

La Contraction Musculaire en Quatre Echelles

Mémoire d'Habilitation à Diriger les Recherches

MATTHIEU CARUEL

La contraction musculaire en quatre échelles

Mémoire d'Habilitation à Diriger les Recherches

Matthieu Caruel

Univ Paris Est Creteil, Univ Gustave Eiffel, CNRS, UMR 8208, MSME, F-94010 Créteil, France

École Doctorale Sciences, Ingénierie et Environnement

Demande d'habilitation évaluée publiquement le 14 Janvier 2025 à Créteil par

Abdul Barakat

Ecole Polytechnique

Rapporteur

Sabine Bensamoun

Université Technologique de Compiègne

Examinatrice

Jocely Etienne

Université Grenoble Alpes, creativecommons

Président

Alf Månsson

Linnaeus University

Rapporteur

Vittorio Sansalone

Université Paris-Est Créteil

Référent

Gudrun Schappacher-Tilp

Joanneum

Rapportrice

Giuseppe Zurlo

University of Galway

Examineur

CC BY-NC-SA 4.0 2025, MATTHIEU CARUEL



This document is published under the Creative Commons license CC BY-NC-SA 4.0 This license enables reusers to distribute, remix, adapt, and build upon the material in any medium or format for noncommercial purposes only, and only so long as attribution is given to the creator. If you remix, adapt, or build upon the material, you must license the modified material under identical terms. For more information, please visit: <https://creativecommons.org/licenses/by-nc-sa/4.0/>

Typeset with the help of Quarto, an Open-source scientific and technical publishing system built on Pandoc.

Allaire, J., Teague, C., Scheidegger, C., Xie, Y., Dervieux, C. and Woodhull, G. (2024). Quarto (Version 1.6) [Computer software].

<https://doi.org/10.5281/zenodo.5960048>

MacFarlane, J., Krewinkel, A., and Rosenthal, J. Pandoc [Computer software].

<https://github.com/jgm/pandoc>

To cite this work:

M. Caruel, “*La Contraction Musculaire en Quatre Echelles*,” Habilitation à Diriger les Recherche, Université Paris-Est Créteil, Créteil, 2025.

Abstract

This work presents a synthesis of the scientific research conducted by Matthieu Caruel between 2008 and 2025. The research focuses on multiscale modeling of muscle contraction, driven by the development of numerical simulation tools for health applications. Starting with the macroscopic description of the tissue within the framework of continuum mechanics, the author introduces the concept of active stress generated by molecular motors. This interaction can be represented by various mathematical models, formulated either in a deterministic framework of population dynamics or in a stochastic framework of Markov processes.

M. Caruel then highlights the role played by mechanical interactions induced by anatomical structures at the micrometric scale in the emergence of collective effects within populations of interacting proteins. These findings suggest a reformulation of the classical modeling framework based so far on a direct coupling between the molecular scale and the tissue scale.

The author emphasizes the necessity of such theoretical developments by presenting various experimental results that have demonstrated the fundamental role of supramolecular mechanical interactions, at the so-called mesoscopic scale, in the physiological processes regulating contraction.

The manuscript is organized as follows. In [Chapter 1](#), we start by giving the essential background on muscle contraction necessary to understand the positioning of the research work and its goals. A macroscopic model of the muscle tissue is presented in [Chapter 2](#), with an emphasis on reduced formulations based on simplified geometries for modeling a muscle fiber and a cardiac ventricle. The force generation process by molecular motors is described in [Chapter 3](#), where we present the classical chemical-mechanical population dynamics approach and more recent stochastic formulations. At the microscale, molecular motors operate in small groups called contractile units. [Chapter 4](#) is dedicated to the modeling of the mechanical coupling of the molecular motors at this scale and its consequences on the force production. The structures connecting contractile units to form muscle fibers within the tissue are introduced in [Chapter 5](#). This chapter addresses the question of the mechanical pathways involved in the regulation of muscle contraction.

All chapters are organized similarly. We start by an introduction providing the technical background and presenting the research challenges, before summarizing M. Caruel's contributions with references to the corresponding publications. A list of perspectives is established at the end of each chapter. [Chapter 6](#) recapitulates these perspectives and briefly discusses potential applications of our work.

Résumé

Cet ouvrage présente une synthèse des travaux scientifiques menés par Matthieu Caruel entre 2008 et 2025. Ces recherches portent sur la modélisation multi-échelle de la contraction musculaire, motivées par le développement d'outils de simulation numérique pour des applications dans le domaine de la santé. En partant de la description macroscopique du tissu dans le cadre de la mécanique des milieux continus, l'auteur introduit la notion de contrainte active générée par les moteurs moléculaires. Cette interaction peut être représentée par divers modèles mathématiques, formulés soit dans un cadre déterministe de dynamique des populations, soit dans un cadre stochastique de processus de Markov.

M. Caruel met ensuite en lumière le rôle des interactions mécaniques induites par les structures anatomiques à l'échelle micrométrique, dans l'émergence d'effets collectifs au sein des populations de protéines interagissantes.

Ces résultats suggèrent une reformulation du cadre classique de modélisation, fondé jusqu'à présent sur un couplage direct entre l'échelle moléculaire et l'échelle tissulaire.

L'auteur souligne la nécessité de ces développements théoriques en s'appuyant sur divers résultats expérimentaux ayant démontré le rôle fondamental des interactions mécaniques supramoléculaires, à l'échelle dite mésoscopique, dans les processus physiologiques régulant la contraction.

Le manuscrit est organisé comme suit. Dans le [Chapitre 1](#), nous présentons les notions essentielles sur la contraction musculaire nécessaires pour comprendre le positionnement et les objectifs des travaux de recherche.

Un modèle macroscopique du tissu musculaire est introduit dans le [Chapitre 2](#), avec une attention particulière portée sur des formulations simplifiées pour modéliser une fibre musculaire et un ventricule cardiaque. Le processus de génération de force par les moteurs moléculaires est détaillé dans le [Chapitre 3](#), où nous exposons l'approche classique de dynamique chimique-mécanique des populations ainsi que des formulations stochastiques plus récentes. À l'échelle microscopique, les moteurs moléculaires fonctionnent en petits groupes appelés unités contractiles. Le [Chapitre 4](#) est consacré à la modélisation du couplage mécanique des moteurs moléculaires à cette échelle et à ses conséquences sur la production de force. Les structures reliant les unités contractiles pour former des fibres musculaires au sein du tissu sont introduites dans le [Chapitre 5](#). Ce chapitre traite des voies mécaniques impliquées dans la régulation de la contraction musculaire.

Tous les chapitres suivent une organisation similaire.

Ils commencent par une introduction fournissant le contexte technique et exposant les défis de

la recherche, avant de résumer les contributions de M. Caruel avec des références aux publications correspondantes.

Une liste de perspectives est établie à la fin de chaque chapitre. Le [Chapitre 6](#) récapitule ces perspectives et discute brièvement les applications potentielles de ces travaux.

Table of contents

| | |
|--|------------|
| Abstract | i |
| Résumé | iii |
| 1 Context and Positioning | 1 |
| 1.1 Muscle contraction in brief | 1 |
| 1.1.1 The contractile structure | 1 |
| 1.1.2 Molecular mechanism of contraction | 2 |
| 1.2 Why study muscle contraction? The example of cardiomyopathies | 3 |
| 1.3 Some motivations | 4 |
| 1.4 Four scales | 5 |
| 1.4.1 Nanoscale: the molecular motor | 5 |
| 1.4.2 Microscale: the contractile unit | 6 |
| 1.4.3 Mesoscale: the sarcomere and the myofibril | 6 |
| 1.4.4 Macroscale: muscle tissue | 7 |
| 1.5 Positionning | 7 |
| 1.5.1 Experimental research | 7 |
| 1.5.2 Mechanical models and heart simulations | 9 |
| 2 Macroscale: contraction at the organ level | 11 |
| 2.1 Background: mechanical models of the heart | 11 |
| 2.1.1 A composite material | 11 |
| 2.1.2 Active strain decomposition | 12 |
| 2.1.3 Model of the contracting muscle tissue | 13 |
| 2.2 Contribution: model reduction for effective calibration and validation | 15 |
| 2.3 Remaining challenges and future work | 17 |
| 3 Nanoscale: molecular motors | 19 |
| 3.1 Background: the myosin molecular motor | 19 |
| 3.1.1 Myosin structure | 19 |
| 3.1.2 Structural aspects of the myosin-actin interaction cycle | 20 |
| 3.1.3 Single molecule force spectroscopy experiments | 21 |
| 3.2 Existing models | 22 |
| 3.2.1 Chemical-mechanical models | 22 |
| 3.2.2 Stochastic ratchet models | 25 |
| 3.3 Challenges | 26 |

| | | |
|----------|--|-----------|
| 3.4 | Contributions | 26 |
| 3.4.1 | The Huxley-Hill formulation revisited | 26 |
| 3.4.2 | Continuous model of the working stroke | 28 |
| 3.4.3 | Jump-diffusion model of the Lymn–Taylor cycle | 29 |
| 3.4.4 | Mean field approximation | 32 |
| 3.4.5 | Reduced models | 34 |
| 3.5 | Ongoing work | 36 |
| 3.5.1 | Molecular dynamics study of the Lymn–Taylor cycle | 36 |
| 3.5.2 | Purely mechanical model of the actin-myosin interaction | 37 |
| 3.6 | Other project: nano diffusion in the bone tissue | 39 |
| 3.7 | Remaining challenges and future work | 40 |
| 3.7.1 | Beyond the mean-field hypothesis | 40 |
| 3.7.2 | Molecular dynamics simulations | 40 |
| 4 | Microscale: the contractile unit | 43 |
| 4.1 | Background: muscle contractile units and models | 43 |
| 4.1.1 | The muscle contractile unit | 43 |
| 4.1.2 | Contractile unit modeling | 44 |
| 4.2 | Challenges | 45 |
| 4.3 | Contributions | 46 |
| 4.3.1 | Fast transient response of muscle fibers | 46 |
| 4.3.2 | Mechanical model of a contractile unit | 47 |
| 4.3.3 | Purely mechanical response of a contractile unit | 47 |
| 4.3.4 | Equilibrium statistical mechanics in length clamp | 49 |
| 4.3.5 | Equilibrium statistical mechanics in soft and mixed devices | 49 |
| 4.3.6 | Effective dynamical model of a contractile unit | 52 |
| 4.3.7 | Application of the contractile unit model to neurotransmission | 53 |
| 4.4 | Perspectives | 54 |
| 5 | Mesoscale: myofibrils and fibers | 55 |
| 5.1 | Background: anatomy of a myofibril | 55 |
| 5.1.1 | Definition of the Mesoscale | 55 |
| 5.1.2 | Cytoskeletal structural elements | 56 |
| 5.1.3 | Three-filament theory of contraction and regulation | 57 |
| 5.1.4 | Contraction regulation mechanisms | 58 |
| 5.1.5 | Non-affine deformation along muscle fibrils | 59 |
| 5.1.6 | Fiber orientations in the muscle tissue | 60 |
| 5.2 | Challenges | 60 |
| 5.3 | Contributions | 61 |
| 5.3.1 | Passive behavior of a simplified sarcomere chain | 61 |
| 5.3.2 | Coupling actin-myosin interaction mechanics and contraction regulation processes | 63 |
| 5.4 | Perspectives | 66 |
| 5.4.1 | Anatomic structures | 66 |

| | | |
|----------|--|-----------|
| 5.4.2 | Modeling activation | 66 |
| 6 | Conclusions, applications, and perspectives | 67 |
| 6.1 | Summary of the main contributions | 67 |
| 6.2 | Applications | 68 |
| 6.2.1 | Collective switching of systems with long-range interactions | 68 |
| 6.2.2 | Simulation of muscle contraction | 69 |
| 6.3 | Perspective and future work | 69 |
| 6.3.1 | Mesoscale modeling | 69 |
| 6.3.2 | Tissue engineering | 70 |
| | References | 73 |

Chapter 1

Context and Positioning

In this chapter, we give the essential background for understanding the principles of muscle contraction. Some elements of this presentation will be refined in appropriate subsequent chapters.

1.1 Muscle contraction in brief

1.1.1 The contractile structure

The human body contains three types of muscles: the skeletal muscles, responsible for motion, the cardiac muscle responsible for the blood circulation, and the smooth muscles found essentially in the digestive apparatus. This manuscript focuses on the group of striated muscles which contains the skeletal and cardiac muscles.

The striated muscle tissue consists in a hierarchy of bundled fibers, with the highest level corresponding to the tissue itself, see Figure 1.1. The skeletal muscles contain fascicles (diameter ~ 1 mm), each one grouping about 10–100 myocytes (diameter ~ 15 μm to 100 μm).

In the skeletal muscle, the myocytes, also called *muscle fibers*, are the centimeter-long fibrillar cells responsible for the contraction. In the cardiac muscle, the contractile cells (cardiomyocytes) are shorter (~ 50 μm to 100 μm) and often branched. The cytoplasm of myocytes and cardiomyocytes contains mostly a parallel arrangement of 2 μm diameter *myofibrils*, in addition to the classical cell organelles (nucleus, mitochondria etc.).

The core of the contractile machinery is embedded in the myofibrils, see Figure 1.2. It consists of a highly regular longitudinal succession of ~ 2 μm -long *sarcomeres*, which are connected by the *Z-lines*. A sarcomere itself is constituted of two antagonist parallel arrays of actin and myosin filaments facing each other on both sides of the *M-lines*.

In the cross-section, actin and myosin filament form a crystalline hexagonal lattice running parallel to the direction of the fiber. The unit cell of this lattice thus contains one thick filament and two thin filaments. When the muscle contracts, the myosin proteins that constitute the thick filaments induce a relative sliding of the surrounding actin filaments that results in the shortening of the sarcomeres. This active shortening is due

Figure 1.1: Hierarchical structure of the skeletal muscle tissue, from McNeill Alexander and Newsom-Davis, “*Striated Muscle; Human Biceps Muscle*” 2015. By courtesy of Encyclopædia Britannica, Inc., ©2017; used with permission.

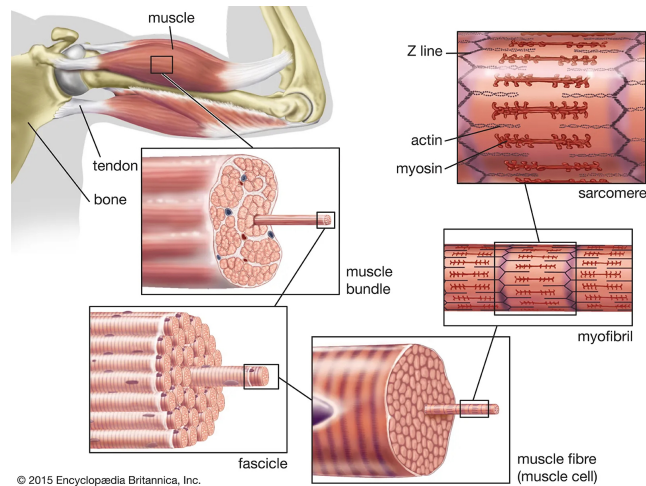
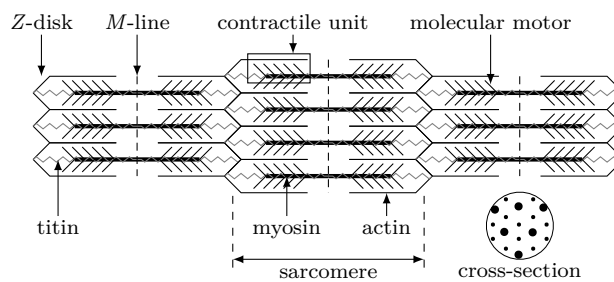


Figure 1.2: Side view of the contractile apparatus inside a myofibril. The cross-section shows the hexagonal lattice formed by the myosin (thick) and actin (thin) filaments. Adapted from Caruel and Truskinovsky, “*Physics of Muscle Contraction*,” 2018.



to the metabolic activity of the myosin proteins which act as *molecular motors*.

The contractile structure also involves other cytoskeletal proteins (see M-lines, Z-disks and titin in Figure 1.2) that will be presented in more details in Section 5.1.1. We will now focus on the molecular mechanism of force generation by the molecular motors.

1.1.2 Molecular mechanism of contraction

The thick filament is a bundle of 600 myosin proteins connected by their tails. They form into two antagonists groups of 300 individuals each, see Figure 1.2. In the rest of this manuscript, we will call a contractile unit an effective bundle of 300 molecular motors constituting a half muosin filament interacting with its surrounding actin filaments. Given the relative proportion of myosin and actin filament, such contractile unit can be effectively represented as a single myosin filament interacting with two actin filaments.

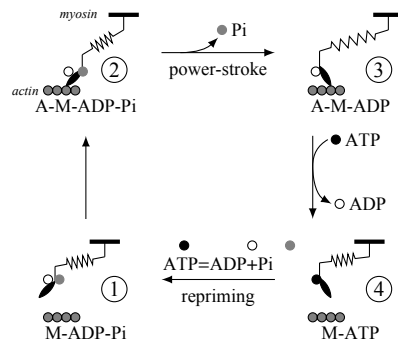
A single myosin protein has a pair of *heads* that points radially, from the myosin filament towards the surrounding thin filaments. It is the cyclic interaction between myosin heads and actin that produces the active force necessary to shorten the sarcomeres. The actin-myosin interaction cycle is referred to as the Lymn and Taylor cycle.¹ see Figure 1.3.

When the muscle contraction is activated² the myosin heads can attach to

¹ “*Mechanism of Adenosine Triphosphate Hydrolysis by Actomyosin*,” 1971. Here we present the classical version contains four steps. Since their fundamental 1971 publication, numerous studies on the molecular mechanism of force generation have contributed to the refinement of this cycle. See for instance the review by Houdusse and Sweeney (“*How Myosin Generates Force on Actin Filaments*,” 2016).

² see Chapter 4 for more details about the activation process.

1.2 Why study muscle contraction? The example of cardiomyopathies



specific actin binding sites regularly positioned along the actin filaments (step 1 \rightarrow 2). While attached, the actin-myosin complex is called a *cross-bridge*. A fundamental characteristic of the myosin protein is its ability to undergo a conformational change, the *working-* (or *power-*) *stroke* (step 2 \rightarrow 3) that results, thanks to a lever-arm, into a 10 nm relative displacement of the two bridged filaments in absence of impairing force.³

After the working stroke has been executed, the myosin detaches from actin (step 3 \rightarrow 4). In the detached state, the working stroke conformational change is reversed, waiting to be triggered again upon the next attachment (step 4 \rightarrow 1). This cocking mechanism requires the hydrolysis of one molecule of Adenosine TriPhosphate (ATP). The hydrolysis products, Adenosine DiPhosphate (ADP) and inorganic phosphate (P_i) are released from within the molecule alongside the power-stroke in the attached state.⁴

The collective actin-myosin interactions, which generate antagonistically oriented working strokes inside each sarcomere, is ultimately responsible for the macroscopic contraction of the muscle fibers.

1.2 Why study muscle contraction? The example of cardiomyopathies

Pathological alterations of the complex contractile apparatus are involved in the development of genetic cardiomyopathies, which, in the most severe cases, lead to Acute Heart Failure (AHF) and sudden death.

The causes of AHF are diverse, which makes it particularly difficult to treat.⁵ The most prevalent genetic cardiomyopathy degenerating into AHF is the Hypertrophic Cardiomyopathy (HCM), affecting 1 individual per 500.⁶ This pathology is often associated with mutations of the myosin protein that result in an increase of the tissue contractility.⁷ Another severe genetic cardiomyopathy leading to AHF is the Dilated Cardiomyopathy (DCM) which accompanies the deterioration of the mechanical properties of the M-lines Z-lines and titin, resulting in the loss of register of the contractile units inside the fibrils (see Figure 1.2), and abnormal inflation of the tissue over time.⁸ The mechanisms underlying HCM and

Figure 1.3: Lymn and Taylor cycle. A myosin protein is represented by a spring with a rotating head (the second head is not represented). The myosin head can attach to specific site located on a surrounding actin filament (step 1 \rightarrow 2). While the head is attached (steps 2 \rightarrow 3) it undergoes a conformational change, the power-stroke (or working stroke) that produces force. After the head detachment (step 3 \rightarrow 4), this conformational change is reversed (steps 4 \rightarrow 1). Adapted from Caruel and Truskinovsky, “*Physics of Muscle Contraction*,” 2018.

³ A. F. Huxley and Simmons, “*Proposed Mechanism of Force Generation in Striated Muscle*,” 1971; Rayment, Holden, et al., “*Structure of the Actin-Myosin Complex and Its Implications for Muscle Contraction*,” 1993; Rayment, Rypniewski, et al., “*Three-Dimensional Structure of Myosin Subfragment-1: A Molecular Motor*,” 1993.

⁴ The exact sequence of events leading to the departure of P_i from the myosin active site and their relationship with the power-stroke not fully resolved. See Debold, “*Recent Insights into the Relative Timing of Myosin’s Powerstroke and Release of Phosphate*,” 2021. For more details about the molecular mechanisms of the enzymatic activity of myosin we refer to Houdusse and Sweeney (“*How Myosin Generates Force on Actin Filaments*,” 2016).

⁵ George et al., “*Novel Drug Targets in Clinical Development for Heart Failure*,” 2014; Rossignol et al., “*Heart Failure Drug Treatment*,” 2019.

⁶ B. J. Maron and M. S. Maron, “*Hypertrophic Cardiomyopathy*,” 2013.

⁷ Morita et al., “*Shared Genetic Causes of Cardiac Hypertrophy in Children and Adults*,” 2008.

⁸ Gerull et al., “*Mutations of TTN, Encoding the Giant Muscle Filament Titin, Cause Familial Dilated Cardiomyopathy*,” 2002; Granzier et al., “*Titin*,” 2005; Hinson et al., “*Titin Mutations in iPS Cells Define Sarcomere Insufficiency as a Cause of Dilated Cardiomyopathy*,” 2015; Lange et al., “*The M-band: The Underestimated Part of the Sarcomere*,” 2019.

DCM are not well understood. The connection between protein alterations at various biological levels and the resulting observable effects on heart function has not been clearly established.

A promising therapeutic approach in AHF, HCM, DCM and other cardiomyopathies is the use of small effector molecules, such as Omecamtiv Mecarbil and Mavacamten, that specifically modulate myosin activity.⁹ For instance, the clinical trials have shown that cardiac function of patients with severe cardiomyopathies can be improved within minutes of inoculation with Omecamtiv Mecarbil.¹⁰ It is worth noticing that Mavacamten has recently been approved by the U.S. Food and Drug Administration.¹¹

Despite the proven clinical efficacy of these molecules, there remains an unclear understanding of their impact on the contraction process, potentially complicating the adjustment of prescriptions. For this reason, and because of their promising impact on diseases, these drugs are under intense experimental scrutiny at the structural, cellular and organ (or body) scales.¹²

1.3 Some motivations

Between the nano- and the macro-scale, a full understanding of how the drugs or pathologic mutation modify the contraction process is still lacking, even at the most basic mechanical level. Practitioners could leverage this understanding in their clinical decisions. For this reason, mutations leading to cardiomyopathies and the associated treatments are considered to be priority research subjects.¹³

Existing experimental studies provide valuable information on the effect of mutation and drugs at specific scales of the tissues. The rationale of research is to leverage this knowledge to design a unified modeling framework to emulate the genotype to phenotype relationship in healthy and diseased muscle tissue. Furthermore, the knowledge of the mechanical and physiological pathways explaining this relationship, would open the possibility to engineer small protein effectors based on the simulation of their desired macroscopic effect.

Another potential outcome of the research efforts in understanding the physical principles governing muscle contraction is to design artificial actuators leveraging similar principles. As an example, we may consider electromechanical actuators being used in machines or vehicles. In some applications, in particular aircraft engineering, critical functions can be impaired by the malfunction of a single actuator. In such situations, critical motions are often ensured by redundant actuators for safety reasons. However, in some cases, redundancy is not permitted, either because of steric hindering (e.g. for helicopters) or because of weight cost (e.g. for spatial application). Muscle resilience originates from its multiscale structure and multileveled neuronal command. The structure and command

⁹ reviewed in Day, Tardiff, and Ostap, "Myosin Modulators," 2022; Houdusse, Auguin, et al., "Small Molecules Modulating Force Production," 2024; RabieeRad et al., "Novel Treatments of Hypertrophic Cardiomyopathy in GDMT for Heart Failure," 2023.

¹⁰ As per 2025, the FDA has not approved the use of Omecamtiv Mecarbil as a treatment of heart failure.

¹¹ Nag et al., "Mavacamten, a Precision Medicine for Hypertrophic Cardiomyopathy," 2023

¹² Houdusse, Auguin, et al., "Small Molecules Modulating Force Production," 2024.

¹³ Velden et al., "Research Priorities in Sarcomeric Cardiomyopathies," 2015.

strategies may be advantageously mimicked to create a new kind of resilient actuator. Moreover, recent advancements in nanomachines constructed from purified muscle proteins suggest the potential design of actuators assembled from genuine proteins.¹⁴

In summary, the goal of our research is to provide models of the contraction at different scales that can be used

- to understand the specific impact of pathological mutations and drugs on the mechanisms of contraction,
- to design artificial devices that mimicks the outstanding properties of muscle cells and tissue.

¹⁴ Pertici, Bongini, et al., “*A Myosin II Nanomachine Mimicking the Striated Muscle*,” 2018; Saper and Hess, “*Synthetic Systems Powered by Biological Molecular Motors*,” 2020.

1.4 Four scales

We view the modeling framework as the integration of four projects, each being specific to one of the following scales:

- the nanoscale,
- the microscale,
- the mesoscale,
- the macroscale.

In the following paragraphs we introduce briefly the context of each scale. More details are available in the dedicated chapters.

1.4.1 Nanoscale: the molecular motor

The typical size of a protein is just a few nanometers. At this scale, the objective is to understand and model:

- The mechanics of allosteric enzymatic activity in myosin, specifically its ability to catalyze ATP hydrolysis within an active site of the molecule, and use this reaction to trigger a significant conformational change at a distant site within the molecule.
- The physical principles underlying the interaction between a single myosin protein and an actin filament.

Our goal at the nanoscale is to provide a physiologically relevant dynamical model of the actin-myosin interaction, based on a minimal set of descriptive variables.

1.4.2 Microscale: the contractile unit

We define a contractile unit a bundle of molecular motors sharing the same myosin filament backbone and interacting with the surrounding actin filaments. Considering the stoichiometry between the two types of filaments, the contractile unit comprises one thick filament and two thin filaments. At this scale, the objective is to understand how the molecular motors cooperate. The cooperative mechanisms emerge from the elastic coupling that is mediated by the filament themselves and by the titin protein.¹⁵ Such coupling plays a fundamental role not only in the basic force production but also in the activation and regulation of this process.¹⁶

Our goal is to understand how the connections between the molecular motors at the scale of a prototypical contractile unit affect their collective functioning, in particular the force production and its regulation.

1.4.3 Mesoscale: the sarcomere and the myofibril

Stacks of contractile units are arranged parallel to form sarcomeres which are, in turn, assembled in series within muscle fibrils and fibers, see Figure 1.2. It is the synchronized contraction of all activated contractile units that enables the macroscopic shortening of the muscle fibers.

The mechanical coupling between the contractile units is facilitated by scaffolding structures (such as Z-lines, M-lines, and titin), which maintain the entire hierarchy in alignment and preserve its integrity. These structures also play a fundamental role in the regulation of the contraction.¹⁷ Finally, it is now clear that mutations affecting the mechanical properties of the M-lines, Z-disks and titin cytoskeletal proteins that constitute this elastic network, are involved in the development of cardiomyopathies, potentially via an alteration of their ability to maintain the sarcomeres in register.¹⁸

Finally, the cardiac tissue being a composite material with active stress fibers embedded in the extracellular matrix, the mesoscale structure is also characterized by the orientation of the fibers within the tissue. Microscope observations show that the fiber orientation distribution in healthy and pathological tissues may greatly differ.¹⁹

Our goals at the mesoscale are to

- provide a physiologically valid model of the network of sarcomeric structural proteins and study how its properties affect the collective functioning of contractile units,
- formulate a homogenized macroscopic behavior law of the tissue that takes into account its composite microstructure.

¹⁵ Caruel and Truskinovsky, “*Physics of Muscle Contraction*,” 2018; Linari, Brunello, et al., “*Force Generation by Skeletal Muscle Is Controlled by Mechanosensing in Myosin Filaments*,” 2015.

¹⁶ Brunello and Fusi, “*Regulating Striated Muscle Contraction*,” 2024.

¹⁷ *ibid.*

¹⁸ Gerull et al., “*Mutations of TTN, Encoding the Giant Muscle Filament Titin, Cause Familial Dilated Cardiomyopathy*,” 2002; Granzier et al., “*Titin*,” 2005; Herwig et al., “*Modulation of Titin-Based Stiffness in Hypertrophic Cardiomyopathy via Protein Kinase D*,” 2020; Hinson et al., “*Titin Mutations in iPSC Cells Define Sarcomere Insufficiency as a Cause of Dilated Cardiomyopathy*,” 2015; Lange et al., “*The M-band: The Underestimated Part of the Sarcomere*,” 2019; Wadmore, Azad, and Gehmlich, “*The Role of Z-disc Proteins in Myopathy and Cardiomyopathy*,” 2021.

¹⁹ Hoshino et al., “*Myocardial Fiber Diameter and Regional Distribution in the Ventricular Wall of Normal Adult Hearts, Hypertensive Hearts and Hearts with Hypertrophic Cardiomyopathy*,” 1983.

1.4.4 Macroscale: muscle tissue

The macroscale is the scale of the contracting tissue itself. Macroscopic data include the typical continuum mechanics fields of displacement, deformation, stresses etc. In the case of the heart they also include the internal pressure, the ventricles or atria volumes and the blood flow rates in and out of the cavities.

The challenge is to provide a model that can reproduce these macroscopic observables using ingredients reminiscent of the actual physiological process. Since these processes are complex, the models may involve many parameters that end up to be difficult to calibrate. Another difficulty lies in the numerical cost of these models which can impair their use in clinical contexts.

1.5 Positioning

In this manuscript, we will position our work mainly with respect to research on the heart contraction in health and disease. However, the models that will be presented can be used with other types of muscle as well.

1.5.1 Experimental research

Muscle contraction mechanisms can be studied experimentally at all scales.

Nanoscale, molecular motors

3D Molecular structures of the various myosin conformations involved in the contraction cycle can be resolved from X-Ray crystallography and/or Cryogenic Electron Microscopy, both in control and in the presence of mutations or small effectors, giving insight into how they could influence the molecular mechanism of force generation.²⁰ These crystallographic structures can be viewed as high resolution snapshots of the protein in different conformations.²¹ It is then possible to use molecular dynamics simulation to get insight into the force generation mechanism over short timescales. The properties of isolated molecular motors can also be probed using mechanical tests in optical tweezers.²²

Finally, taking advantage of the crystalline nature of the muscle myofibrils, X-ray diffraction can be used in-situ to probe nanoscale structural change in real time, while performing a mechanical test on a macroscopic sample.²³ In the latter type of experiment, the average behavior of a motor can be monitored with nanometer resolution while it interacts with other motors in near to physiological conditions.

Microscale, contractile units

²⁰ Robert-Paganin et al., “*Force Generation by Myosin Motors*,” 2020.

²¹ Houdusse and Sweeney, “*How Myosin Generates Force on Actin Filaments*,” 2016.

²² Arbore et al., “*Probing Force in Living Cells with Optical Tweezers*,” 2019; Woody, Winkelmann, et al., “*Single Molecule Mechanics Resolves the Earliest Events in Force Generation by Cardiac Myosin*,” 2019; Woody, Greenberg, et al., “*Positive Cardiac Inotrope Ome-camtiv Mecarbil Activates Muscle despite Suppressing the Myosin Working Stroke*,” 2018; Yanagida et al., “*Single Molecule Analysis of the Actomyosin Motor*,” 2000.

²³ Piazzesi, Reconditi, Linari, Lucii, Bianco, et al., “*Skeletal Muscle Performance Determined by Modulation of Number of Myosin Motors Rather Than Motor Force or Stroke Size*,” 2007.

²⁴ Marston, “Force Measurements From Myofibril to Filament,” 2022.

²⁵ Holzbaur and Goldman, “Coordination of Molecular Motors,” 2010; D. Warshaw, “The In Vitro Motility Assay,” 1996.

²⁶ Buonfiglio et al., “Force and Kinetics of Fast and Slow Muscle Myosin Determined with a Synthetic Sarcomere-like Nanomachine,” 2024; Pertici, Bianchi, et al., “A Myosin II-Based Nanomachine Devised for the Study of Ca²⁺-Dependent Mechanisms of Muscle Regulation,” 2020; Pertici, Bongini, et al., “A Myosin II Nanomachine Mimicking the Striated Muscle,” 2018, see also Cheng, Leite, and Rassier, “The Load Dependence and the Force-Velocity Relation in Intact Myosin Filaments from Skeletal and Smooth Muscles,” 2020; Hwang et al., “A Reverse Stroke Characterizes the Force Generation of Cardiac Myofilaments, Leading to an Understanding of Heart Function,” 2021; Kaya et al., “Coordinated Force Generation of Skeletal Myosins in Myofilaments through Motor Coupling,” 2017.

²⁷ Herzog and Schappacher-Tilp, “Molecular Mechanisms of Muscle Contraction,” 2023; Leite and Rassier, “Sarcomere Length Non-Uniformity and Force Regulation in Myofibrils and Sarcomeres,” 2020; Linke, “Stretching the Story of Titin and Muscle Function,” 2023.

²⁸ Ait-Mou et al., “Titin Strain Contributes to the Frank-Starling Law of the Heart by Structural Rearrangements of Both Thin- and Thick-Filament Proteins,” 2016; Brunello and Fusi, “Regulating Striated Muscle Contraction,” 2024; Caremani, Marcello, et al., “The Force of the Myosin Motor Sets Cooperativity in Thin Filament Activation of Skeletal Muscles,” 2022; Linke and Krüger, “The Giant Protein Titin as an Integrator of Myocyte Signaling Pathways,” 2010.

²⁹ Squarci et al., “Titin Activates Myosin Filaments in Skeletal Muscle by Switching from an Extensible Spring to a Mechanical Rectifier,” 2023.

³⁰ Hoshino et al. (“Myocardial Fiber Diameter and Regional Distribution in the Ventricular Wall of Normal Adult Hearts, Hypertensive Hearts and Hearts with Hypertrophic Cardiomyopathy,” 1983); Damon et al. (“Skeletal Muscle Diffusion Tensor-MRI Fiber Tracking,” 2017)

Interactions between molecular motors within contractile units can be observed in artificial preparations.²⁴ In in-vitro motility assays for instance, large groups of myosin motors are fixed on a plane surface and moving actin filament put on to of them.²⁵ Contractile units involving a controlled number of motors can also be manipulated in vitro. Recently the team lead by Dr. P. Bianco from the PhysioLab (University of Florence, Italy) has succeeded in reconstructing a minimal functional contractile unit out of purified actin and myosin proteins, able to reproduce the performance of the functional unit of the muscle.²⁶ These experimental setups provide ideal platforms for testing the basic effect of new drugs and for designing artificial biomimetic devices.

Mesoscale, Inter-sarcomere dynamics and regulation

Over the past two decades, experimental studies at the scale of single myofibrils or fibers have revealed the existence of non-uniformities (non-affine behavior) of the sarcomere lengths during contraction. The direct observation can come from single fibrils tested in optical tweezer setups or from single cell preparations using fast confocal microscopy. Recent reviews of these studies report on the important role played by the elastic network that connects the sarcomeres together in tailoring these non-uniformities.²⁷

It is also hypothesized that these sarcomeric proteins participate in fundamental regulation pathways involving mechanical feedback-loops: the force transmitted via the elastic scaffold may enhance contractile units’ activation.²⁸ Recording myosin based reflexions gives access to the footprint of titin modulation of the regulatory state of the myosin filament. This approach allowed understanding of how the titin react to activation signals and how it can activate the molecular motors.²⁹

Finally, the distribution of fiber orientation in the tissue can be quantified post-mortem using standard microscopy or using diffusion-weighted MR imaging (DW-MRI).³⁰

Macroscale, experiments on intact trabeculae

The majority of experimental data are obtained from mechanical tests performed on multicellular preparations. These tests allow studying the effects of drugs and mutations on the tissue contraction. For skeletal muscles, in situ experiments are performed either on single fibers or directly on intact muscle preparations. For the heart muscle, a large body of experimental data is obtained from mechanical tests performed on multicellular preparations—typically the pillar-shaped cardiac trabecula³¹—isolated from ventricles.³²

The mechanisms of contraction can then be tested in a wide range of conditions by varying the content of the bathing solution, the temperature and the mechanical loading. As mentioned above, this type of experiment, can be coupled with nanometer resolution X-ray diffraction measurements.³³

At the scale of the organ, macroscopic deformation maps can be recovered from tagged cine MRI,³⁴ and catheter pressure probes inserted in the heart allow recording pressure-volume loops.³⁵

1.5.2 Mechanical models and heart simulations

The interest of having a physiologically relevant model at organ-scale is obvious: it allows simulating the contraction and have access to various indicators that can be compared to clinical data on the one hand but also estimates of internal parameters that are not directly accessible by macroscale measurements, such as internal stresses.

To link these internal parameters to the macroscopic observables, comprehensive models of the heart covering all physiological aspects of its functioning are already available. International research consortia are already using this kind of models to study cardiomyopathies and their treatments, see for instance the work of the [SilicoFCM consortium](#) or the [MATHCARD project](#).

In the last decade, computer methods have been developed to simulate realistic muscle behavior, especially for the heart.³⁶ Essential underlying model elements are the force generation by molecular acto-myosin motors, the activation processes regulating contraction, the perfusion mechanisms (for the heart), and the passive viscoelastic properties of the tissue.

All the existing approaches share similar background based on three essential assumptions.

1. The molecular motors' behavior can be represented as a jump process between a set of states characterizing the conformation of the myosin motors, its attachment to actin (attached or detached) and its biochemical state (ATP hydrolysis stage within the active site). The transition rates between these states are dependent on conformational and positional mechanical degrees of freedom. Hence, the designation *chemical-mechanical models*.
2. The bulk density of motors within the tissue is sufficiently large for a mean-field description to be valid. The motors population dynamics is then governed by a (potentially large) system of Partial Differential Equations on the probability distributions characterizing each "chemical state" of the motors. Mathematical simplifications (surrogate models) and associated numerical schemes have been developed to make this system of governing equations suitable for organ-scale finite elements simulations³⁷
3. The equations describing the population of motors are directly coupled to the equilibrium laws of continuum mechanics, using rheological lumped elements that represent the contribution of cytoskeletal structural proteins to the passive viscoelastic properties of the tissue. It is usually assumed that active fibers are homogeneous and that a unique fiber direction can be defined at each material point.

³¹ the trabeculae muscle (or trabeculae carneae) are muscular columns that project from the inner surface of the right and left ventricles. They may form simple ridges, or be fixed at both extremities. Papillary muscles are examples of trabeculae that holds the tendinous chords holding the cusps of the valves. Trabeculae muscles are used in experiments because they are essentially one dimensional objects with aligned fibers.

³² Ait Mou et al., "Altered Myofibril Structure and Function in Dogs with Duchenne Muscular Dystrophy Cardiomyopathy," 2018; Caremani, Pinzauti, et al., "Size and Speed of the Working Stroke of Cardiac Myosin in Situ," 2016; de Tombe and ter Keurs, "Force and Velocity of Sarcomere Shortening in Trabeculae from Rat Heart. Effects of Temperature." 1990; Pinzauti et al., "The Force and Stiffness of Myosin Motors in the Isometric Twitch of a Cardiac Trabecula and the Effect of the Extracellular Calcium Concentration," 2018.

³³ Piazzesi, Reconditi, Linari, Lucii, Bianco, et al., "Skeletal Muscle Performance Determined by Modulation of Number of Myosin Motors Rather Than Motor Force or Stroke Size," 2007.

³⁴ Chabiniok et al., "Multiphysics and Multiscale Modelling, Data-Model Fusion and Integration of Organ Physiology in the Clinic," 2016.

³⁵ Bastos et al., "Invasive Left Ventricle Pressure-Volume Analysis," 2020; Foëx and Leone, "Pressure-Volume Loops," 1994; Protti et al., "Looking Back, Going Forward," 2024.

³⁶ Chabiniok et al., "Multiphysics and Multiscale Modelling, Data-Model Fusion and Integration of Organ Physiology in the Clinic," 2016; Regazzoni, Dedè, and Quarteroni, "Biophysically detailed mathematical models of multiscale cardiac active mechanics," 2020; Stojanovic et al., "Multi-scale Striated Muscle Contraction Model Linking Sarcomere Length-dependent Cross-bridge Kinetics to Macroscopic Deformation," 2019; Sugiura, Washio, et al., "Multi-Scale Simulations of Cardiac Electrophysiology and Mechanics Using the University of Tokyo Heart Simulator," 2012.

³⁷ Kimmig and Caruel, “*Hierarchical Modeling of Force Generation in Cardiac Muscle*,” 2020; Milićević et al., “*Huxley Muscle Model Surrogates for High-Speed Multi-Scale Simulations of Cardiac Contraction*,” 2022; Regazzoni, Salvador, et al., “*A Machine Learning Method for Real-Time Numerical Simulations of Cardiac Electromechanics*,” 2022.

³⁸ Moo and Herzog, “*Single Sarcomere Contraction Dynamics in a Whole Muscle*,” 2018; Squarci et al., “*Titin Activates Myosin Filaments in Skeletal Muscle by Switching from an Extensible Spring to a Mechanical Rectifier*,” 2023.

³⁹ Lange et al., “*The M-band: The Underestimated Part of the Sarcomere*,” 2019.

⁴⁰ Hoshino et al., “*Myocardial Fiber Diameter and Regional Distribution in the Ventricular Wall of Normal Adult Hearts, Hypertensive Hearts and Hearts with Hypertrophic Cardiomyopathy*,” 1983.

In view of these modeling hypotheses, we can point several limitations of the existing frameworks.

1. The chemical-mechanical model of the molecular motor functioning is in fact an asymptotic representation of a high-dimensional stochastic system describing the motion of interconnected atoms or amino-acids. There is no systematic derivation such asymptotic model reduction, which is in fact valid only if the so-called states represent deep enough energy wells. There is also no formal link between the chemical-mechanical model and the underlying structural mechanisms and conformational changes.
2. The mean-field assumption made to describe a large population of molecular motors neglects the mechanical interactions that can exist at the level of single contractile units, i.e. where a finite size system of molecular motors are coupled via the myofilaments. It also corresponds to an asymptotic limit that would need to be mathematically justified.
3. Using the assumption of a direct coupling between the molecular scale processes and the macroscopic mechanical balance laws, current models consider that a muscle fiber can be viewed as a homogenous 1D continuum, without detailed modeling of the cytoskeletal proteins at the mesoscale and without questioning the validity of having a single fiber orientation per material point. However, as mentioned in the previous sections, experiments have shown that the cytoskeletal proteins play a role in maintaining contractile units in register, notably during activation.³⁸ Alteration of their mechanical properties may lead to non-affine deformations which could contribute to the development of cardiomyopathies.³⁹ Direct observation have also shown that in pathological situation, the definition of a clear fiber orientation was not possible.⁴⁰

For these reasons, there is no truly multiscale framework linking the molecular structural alterations induced by cardiomyopathies and their associated pharmacology, with their consequences on the heart.

In the following chapters, we will review the different scales of modeling and present an overview of the current state of research, of our contribution to this research, and sketch further developments.

Chapter 2

Macroscale: contraction at the organ level

In this chapter, we present the framework for modeling the heart contraction at the macroscale. We will here focus on the continuum mechanics formulation to make clear where the active component of the model enters the description. The modeling of the internal variables that represent the underlying active processes will be presented in the next chapter.

i Associated publications

The contributions summarized in this chapter can be found in “*Dimensional Reductions of a Cardiac Model for Effective Validation and Calibration*,” 2014 by Caruel et al.; and “*Hierarchical Modeling of Force Generation in Cardiac Muscle*,” 2020 by Kimmig and Caruel. The general approach used in these two references is quite representative of the literature.

2.1 Background: mechanical models of the heart

2.1.1 A composite material

From the macroscale point of view, the cardiac muscle tissue can be represented as a composite material consisting in a hyperelastic polymer matrix with embedded active stress fibers, see Figure 2.1. The fibers’ orientation vary continuously from $+60^\circ$ at the endocardium to -60° at the epicardium¹. Locally parallel fibers are themselves grouped in fascicles of 5 to 10 individuals surrounded by *sheetlets* of collagen, whose orientation also vary from the endocardium to the pericardium.²

Macroscale models are formulated using the laws of continuum mechanics which assume the existence of an elementary representative microscopic volume. For the muscle tissue, the usual elementary representative volume is constituted of a hyper-viscoelastic material representing the extracellular matrix, in which a 1D contractile fiber—characterized by its local orientation $\underline{\tau}$ —is embedded, see Figure 2.2 (a).³ This represen-

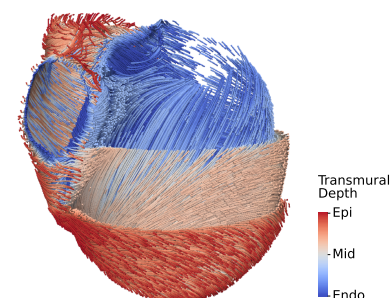


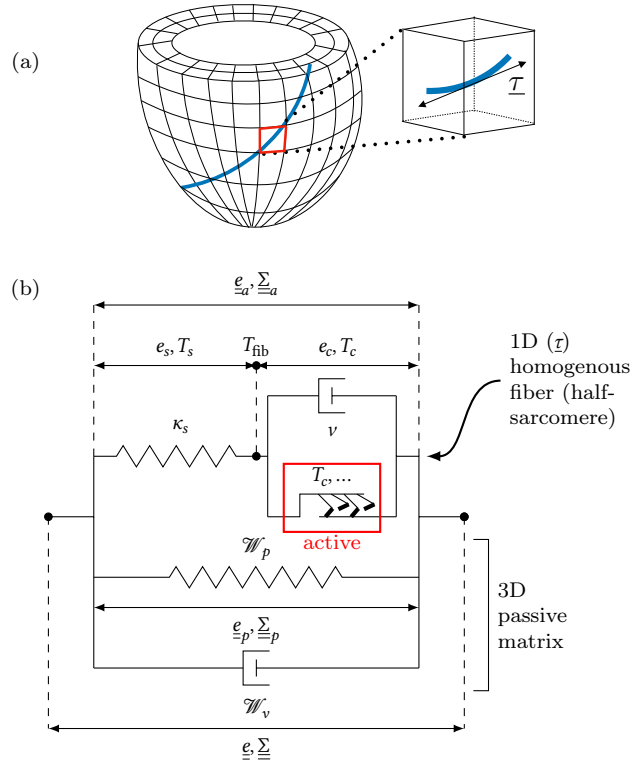
Figure 2.1: Reconstruction of fibers orientation in the cardiac tissue. From *ibid.* (unmodified, CC BY 4.0).

¹ Streeter Jr. and Bassett, “*An Engineering Analysis of Myocardial Fiber Orientation in Pig’s Left Ventricle in Systole*,” 1966

² LeGrice et al., “*Laminar Structure of the Heart*,” 1995; NIELLES-VALLESPIN et al., “*Assessment of Myocardial Microstructural Dynamics by In Vivo Diffusion Tensor Cardiac Magnetic Resonance*,” 2017.

³ In this presentation we neglect the sheetlets organization and refer to Tuani, Allain, and Genet (“*On the Structural Origin of the Anisotropy in the Myocardium*,” 2023) for a presentation of a model that takes it into account.

Figure 2.2: Rheological model of the muscle tissue. (a) Geometry of the heart showing one fiber (blue line) and the local fiber orientation $\underline{\tau}$. (b) Rheological model. Adapted from Kimmig, Chapelle, and Moireau, “*Thermodynamic Properties of Muscle Contraction Models and Associated Discrete-Time Principles*,” 2019 (CC BY 4.0).



tation assumes the possibility to define a preferred fiber direction at each material point.

2.1.2 Active strain decomposition

We start the model presentation by mentioning that our approach is based on the so-called “active stress” assumption. The alternative “active strain” approach is based on the multiplicative decomposition of the deformation gradient tensor

$$\underline{\underline{F}} = \underline{\underline{F}}_p \cdot \underline{\underline{F}}_a,$$

where $\underline{\underline{F}}_a$ and $\underline{\underline{F}}_p$ represent the active and passive deformations, respectively.⁴ As an example, Colorado-Cervantes et al.⁵ proposed the following expression for the active strain

$$\underline{\underline{F}}_a = \lambda_{\parallel} \underline{\tau} \otimes \underline{\tau} + \frac{1}{\sqrt{\lambda_{\parallel}}} (\underline{\underline{1}} - \underline{\tau} \otimes \underline{\tau}),$$

where λ_{\parallel} measures the contraction along the fibers. Models of this type then provide a phenomenological relation between the parameter λ_{\parallel} and an activation field linked for instance to the transmembrane electric potential.⁶

We chose to follow a different approach based on a formulation that naturally describes the internal microscopic kinematics of a fiber and that can be closely linked to the actual molecular force generation process. This approach can thus benefit from a large set of experimental data targeting

⁴ The theory is developed in the following references: Göktepe, Menzel, and Kuhl, “*The Generalized Hill Model*,” 2014; Nardinocchi and Teresi, “*On the Active Response of Soft Living Tissues*,” 2007; Nobile, Quarteroni, and Ruiz-Baier, “*An Active Strain Electromechanical Model for Cardiac Tissue*,” 2012.

⁵ Colorado-Cervantes et al., “*Patient-Specific Modeling of Left Ventricle Mechanics*,” 2022.

⁶ Göktepe, Menzel, and Kuhl, “*The Generalized Hill Model*,” 2014.

these microscale processes and from which different model ingredients can be specifically calibrated.

2.1.3 Model of the contracting muscle tissue

The proposed macroscale muscle tissue model originates from the work of Chapelle et al.⁷ It is based on the Hill-Maxwell rheology represented in Figure 2.2 (b). This model was used in Caruel, Chabiniok, et al., “*Dimensional Reductions of a Cardiac Model for Effective Validation and Calibration*,” 2014, and has been refined in Kimmig, Chapelle, and Moireau, “*Thermodynamic Properties of Muscle Contraction Models and Associated Discrete-Time Principles*,” 2019. We here summarize the latter formulation.

The tissue model is decomposed of two parallel branches: a 3D branch representing the extracellular matrix and a 1D branch representing the fiber. The Green-Lagrange deformation tensors of the extracellular matrix and the contractile fiber are denoted by \underline{e}_p and \underline{e}_a , respectively. Since the passive and active branch are in parallel, the global Green-Lagrange tensor reads $\underline{e} = \underline{e}_p = \underline{e}_a$. The fiber is usually viewed as a one dimensional homogenous medium where the global deformation can be mapped to the deformation of single half-sarcomere. Denoting by ℓ_{fib} the characteristic length of a half sarcomere and by $\delta\ell_{\text{fib}}$ its variation, we define the total extension of the fiber by

$$e_{\text{fib}} = \frac{\delta\ell_{\text{fib}}}{\ell_{\text{fib}}} = (1 + 2\tau \cdot \underline{e} \cdot \underline{\tau})^{\frac{1}{2}} - 1.$$

A mechanical geometrical representation of a single half-sarcomere that have been validated by numerous in situ mechanical experiments consists in a series connexion of two elements:⁸ (i) a passive element representing the elastic deformation of the myofilaments and other non-contractile sarcomeric structure, like the Z-disks, the M-line and titin,⁹ and (ii) an active element representing the array of myosin molecular motors interacting with the surrounding actin filaments, see Figure 2.2 (b).

Following this assumption, we can decompose the extension $\delta\ell_{\text{fib}}$ into

$$\delta\ell_{\text{fib}} = \delta\ell_c + \delta\ell_s,$$

where $\delta\ell_c$ and $\delta\ell_s$ denote the extensions of the active and passive series elements, respectively. We further define the associated deformations $e_c = \delta\ell_c/\ell_{\text{fib}}$ and $e_s = \delta\ell_s/\ell_{\text{fib}}$, which verify $e_{\text{fib}} = e_c + e_s$.

We denote by T_{fib} the active force in the direction of the fiber per unit area of transverse cross-section considered in the reference configuration. The stress T_{fib} combines the force produced by the contractile machinery T_c and a viscous drag that is considered linear, so that

$$T_{\text{fib}} = T_c + \nu\dot{e}_c = \kappa_s e_s. \quad (2.1)$$

⁷ “An Energy-Preserving Muscle Tissue Model: Formulation and Compatible Discretizations,” 2012.

⁸ Caruel and Truskinovsky, “*Physics of Muscle Contraction*,” 2018; Pertici, Caremani, and Reconditi, “*A Mechanical Model of the Half-Sarcomere Which Includes the Contribution of Titin*,” 2019, and references therein. The kinematic decomposition is based on the work of Ford, A. F. Huxley, and Simmons (“*The Relation between Stiffness and Filament Overlap in Stimulated Frog Muscle Fibres*,” 1981).

⁹ for more details about the sarcomeric proteins and their role in the contraction mechanism, see Chapter 5.

The first Piola-Kirchhoff active stress tensor T_{fib} can finally be mapped to the second Piola-Kirchhoff stress tensor

$$\underline{\underline{\Sigma}}_a = \frac{T_{\text{fib}}}{(1 + 2\underline{\underline{\tau}} \cdot \underline{\underline{e}} \cdot \underline{\underline{\tau}})^{\frac{1}{2}}} \underline{\underline{\tau}} \otimes \underline{\underline{\tau}}.$$

The extracellular matrix is endowed with a 3D visco-hyperelastic constitutive law derived from a hyperelastic potential \mathcal{W}_p and a viscous pseudo-potential \mathcal{W}_v . The resulting passive second Piola-Kirchhoff stress tensor is

$$\underline{\underline{\Sigma}}_p = \frac{\partial \mathcal{W}_p}{\partial \underline{\underline{e}}} + \frac{\partial \mathcal{W}_v}{\partial \underline{\underline{\dot{e}}}}.$$

Finally, the total stress tensor aggregates the stresses in the active and passive branches

$$\underline{\underline{\Sigma}} = \underline{\underline{\Sigma}}_p + \underline{\underline{\Sigma}}_a = \frac{\partial \mathcal{W}_p}{\partial \underline{\underline{e}}} + \frac{\partial \mathcal{W}_v}{\partial \underline{\underline{\dot{e}}}} + \frac{T_c + \nu \dot{e}_c}{(1 + 2\underline{\underline{\tau}} \cdot \underline{\underline{e}} \cdot \underline{\underline{\tau}})^{\frac{1}{2}}} \underline{\underline{\tau}} \otimes \underline{\underline{\tau}}. \quad (2.2)$$

The principle of virtual work can then be written for any admissible displacement field \underline{w} on the reference configuration Ω_0 with boundary S_0 :

$$\int_{\Omega_0} \rho_0 \underline{\underline{y}} \cdot \underline{w} \, d\Omega + \int_{\Omega_0} \underline{\underline{\Sigma}} : \underline{d}_{\underline{\underline{y}} \underline{\underline{e}}} \cdot \underline{w} \, d\Omega_0 = \int_{S_0} \underline{t} \cdot \underline{w} \, dS, \quad (2.3)$$

where, ρ_0 is the mass density of the tissue in the reference configuration, \underline{y} is the displacement field, \underline{t} is a force field actin on the boundary S_0 of the domain Ω_0 and

$$\underline{d}_{\underline{\underline{y}} \underline{\underline{e}}} \cdot \underline{w} = \frac{1}{2} \left[\underline{\underline{\nabla}} \underline{w} + (\underline{\underline{\nabla}} \underline{w})^\top + (\underline{\underline{\nabla}} \underline{y})^\top \cdot \underline{\underline{\nabla}} \underline{w} + (\underline{\underline{\nabla}} \underline{w})^\top \cdot \underline{\underline{\nabla}} \underline{y} \right].$$

In cardiac simulation the external load results typically from the intraventricular blood pressure and contact forces at the pericardium. To reproduce a cardiac cycle, Eq. 2.3 have to be supplemented with an external circulation model and opening/closing valve laws that define the relationship between the internal pressure and the blood outflow.¹⁰

The coupling between the macroscopic behavior and the process of force generation by the molecular motors is contained in the active stress T_c appearing in Eq. 2.2, which will depend on local internal variable characterizing the state of the force production machinery. The usual hypothesis is to consider that the macroscopic stress T_c can be obtained by a simple rescaling of the force produced by a single molecular motor τ_c in a mean-field-like approach:

$$T_c = \rho_m \tau_c,$$

where ρ_m is the number of myosin molecular motors in a layer of thickness ℓ_{fib} per unit cross-sectional area.

We delay the presentation of the molecular motors models behind the active force τ_c to Chapter 3, but note here that the current framework directly connect the macroscale continuum mechanics balance laws with the nanoscale force generation dynamics. In this sense, the presented model, like most of the existing muscle tissue models is not multiscale, indeed. This aspect is further discussed in Chapter 4 and Chapter 5.

¹⁰ Caruel, Chabiniok, et al., "Dimensional Reductions of a Cardiac Model for Effective Validation and Calibration," 2014.

2.2 Contribution: model reduction for effective calibration and validation

To illustrate the model summarized in Section 2.1.3, we present the results obtained by Caruel, Chabiniok et al.¹¹. In this work we introduced two reduced models for the purpose of fast calibration and simulation.

The first model is a unidimensional representation of a muscle fiber aiming at reproducing uniaxial experiments. The formulation assumes a displacement field in the direction of the fiber. With this assumption, the principle of virtual work (Eq. 2.3) reduced to a one dimensional partial differential equation and eventually an ordinary differential equation (0D model) if a uniform deformation is assumed. This uniform formulation is usually used for simulating the experiment performed on fibers. We will present some results of this approach in Chapter 3.¹²

We here present another reduced model, that was formulated for fast simulation of the left ventricle cardiac cycle, using a spherical representation of that ventricle. Originally formulated by Caruel et al., this reduction was rewritten by Manganotti et al.¹³ to take into account the kinematics introduced by Kimmig, Chapelle and Moireau¹⁴, see Section 2.1.3.

The cardiac ventricle is represented by a thick sphere with radius R and thickness d , see Figure 2.3. In the reference configuration, $R = R_0$ and $d = d_0$. We denote by y the uniform radial displacement and V the volume of the cavity such that

$$R(y) = R_0 + y, \quad d(y) = d_0 \left(1 + \frac{y}{R_0}\right)^{-2} \quad \text{and}$$

$$V(y) = \frac{4}{3}\pi \left(R(y) - \frac{d(y)}{2}\right)^3,$$

The passive component of the stress (extracellular matrix) can be derived from the hyperelastic potential

$$\mathcal{W}_p(\underline{e}) = C_0 \exp [C_1 (J_1(\underline{e}) - 3)^2] + C_2 \exp [C_3 (J_4(\underline{e}) - 1)^2] \quad (2.4)$$

that depends on the reduced invariant of the Green-Lagrange strain tensor J_1 and J_4 ,¹⁵ on the viscous potential $\mathcal{W}_v(\underline{e}) = \eta \dot{\underline{e}} : \dot{\underline{e}}$ and on four material parameters: C_1 , C_2 , C_3 and C_4 .

Combined with the sphere kinematics, Eq. 2.3 and Eq. 2.1 become

$$\begin{cases} \rho_0 |\Omega_0| \ddot{y} + \frac{|\Omega_0|}{R_0} \kappa_s \left(\frac{y}{R_0} - e_c \right) + \frac{\partial \mathcal{W}_p}{\partial y}(y) + \Lambda_v(y, \dot{y}) = P_v \frac{\partial V}{\partial y}, \\ \kappa_s \left(\frac{y}{R_0} - e_c \right) - \nu \dot{e}_c = \tau_c, \end{cases}$$

¹¹ *ibid.*

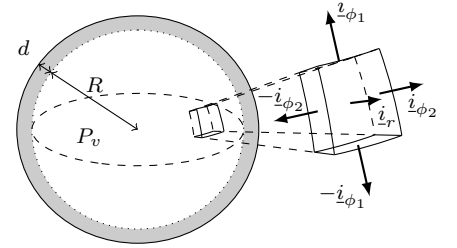


Figure 2.3: 0D model of a cardiac ventricle. Adapted from *ibid.*, reproduced with permission from SNCSC.

¹² For details about the formulation inhomogenous 1D model and some illustrations, we refer to *ibid.*

¹³ “Coupling Reduced-Order Blood Flow and Cardiac Models through Energy-Consistent Strategies,” 2021

¹⁴ “Thermodynamic Properties of Muscle Contraction Models and Associated Discrete-Time Principles,” 2019

¹⁵ Denoting by \underline{C} the righth Cauchy-Green deformation tensor we have $J_1 = I_1 I_3^{-\frac{1}{3}}$ and $J_4 = I_4 I_3^{-\frac{1}{3}}$ where $I_1 = \text{tr}(\underline{C})$ and $I_3 = \det(\underline{C})$, and $J_4 = \underline{\tau} \cdot \underline{C} \cdot \underline{\tau}$

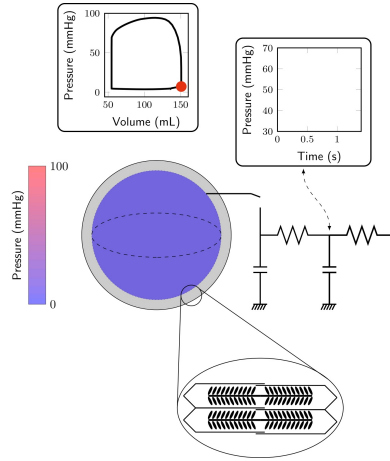


Figure 2.4: Simulation of the cardiac cycle using the 0D model. Video available only on HTML version of the document. Courtesy of François Kim-mig.

where $|\Omega_0|$ is the volume of the cavity in the reference configuration, P_v is the ventricular pressure and

$$\begin{aligned} \mathcal{W}_p(y) &= |\Omega_0| \left[C_0 e^{C_1 \left[2 \left(1 + \frac{y}{R_0} \right)^2 + \left(1 + \frac{y}{R_0} \right)^4 - 3 \right]^2} + C_2 e^{C_3 \left[\left(1 + \frac{y}{R_0} \right)^2 - 1 \right]^2} \right] \\ \Lambda(y, \dot{y}) &= 2\eta |\Omega_0| \left(1 + \frac{y}{R_0} \right)^2 \left[1 + 2 \left(1 + \frac{y}{R_0} \right)^{-12} \right] \dot{y}. \end{aligned}$$

To compute the ventricular pressure P_v , the 0D model is coupled to a Windkessel representation of the blood circulation, which closes the system of equations. In this framework, the circulation system is analog to an electric circuit containing diodes, representing the valves, resistances representing the head loss in arteries and capacitances representing the elasticity of the arteries.¹⁶ The application of the classical Kirchhoff laws leads the closure of the system of equation driving the dynamics of the cavity contractile cycle.

The parameters of the model are:

- the material parameters C_i , characterizing the hyperelastic potential (2.4),
- the activation of the force generation process, here represented by the active force τ_c (see Chapter 3 for more details),
- the atrial pressure, which is a given function of time if one considers only the left ventricle,
- the characteristics of the circulation model.

A cardiac cycle simulation performed using the 0D model is illustrated in Figure 2.4. The model was calibrated using experimental data obtained from mechanical test on heart papillary muscles mechanical tests.¹⁷ In

¹⁶ see Manganotti et al., “Coupling Reduced-Order Blood Flow and Cardiac Models through Energy-Consistent Strategies,” 2021, for an example of a two-stage Windkessel model.

¹⁷ Caruel, Chabiniok, et al., “Dimensional Reductions of a Cardiac Model for Effective Validation and Calibration,” 2014.

this model, the active stress τ_c is computed using a reduced model of the actin-myosin interaction that will be discussed in Chapter 3.

2.3 Remaining challenges and future work

Simulation platforms that produce physiologically relevant macroscale simulations of the heart contraction are now available.¹⁸ Such simulations in patient specific geometries are costly, but strategies have been developed to accelerate that process, using surrogate models based on asymptotic methods or AI assisted methods.¹⁹ Now these models can be used also for predicting the effect of drugs and mutations in the context of developed cardiomyopathies and large consortium are being set to develop clinical applications.

The most recent advances in cardiac research concerns the activation and regulation pathways. We will report in Chapter 5 that the cytoskeletal proteins linking the muscle contractile unit together in the tissue play a major role in these fundamental processes. These mechanisms thus operate at a scale lying between the tissue scale and the molecular motors scale. The problem is that the large majority of available heart models are formulated using similar hypotheses as the ones used in this chapter. Two hypotheses have to be reconsidered if one wants to incorporate a realistic description of the intrinsic contraction and regulation pathways into a heart simulation framework:

1. The contractile force in the macroscale mechanical formulation is obtained by a direct rescaling of the molecular motor force,
2. The muscle fibers are locally homogenous.

At the time this manuscript is being writted, there seems to be no mechanical model available that provides convincing representation of the intermediate scales, bridging the nanoscale and the macroscale. This issue is explained in more details in Chapter 5.

¹⁸ Chabiniok et al., “*Multiphysics and Multiscale Modelling, Data-Model Fusion and Integration of Organ Physiology in the Clinic*,” 2016; Filipovic et al., “*SIL-ICOFCM Platform, Multiscale Modeling of Left Ventricle from Echocardiographic Images and Drug Influence for Cardiomyopathy Disease*,” 2022; Regazzoni, Dedè, and Quarteroni, “*Biophysically detailed mathematical models of multiscale cardiac active mechanics*,” 2020; Sugiura, Okada, et al., “*UT-Heart*” 2022.

¹⁹ Kimmig, Moireau, and Chapelle, “*Hierarchical Modeling of Length-Dependent Force Generation in Cardiac Muscles and Associated Thermodynamically-Consistent Numerical Schemes*,” 2021; Milićević et al., “*Huxley Muscle Model Surrogates for High-Speed Multi-Scale Simulations of Cardiac Contraction*,” 2022; Regazzoni, Salvador, et al., “*A Machine Learning Method for Real-Time Numerical Simulations of Cardiac Electromechanics*,” 2022.

Chapter 3

Nanoscale: molecular motors

In Chapter 2, we presented a modeling framework of the cardiac tissue relying on the additive decomposition of the total stress into a passive and an active contribution. The active stress in the direction of the fiber was written

$$\underline{\underline{\Sigma}}_a = \frac{T_{\text{fib}}}{(1 + 2\underline{\underline{\tau}} \cdot \underline{\underline{e}} \cdot \underline{\underline{\tau}})^{\frac{1}{2}}} \underline{\underline{\tau}} \otimes \underline{\underline{\tau}}, \quad \text{with } T_{\text{fib}} = \rho_m \tau_c + \nu \dot{e}_c,$$

where ρ_m is the number of myosin molecular motors in a layer of thickness ℓ_{fib} per unit cross-sectional area, τ_c is the force produced by a single moto and \dot{e}_c is the deformation rate of the half-sarcomere. This chapter summarizes our contribution to the modeling of this force.

i Associated publications

The results summarized here are from Caruel, Moireau, and Chapelle, “*Stochastic Modeling of Chemical–Mechanical Coupling in Striated Muscles*,” 2019; Kimmig and Caruel, “*Hierarchical Modeling of Force Generation in Cardiac Muscle*,” 2020; Chaintron, Caruel, and Kimmig, “*Modeling Actin-Myosin Interaction: Beyond the Huxley–Hill Framework*,” 2023, and Chaintron et al., “*A Jump-Diffusion Stochastic Formalism for Muscle Contraction Models at Multiple Timescales*,” 2023.

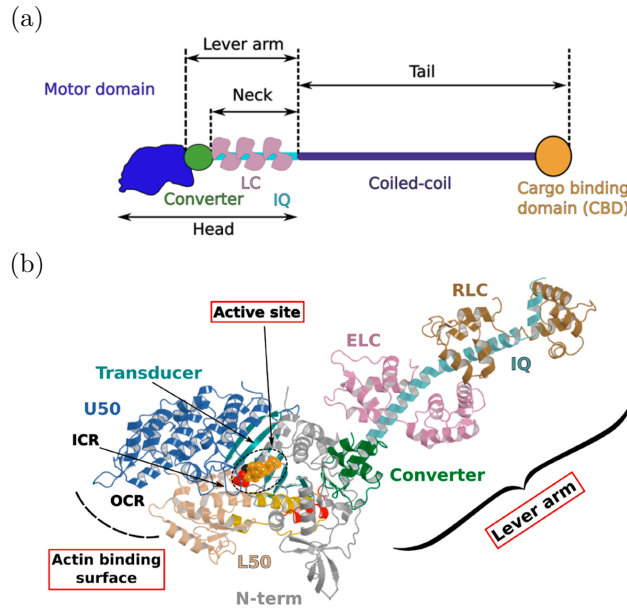
We recall that most of existing heart models use a direct rescaling of the average force generated by an infinitely large population of independent molecular motors, which is equivalent to rescaling the force produced by a single representative motor.

3.1 Background: the myosin molecular motor

3.1.1 Myosin structure

The myosin II protein responsible for muscle contraction consists of two heavy chains containing about 2000 amino-acids each. The two chains are coiled together by their *tail* regions while their *head* regions remain independent. A schematic representation one of the chains is shown in figure Figure 3.1 (a).

Figure 3.1: The myosin protein. (a) Schematic representation of a myosin protein (here a processive myosin isoform). It consists of two heavy chains coiled together by their tails. Each chain contains a motor (head) domain that interacts with actin and that contains the active site of ATP hydrolysis. The force is generated upon conformational changes of the motor domain that gets amplified by the lever arm structure. (b) Ribon representation of the motor domain of a scallop myosin II molecule. Structure PDB ID 1QVI from the protein databank. Adapted with permission from Robert-Paganin et al., “Force Generation by Myosin Motors,” 2020. ©2020 from the American Chemical Society.



¹ Dominguez et al., “Crystal Structure of a Vertebrate Smooth Muscle Myosin Motor Domain and Its Complex with the Essential Light Chain,” 1998; Rayment, Holden, et al., “Structure of the Actin-Myosin Complex and Its Implications for Muscle Contraction,” 1993; Robert-Paganin et al., “Force Generation by Myosin Motors,” 2020.

² Dominguez et al., “Crystal Structure of a Vertebrate Smooth Muscle Myosin Motor Domain and Its Complex with the Essential Light Chain,” 1998.

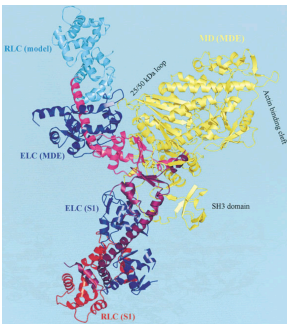


Figure 3.2: Structures of the pre- and post-power stroke conformations of myosin II. The superimposed motor domains are highlighted in yellow. The pre-power stroke conformation has the upward lever-arm (pink, blue, and cyan). The total displacement between the ends of the two lever arm configuration is about 12 nm. Reprinted from *ibid.*, ©1998, with permission from Elsevier.

The motor domain is the part of the protein that interacts directly with the actin filament during the contraction. It is connected to a coiled coil called the *lever arm*, whose crystallographic structure has been resolved in the 90s.¹ The motor domain itself is decomposed into several subdomains that surround the *active site*, where the ATP hydrolysis occurs, see Figure 3.1 (b). A structure of the motor domain of a myosin head (without the lever arm) bound to actin shown in Figure 3.1 (b).

An important aspect of the force generation mechanism is the ability of the myosin motor domain to undergo a conformational change that gets amplified by the lever arm. In the absence of impairing force (load free condition), the motion of the tip of the lever arm generates a relative displacement of about 10 nm of the myosin filament with respect to the actin filament. This conformational change, called the *power stroke* (or *working stroke*) has been characterized from the structural point of view by Dominguez et al.² A representation of the pre- and post-power stroke structures is shown in Figure 3.2.

3.1.2 Structural aspects of the myosin-actin interaction cycle

In our [Introduction](#), we presented a simplified version of the Lymn and Taylor cycle, see Figure 1.3. This cycle has been refined since then based on numerous studies that revealed the structures corresponding to various intermediate steps. As an example, the cycle proposed by Houdusse and Sweeney³ is shown in Figure 3.3.

While structural studies undeniably offer valuable insights into the molecular processes of force generation, they do not capture the dynamics of the transitions between the states. However, these structures can serve as initial conditions of Molecular Dynamics (MD) Simulations

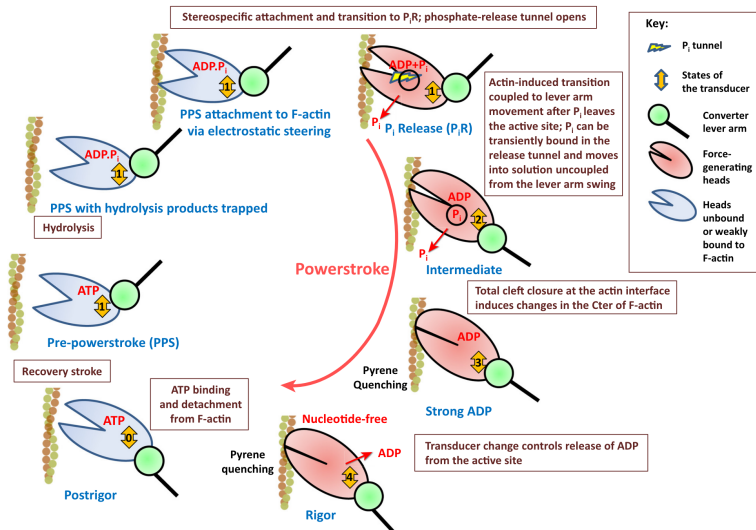


Figure 3.3: Representation of the actin-myosin interaction cycle emphasizing the state of the motor domain and the position of the lever arm. Reprinted from Houdusse and Sweeney, “*How Myosin Generates Force on Actin Filaments*,” 2016, ©2016, with permission from Elsevier.”

that can be performed to compute the free energy landscapes between the states as well as and short timescale dynamics.⁴ Different levels of description are available: all atoms or with different degrees of coarse-graining.⁵ These costly simulations, even the most coarse-grained ones, can cover timescales up to $\sim 1 \mu\text{s}$, which is ineffective to simulate the conformational changes involved in force production which last more than 1 ms.⁶ Moreover, current MD studies focus on single transitions of the actin-myosin interaction cycle (see Figure 3.3). Simulating the entire ATPase cycle for even a single motor therefore remains a significant challenge.

These simulations however provide valuable information on the effective mechanical properties of the proteins and help to determine the collective variables that can be used to characterize the different transitions within the cycle. Starting from an all atom dynamics in a space of very high dimension, the strategy is to project this dynamics on lower-dimension manifold parametrized by a set of collective variables to obtain a reduced model.

The highest degree of simplification is when the reduced dynamics becomes a jump process between discrete states, as depicted in Figure 3.3. This description thus views the actin-myosin interaction cycle as a sequence of chemical reactions whose rates determine the dynamics of the system. Most of the currently used molecular motors models are based on this idea, see Section 3.2 for examples.

3.1.3 Single molecule force spectroscopy experiments

Nanomanipulation techniques such as optical tweezers, Atomic Force Microscopy or Scanning probe microscopy, have been developed since the 1990s to study mechanotransduction phenomena of the living cells and in particular force generation by molecular motors.⁷ They have been particularly successful at determining the functioning of processive molecular motors, i.e. motors that operate individually⁸ or slow muscles

³ Houdusse and Sweeney, “*How Myosin Generates Force on Actin Filaments*,” 2016.

⁴ Baker and Voth, “*Effects of ATP and Actin-Filament Binding on the Dynamics of the Myosin II S1 Domain*,” 2013; Fischer et al., “*Structural Mechanism of the Recovery Stroke in the Myosin Molecular Motor*,” 2005.

⁵ Tozzini, “*Coarse-Grained Models for Proteins*,” 2005.

⁶ A. F. Huxley and Simmons, “*Proposed Mechanism of Force Generation in Striated Muscle*,” 1971.

⁷ Spudich et al., “*Optical Traps to Study Properties of Molecular Motors*,” 2011.

⁸ Kinesin, Myosin VI etc., see Block, Goldstein, and Schnapp, “*Bead Movement by Single Kinesin Molecules Studied with Optical Tweezers*,” 1990; Ménétrey et al., “*The Structure of the Myosin VI Motor Reveals the Mechanism of Directionality Reversal*,” 2005; Rock et al., “*Myosin VI Is a Processive Motor with a Large Step Size*,” 2001; Svoboda et al., “*Direct Observation of Kinesin Stepping by Optical Trapping Interferometry*,” 1993.

⁹ Veigel et al., “Load-Dependent Kinetics of Force Production by Smooth Muscle Myosin Measured with Optical Tweezers,” 2003.

¹⁰ Finer, Simmons, and Spudich, “Single Myosin Molecule Mechanics,” 1994; Molloy et al., “Single-Molecule Mechanics of Heavy Meromyosin and Si Interacting with Rabbit or Drosophila Actins Using Optical Tweezers,” 1995; Veigel et al., “Load-Dependent Kinetics of Force Production by Smooth Muscle Myosin Measured with Optical Tweezers,” 2003.

¹¹ Capitanio et al., “Ultrafast Force-Clamp Spectroscopy of Single Molecules Reveals Load Dependence of Myosin Working Stroke,” 2012.

¹² Woody, Winkelmann, et al., “Single Molecule Mechanics Resolves the Earliest Events in Force Generation by Cardiac Myosin,” 2019.

¹³ Veigel et al., “Load-Dependent Kinetics of Force Production by Smooth Muscle Myosin Measured with Optical Tweezers,” 2003.

¹⁴ Woody, Greenberg, et al., “Positive Cardiac Inotrope Omecamtiv Mecarbil Activates Muscle despite Suppressing the Myosin Working Stroke,” 2018.

¹⁵ Malik et al., “Cardiac Myosin Activation,” 2011.

myosins.⁹ Unlike muscle Myosin II, processive molecular motors stay permanently in contact with their track thanks to their pair of heads actin like coordinated legs. Non processive motors like muscle Myosin II spend only a small fraction of their cycle attached to their track. Studying these short-lived attached configuration requires sub-millisecond resolution of the loading device, which is a technical limitation of single molecule techniques.¹⁰

The development of ultrafast force clamp single molecule spectroscopy over the past decade,¹¹ allows detecting events occurring at timescales comparable to that of the power stroke,¹² which partially remove the previous limitations. Before that however, we can mention the work of Veigel et al. on the slower smooth muscle myosin who showed that the myosin detachment rate is load-dependent: it is larger when the molecule is in compression than when in tension.¹³

A contemporary promising application of single-molecule biophysical experiments is the in-vitro testing of mutated proteins and specific modulators used as treatments of muscular diseases. A recent example is provided by Woody et al.¹⁴ where a dual-laser optical trapping setup was used to study the effect of Omecamtiv Mecarbil, a small positive cardiac inotropic agent that increases cardiac performance in acute heart failure situations.¹⁵

Since our work is focused on the modeling of non-processive motors, the systematic comparison of the model predictions with single molecule experimental results was not pursued, though it is not excluded for future model calibration procedures.

3.2 Existing models

3.2.1 Chemical-mechanical models

i Associated publications

The following is a presentation of the most widely used class of actin-myosin interaction models. While the original formulation dates back to the 1950s and 1970s, more recent presentations with additional mathematical and numerical developments can be found in Kimmig, Chapelle, and Moireau, “*Thermodynamic Properties of Muscle Contraction Models and Associated Discrete-Time Principles*,” 2019; and Chaintron, Caruel, and Kimmig, “*Modeling Actin-Myosin Interaction: Beyond the Huxley–Hill Framework*,” 2023. The following paragraphs are adapted from these references.

The typical representation of the actin-myosin dynamics is a discrete jump process between states endowed with mechanical degrees of freedom. The first model of this kind was proposed by A.F. Huxley in 1957.¹⁶ It has later been formalized and generalized by T.L. Hill and co-workers

¹⁶ “Muscle Structure and Theories of Contraction,” 1957.

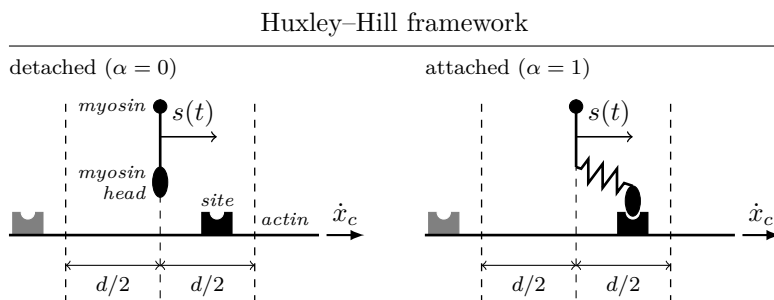


Figure 3.4: The original two-state Huxley model (*“Muscle Structure and Theories of Contraction,”* 1957) is parametrized by the distance $s(t)$ separating the myosin anchor from its nearest binding site. The distance between two consecutive sites is denoted by d . After attachment, the formed cross-bridge is represented as a spring of length $s(t)$. Adapted from Chaintron, Caruel, and Kimmig, *“Modeling Actin-Myosin Interaction: Beyond the Huxley–Hill Framework,”* 2023, CC BY 4.0.

in 1974.¹⁷ Its formulation is illustrated in Figure 3.4.¹⁸ The model is parametrized by the distance $s(t)$ separating the myosin anchor from its nearest binding site. The distance between two consecutive sites is denoted by d . A fundamental hypothesis is that a given head can interact only with the nearest binding site. A myosin head exists in two states: detached or attached to actin, with attachment and detachment events being modeled as a “chemical” jump process with rates that depend on the distance to the nearest binding site s . The Huxley’ 57 model sets the foundation for all subsequent models that use this so-called *chemical-mechanical* approach.

The collective variable that lumps the high dimensional space of protein configurations is here the discrete variable $\alpha_t \in \{0, 1\}$. This variable characterizes the attachment state of the myosin head, taking the value $\alpha_t = 1$ if the head is attached, and the value $\alpha_t = 0$ if the head is detached. After attachment, the formed cross-bridge is represented as a spring of elongation $s(t)$, see Figure 3.4.

The model assumes a large population of *independent* myosin proteins having their closest attachment sites distributed uniformly in the interval $(-d/2, +d/2)$. Non symmetric interval of type (s_-, s_+) with $s_+ - s_- = d$ can also be considered. The function $(t, s) \mapsto P_1(t, s)$, represents the fraction of this population that is attached at time t . Similarly, the function $(t, s) \mapsto P_0(t, s) := 1 - P_1(t, s)$ represents the fraction of this population that is detached at time t .

The stochastic jumps dynamics associated with α_t involves four transition rates (see Figure 3.5 (a)):

- $k_{0 \rightarrow 1}(s)$ associated with the jump $0 \rightarrow 1$ (direct attachment);
- $k_{0 \rightarrow 1}^{\text{rev}}(s)$ associated with the jump $1 \rightarrow 0$ (reverse attachment);
- $k_{1 \rightarrow 0}(s)$ associated with the jump $1 \rightarrow 0$ (direct detachment);
- $k_{1 \rightarrow 0}^{\text{rev}}(s)$ associated with the jump $0 \rightarrow 1$ (reverse detachment).

¹⁷ “Theoretical Formalism for the Sliding Filament Model of Contraction of Striated Muscle Part I,” 1974.

¹⁸ Chaintron, Caruel and Kimmig (*“Modeling Actin-Myosin Interaction: Beyond the Huxley–Hill Framework,”* 2023) discuss the well-posedness conditions of the Huxley-Hill model and suggest an alternative formulation based on the use of Poisson random measures. We determine conditions that ensure the model’s compatibility with the thermodynamic principles.

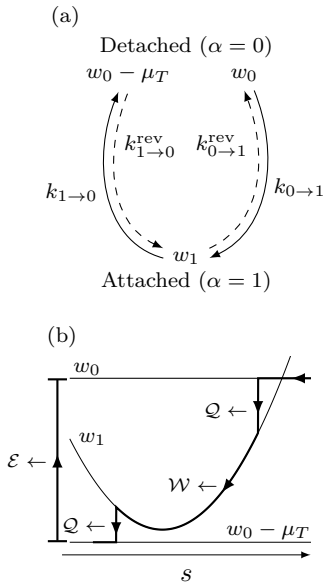


Figure 3.5: Stochastic jump process dynamics and energetics. (a) illustration of the transition rates between the attached and the detached states. (b) illustration of the first principle. Adapted from Chaintron, Caruel, and Kimmig, “*Modeling Actin-Myosin Interaction: Beyond the Huxley-Hill Framework*,” 2023, CC BY 4.0.

¹⁹ This formulation corresponds to the one formulated by Huxley (“*Muscle Structure and Theories of Contraction*,” 1957).

²⁰ Hill, “*Theoretical Formalism for the Sliding Filament Model of Contraction of Striated Muscle Part I*,” 1974, “*Theoretical Formalism for the Sliding Filament Model of Contraction of Striated Muscle Part II*,” 1976

²¹ Chaintron, Caruel, and Kimmig, “*Modeling Actin-Myosin Interaction: Beyond the Huxley-Hill Framework*,” 2023; Jülicher and Prost, “*Cooperative Molecular Motors*,” 1995.

These rates can be aggregated by defining $f(s) = k_{0 \rightarrow 1}(s) + k_{1 \rightarrow 0}^{\text{rev}}(s)$ and $g(s) = k_{1 \rightarrow 0}(s) + k_{0 \rightarrow 1}^{\text{rev}}(s)$. The fraction of attached myosin heads then verifies the following PDE,¹⁹ for $t > 0$, $s \in (-\frac{d}{2}, +\frac{d}{2})$

$$\begin{cases} \partial_t P_1 + \dot{x}_c(t) \partial_s P_1 = -g(s) P_1 + f(s) [1 - P_1], \\ P_1(t, \pm d/2) = 0, t \geq 0, \\ P_1(0, s) = P_1^{\text{ini}}(s), s \in [-\frac{d}{2}, +\frac{d}{2}], \end{cases} \quad (3.1)$$

where \dot{x}_c is the relative sliding velocity between the two filaments, see Figure 3.4.

The tension generated by the attached motors at a given sliding velocity \dot{x}_c is then defined as

$$\tau_c(t) := \frac{1}{d} \int_{-d/2}^{+d/2} \partial_s w_1(s) P_1(t, s) ds,$$

where w_1 is the energy of the protein in the attached state. If the attached protein is viewed as an elastic spring, then $w_1(s) = (\kappa/2)(s - s_0)^2$, where κ is the stiffness and s_0 the reference length, see Figure 3.5 (b). This tension is finally rescaled to obtain the macroscopic active stress T_c that appears the macroscopic behavior law, see Section 2.1.3 and Eq. 2.2 in particular.

Overall, the thermodynamic properties of the models are defined by the energy landscapes w_α and by the transition rates. There is no a priori guarantee that for an arbitrary choice of these parameters, the system would be compatible with the principle of thermodynamics. These energetic aspects of the chemical mechanical models have been clarified in the work of Hill.²⁰ In particular, it was shown that the system satisfies the second principle of thermodynamics if for each transition between two states A and B of the cycle, the associated transition rates $K_{A \rightarrow B}$ and $K_{B \rightarrow A}$ verify the detailed balance condition

$$\frac{K_{A \rightarrow B}}{K_{B \rightarrow A}} = \exp \left[-\frac{w_B - w_A}{k_B T} \right],$$

where w_A and w_B are the energies of states A and B , respectively.

In the case of the two state model illustrated in Figure 3.5 (a), this property reads

$$\begin{aligned} \frac{K_{0 \rightarrow 1}(s)}{K_{0 \rightarrow 1}^{\text{rev}}(s)} &= \exp \left[-\frac{w_1(s) - w_0(s)}{k_B T} \right], \\ \frac{K_{1 \rightarrow 0}(s)}{K_{1 \rightarrow 0}^{\text{rev}}(s)} &= \exp \left[-\frac{(w_0(s) - \mu_T) - w_1(s)}{k_B T} \right] \end{aligned} \quad (3.2)$$

Notice that, in the second equation, the energy of the detached state is $w_0 - \mu_T$ and not w_0 . The difference is the free energy μ_T harvested from the hydrolysis of ATP. In isometric condition ($\dot{x}_c = 0$), if $\mu_T = 0$, then it can be shown that there is no net flux in the cycle and no force is produced.²¹

A typical cycle is shown by the thick line in Figure 3.5 (b), where we illustrate for each sequence of that cycle, the associated first principle quantity: work (W), heat (Q) and energy input (\mathcal{E}). Having $\mu_t > 0$ ensures that, on average the overall free energy decays at each cycle, which maintain non-equilibrium.²²

The class of chemical-mechanical models was intensely studied in the late 90's and up to the late 2010's, in particular in relation with the development of biomimetic in vitro experiments.²³ These works shed light on a variety of dynamical behaviors akin to spontaneous oscillations, emerging particularly when a cluster of motors is coupled to a common elastic substrate.²⁴ Today, the vast majority of existing models pertains to this category and differ from the original Huxley-Hill two state formulation essentially by the number of chemical states involved and by the nature of the spring (linear or nonlinear).²⁵

In summary, the chemical-mechanical models project the high dimensional molecular dynamics on a discrete space of states. The originality of the approach vis a vis a purely chemical system is the association of each state with a mechanical degree of freedom (here denoted as $s(t)$). The resulting energy landscape is thereby coupled to the relative position of the two filaments.

3.2.2 Stochastic ratchet models

An alternative to the Huxley-Hill-type models is to consider a less drastic dimensional reduction of the molecular motors' molecular dynamics, by keeping a description of the "internal motion" of the proteins. Using such approach, the state of the motor is parametrized by a vector of continuous stochastic (collective) variables X_t evolving in a low dimensional space. The dynamics of X_t follows the gradient of an energy landscape which represent the projection of the all-atom potential on the lower dimension space of collective variables.

A prototype model this kind was proposed by Magnasco.²⁶ The molecular motor is a particle $X_t \in \mathbb{R}$ evolving on a unidimensional periodic energy landscape according to Langevin stochastic differential equation

$$dX_t = -[\phi'(X_t) + f(t) + q]dt + \sqrt{2D}dB_t. \quad (3.3)$$

In Eq. 3.3, ϕ is a non-symmetric periodic potential mimicking the interaction with the actin track, q is the external load, D is the diffusion coefficient and dB_t is a brownian motion increment. The term $f(t)$ represent a so-called *colored* component of the noise, as opposed to the pure *white* noise represented by the term dB_t . In the case of Magnasco's model, it is represented by a deterministic piecewise constant force of the form $f(t) = A(-1)^{n(t)}$ with $n(t) = \lfloor 2t/\tau \rfloor$. The average of this force over a period τ is equal to 0, implying that f has no net effect, but combined with the uncorrelated brownian motion and the non-symmetric periodic

²² This point is discussed in a general context by Jülicher, Ajdari and Prost ("Modeling Molecular Motors," 1997), see also Jülicher and Prost, "Cooperative Molecular Motors," 1995; H. Wang and Oster, "Ratchets, Power Strokes, and Molecular Motors," 2002.

²³ Holzbaur and Goldman, "Coordination of Molecular Motors," 2010; Pollard, "Evolution of Research on Cellular Motility over Five Decades," 2018.

²⁴ We refer to T. A. J. Duke, "Molecular Model of Muscle Contraction," 1999; Guérin, Prost, Martin, et al., "Coordination and Collective Properties of Molecular Motors," 2010; Jülicher and Prost, "Cooperative Molecular Motors," 1995; Jülicher, Ajdari, and Prost, "Modeling Molecular Motors," 1997; Plaçais et al., "Spontaneous Oscillations of a Minimal Actomyosin System under Elastic Loading," 2009 and Guérin, Prost, and Joanny, "Dynamical Behavior of Molecular Motor Assemblies in the Rigid and Crossbridge Models," 2011 for further details.

²⁵ Caremani, Melli, et al., "Force and Number of Myosin Motors during Muscle Shortening and the Coupling with the Release of the ATP Hydrolysis Products," 2015; T. A. J. Duke, "Molecular Model of Muscle Contraction," 1999; A. F. Huxley and Simmons, "Proposed Mechanism of Force Generation in Striated Muscle," 1971; Månsson, "Actomyosin-ADP States, Interhead Cooperativity, and the Force-Velocity Relation of Skeletal Muscle," 2010, "Actomyosin Based Contraction," 2016, "Hypothesis: Single Actomyosin Properties Account for Ensemble Behavior in Active Muscle Shortening and Isometric Contraction," 2020; Pertici, Bongini, et al., "A Myosin II Nanomachine Mimicking the Striated Muscle," 2018; Piazzesi and Lombardi, "A Cross-Bridge Model That Is Able to Explain Mechanical and Energetic Properties of Shortening Muscle," 1995; D. A. Smith and Mijailovich, "Toward a Unified Theory of Muscle Contraction. II," 2008; D. Smith and M. Geeves, "Strain-Dependent Cross-Bridge Cycle for Muscle," 1995a, "Strain-Dependent Cross-Bridge Cycle for Muscle. II. Steady-state Behavior," 1995b; D. Smith, M. Geeves, et al., "Towards a Unified Theory of Muscle Contraction. I," 2008.

²⁶ "Forced Thermal Ratchets," 1993.

landscape, it can effectively generate a directional motion in the direction opposite to an applied external force. This description is a way to represent the chemical energy input from the ATP hydrolysis as a purely mechanical element.

3.3 Challenges

At the scale of the molecular motor several challenges can be stated.

1. Not all the crystallographic structures associated with the different steps of the Lymn–Taylor cycle are resolved, and MD simulations only provides very short time dynamics, so one cannot use this technique to simulate the entire interaction cycle. The challenge here is to formulate new methodologies allowing to use the data generated by these simulations to formulate simplified models of the actin-myosin interaction, like for instance the chemical-mechanical models.
2. A salient feature of the existing chemical-mechanical models is the use of functions to parametrize the transition rates between the states, see f and g in Eq. 3.1. These rates are difficult to calibrate in an unequivocal way as they represent a virtually infinite set of parameters. Currently, the data available to constrain their calibration come mostly from experiments dealing with many motors in interaction, different animal species and heterogenous experimental conditions. Other data can be extracted from single molecule experiments. One could also leverage the results of the molecular dynamics simulations on single proteins to complement experiments involving many motors.
3. The calibration is greatly facilitated by the mean-field assumption mentioned in Section 2.1.3, since it implies a rather direct coupling between the experimental observables and the single motor characteristics. This fundamental assumption can be questioned.

3.4 Contributions

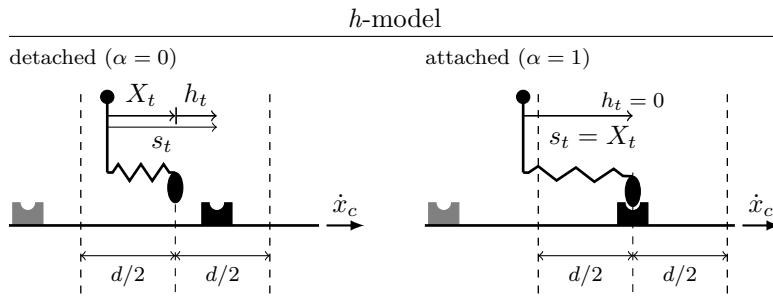
3.4.1 The Huxley-Hill formulation revisited

i Associated reference

This section is an abstract of the model and results presented in Chaintron, Caruel, and Kimmig, “*Modeling Actin-Myosin Interaction: Beyond the Huxley–Hill Framework*,” 2023.

²⁷ *ibid.*

Recently, Chaintron, Caruel and Kimmig published a slightly modified formulation of the Huxley-Hill model,²⁷ see Figure 3.6. In this new formu-



lation, called the *h*-model, the state of the myosin motor is characterized by three stochastic variables:

- X_t , the position of the head with respect to the myosin's anchor on the thick filament,
- h_t , the position of the nearest actin site with respect to X_t .
- α_t , the attachment state ($\alpha_t = 0$ is the motor is detached and $\alpha_t = 1$ if it is attached),

The main difference with the original formulation is that the position of the nearest binding h_t site is not anymore defined with respect to the anchor on the thick filament, see Figure 3.4. The two models are linked formally by the relation $s_t = X_t + h_t$.²⁸ Upon attachment, the variable h_t jumps to 0 so that $X_t = s_t$ after attachment.

The consequence of this seemingly innocent change is that the myosin head can now attach to any site on the real axis without having to resolve to an explicitly multi-site formulation.²⁹ Using a multi-site model comes at the price of having to define four rates per additional site. While we still enforce the myosin head to interact with only one site at a time, it can now be any site with only four rates to calibrate.

Chaintron Caruel and Kimmig³⁰ formulate this new approach using the concept of Poisson random measures,³¹ and establish the conditions of its well posedness. We adapt the detailed balance condition (3.2) and show the ensuing model's compatibility with the second principle. We then propose a reduction strategy that allows to adiabatically eliminate the variable h_t . The resulting reduced model has only two degrees of freedom, namely s and α , like the Huxley-Hill model. The associated PDE formulation is analog to Eq. 3.1 with a correction term. This shows that by extrapolation, more complex chemical-mechanical models (i.e. with more states) could be reformulated using this new framework. The paper also provide numerical illustrations of the *h*-model and of its reduced version.

Figure 3.6: New formulation of the Huxley-Hill model proposed by Chaintron, Caruel and Kimmig. In this new formulation, called the *h*-model, the dynamics of the position of the detached head X_t relative to the same anchor point is described. The position of the nearest binding site, denoted by h_t is now defined with respect to this position X_t and not anymore with respect to the anchor of the myosin head in the thick filament, see Figure 3.4 for comparison. Adapted from Chaintron, Caruel, and Kimmig, “*Modeling Actin-Myosin Interaction: Beyond the Huxley-Hill Framework*,” 2023, CC BY 4.0.

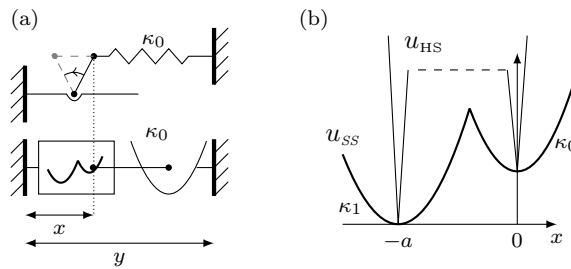
²⁸ Note that here $s(t)$ is the distance between the anchor on the myosin filament and the site closest to X_t , which is different from the Huxley-Hill model.

²⁹ multisite models in the classical framework can be found in Kimmig, Chapelle, and Moireau, “*Thermodynamic Properties of Muscle Contraction Models and Associated Discrete-Time Principles*,” 2019 and Månsson, “*Comparing Models with One versus Multiple Myosin-Binding Sites per Actin Target Zone: The Power of Simplicity*,” 2019.

³⁰ “*Modeling Actin-Myosin Interaction: Beyond the Huxley-Hill Framework*,” 2023

³¹ The interested reader can find a short pedagogical introduction to the concept of Poisson Random measured in section 2.2 of *ibid*.

Figure 3.7: Continuous model of the working stroke. (a) Schematic representation of the cross-bridge model consisting of two degrees of freedom, the total elongation y and the variable x representing the conformation. (b) Conformational energy for chemical-mechanical framework introduced in A. F. Huxley and Simmons, “*Proposed Mechanism of Force Generation in Striated Muscle*,” 1971 (thin) or in the regularized continuous framework proposed in Marcucci and Truskinovsky, “*Mechanics of the Power Stroke in Myosin II*,” 2010 (thick).



3.4.2 Continuous model of the working stroke

i Associated publications

This work was initiated by Marcucci and Truskinovsky (“*Mechanics of the Power Stroke in Myosin II*,” 2010) and continued during M. Caruel’s PhD. Details about the model can be found in the following references: Caruel, Allain, and Truskinovsky, “*Muscle as a Metamaterial Operating Near a Critical Point*,” 2013 and Caruel and Truskinovsky, “*Physics of Muscle Contraction*,” 2018. Note also that the latter reference is already a review of several papers by Caruel and Truskinovsky.

³² Caruel and Truskinovsky, “*Physics of Muscle Contraction*,” 2018; A. F. Huxley and Simmons, “*Proposed Mechanism of Force Generation in Striated Muscle*,” 1971; Marcucci and Truskinovsky, “*Mechanics of the Power Stroke in Myosin II*,” 2010.

³³ Caremani, Melli, et al., “*Force and Number of Myosin Motors during Muscle Shortening and the Coupling with the Release of the ATP Hydrolysis Products*,” 2015; A. F. Huxley and Simmons, “*Proposed Mechanism of Force Generation in Striated Muscle*,” 1971; Månsson, “*Actomyosin Based Contraction*,” 2016; D. Smith, M. Geeves, et al., “*Towards a Unified Theory of Muscle Contraction. I*,” 2008.

³⁴ Dominguez et al., “*Crystal Structure of a Vertebrate Smooth Muscle Myosin Motor Domain and Its Complex with the Essential Light Chain*,” 1998.

³⁵ E. Eisenberg and Hill, “*A Cross-Bridge Model of Muscle Contraction*,” 1979.

³⁶ A. F. Huxley and Simmons, “*Proposed Mechanism of Force Generation in Striated Muscle*,” 1971.

The working stroke is the force-generating step of the actin-myosin interaction cycle, see Figure 1.3. It corresponds to a conformational change of the protein executed while it is attached to the actin filament. This transition can be interpreted as the swift relaxation towards thermal equilibrium of the internal degrees of freedom characterizing the conformation of the myosin protein, with an associated timescale of a few milliseconds. This timescale is short compared to the time to complete the Lymnn-Taylor cycle (about 30 ms), which suggests that the power stroke is a purely mechanical phenomenon.³²

In the classical framework of chemical-mechanical models presented in Section 3.2.1, the power stroke is viewed as a sequence of three or more chemical transitions.³³ While the molecular structures of the pre- and post-power-stroke conformations have been clearly identified,³⁴ additional states are not yet associated with stable structure.

Furthermore, since the motion of the lever arm is by essence constrained by the relative motion of the myosin and actin filaments, which is not a discrete process, it seems natural to view the power-stroke as a continuous process, an idea that was originally coined by Eisenberg and Hill.³⁵ Finally, from a mathematical point of view, studying the low temperature limit of a continuous power-stroke model could help to justify the discrete approach.

Based on the experimental observation, first made by Huxley and Simmons³⁶, that the power stroke operates at fast timescales, Marcucci and Truskinovsky developed a model of the working stroke, where the conformational change is represented as a one-dimensional Langevin process

in a double-well potential instead of a jump process, see Figure 3.7. This model can be considered as a regularized version of the original chemo-mechanical representation of the working stroke proposed by Huxley and Simmons.

The model was introduced to model the collective response of groups of connected molecular motors to rapid load changes. This topic will be discussed in details in Chapter 4. We now present how this continuous model of the power stroke can be coupled to a more classical “chemical” representation of the attachment-detachment process, to result in a hybrid jump-diffusion model actin-myosin interaction model.

3.4.3 Jump-diffusion model of the Lymn–Taylor cycle

i Associated publications

The formulation of the model and its first validation are from Caruel, Moireau, and Chapelle, “*Stochastic Modeling of Chemical–Mechanical Coupling in Striated Muscles*,” 2019. The model was further refined and calibrated to reproduce cardiac muscle data during the PhD of F. Kimmig in Kimmig and Caruel, “*Hierarchical Modeling of Force Generation in Cardiac Muscle*,” 2020. Recently the formulation of the model was significantly improved, with the contribution of L. P. Chaintron, to strengthen its mathematical well-posedness and assess its compatibility with the thermodynamic principles in Chaintron et al., “*A Jump-Diffusion Stochastic Formalism for Muscle Contraction Models at Multiple Timescales*,” 2023.

To extend the Marcucci and Truskinovsky model³⁷ of the power stroke, and describe the whole Lymn–Taylor cycle, Caruel, Moireau and Chapelle proposed a jump-diffusion hybrid model,³⁸ illustrated in 3.8 (a). The state of the myosin motor is parametrized by the following stochastic variables

- X_t , the position of the myosin head with respect to its fixed location on the myosin filament,
- Y_t , the conformation of the head (power stroke),
- α_t , the state of attachment (equal to 0 when the motor is detached and equal to 1 when the motor is attached).

As in the classical Huxley-Hill model, the myosin head can attach only to the nearest actin site, located at a distance s from the myosin anchor in the thick filament. When an attachment event ($\alpha = 0 \rightarrow \alpha = 1$) occurs, the head position jumps to the value $X_t = s(t)$.

The stochastic jump dynamics is formulated by Chaintron et al. using the concept of Poisson random measures, which allows to write the stochastic differential equation describing the dynamics of the discrete variable α_t .³⁹ The jump process involves four transition rates

³⁷ “*Mechanics of the Power Stroke in Myosin II*,” 2010.

³⁸ “*Stochastic Modeling of Chemical–Mechanical Coupling in Striated Muscles*,” 2019.

³⁹ “*A Jump-Diffusion Stochastic Formalism for Muscle Contraction Models at Multiple Timescales*,” 2023

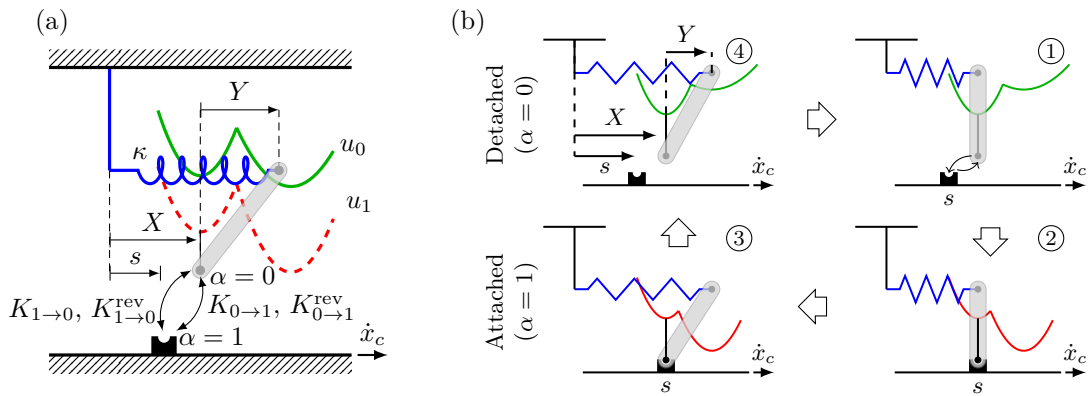


Figure 3.8: Jump-diffusion model proposed by Chaintron et al. (*"A Jump-Diffusion Stochastic Formalism for Muscle Contraction Models at Multiple Timescales,"* 2023). (a) The state of the myosin head is characterized by three stochastic variables: X_t , Y_t and α_t , which represent the position of the head, its conformation and the state of attachment, respectively. The position of the nearest binding site is denoted by s . The attachment-detachment process is characterized by four jumps whose rates are denoted $k_{0 \rightarrow 1}$, $k_{0 \rightarrow 1}^{\text{rev}}$, $k_{1 \rightarrow 0}$ and $k_{1 \rightarrow 0}^{\text{rev}}$. The energy landscape has two main ingredients: a quadratic term representing the elasticity of the head (stiffness κ) and a double-well potential u_α associated with the conformational change. The latter potential depends on the attachment state. (b) illustration fo the Lymn-Taylor cycle with 1 \rightarrow 2: attachment; 2 \rightarrow 3: power stroke; 3 \rightarrow 4: detachment, and 4 \rightarrow 1 recovery stroke. (a) is adapted from Chaintron et al., *"A Jump-Diffusion Stochastic Formalism for Muscle Contraction Models at Multiple Timescales,"* 2023 with the permission of AIP Publishing, ©2023

- $K_{0 \rightarrow 1}(x, y, s)$ associated with the jump $0 \rightarrow 1$ (direct attachment);
- $K_{0 \rightarrow 1}^{\text{rev}}(x, y, s)$ associated with the jump $1 \rightarrow 0$ (reverse attachment);
- $K_{1 \rightarrow 0}(x, y, s)$ associated with the jump $1 \rightarrow 0$ (direct detachment);
- $K_{1 \rightarrow 0}^{\text{rev}}(x, y, s)$ associated with the jump $0 \rightarrow 1$ (reverse detachment).

The conformation variable Y_t and the detached head position X_t both follow Langevin dynamics. As in the classical Huxley-Hill formulation, the internal energy of the myosin motor depends on the attachment state. A typical actin-myosin interaction cycle is illustrated in 3.8 (b). Within this theoretical formalism, the complete jump-diffusion stochastic differential system can be written as

$$\left\{ \begin{array}{l} d\alpha_t = \mathbb{1}_{\alpha_{t^-}=0} \left[\int_{\mathbb{R}_+} \mathbb{1}_{z \leq K_{0 \rightarrow 1}(X_{t^-}, Y_t, s(t))} N_{0 \rightarrow 1}(dt, dz) + \int_{\mathbb{R}_+} \mathbb{1}_{z \leq K_{1 \rightarrow 0}^{\text{rev}}(X_{t^-}, Y_t, s(t))} N_{1 \rightarrow 0}^{\text{rev}}(dt, dz) \right] \\ \quad - \mathbb{1}_{\alpha_{t^-}=1} \left[\int_{-d/2}^{+d/2} \int_{\mathbb{R}_+} \mathbb{1}_{z \leq K_{1 \rightarrow 0}(x, Y_t, s(t))} N_{1 \rightarrow 0}(dt, dx, dz) \right. \\ \quad \quad \left. + \int_{-d/2}^{+d/2} \int_{\mathbb{R}_+} \mathbb{1}_{z \leq K_{0 \rightarrow 1}^{\text{rev}}(x, Y_t, s(t))} N_{1 \rightarrow 0}^{\text{rev}}(dt, dx, dz) \right], \\ dX_t = \mathbb{1}_{\alpha_{t^-}=0} \left[-\eta_x^{-1} \partial_x w_0(X_t, Y_t) dt + \sqrt{2\eta_x^{-1} k_B T} dB_t^x \right] + \mathbb{1}_{\alpha_{t^-}=1} \dot{x}_c(t) dt \\ \quad + \mathbb{1}_{\alpha_{t^-}=0} \left[\int_{\mathbb{R}_+} (s(t) - X_{t^-}) \mathbb{1}_{z \leq K_{0 \rightarrow 1}(X_{t^-}, Y_t, s(t))} N_{0 \rightarrow 1}(dt, dz) \right. \\ \quad \quad \left. + \int_{\mathbb{R}_+} (s(t) - X_{t^-}) \mathbb{1}_{z \leq K_{1 \rightarrow 0}^{\text{rev}}(X_{t^-}, Y_t, s(t))} N_{1 \rightarrow 0}^{\text{rev}}(dt, dz) \right] \\ \quad + \mathbb{1}_{\alpha_{t^-}=1} \left[\int_{-d/2}^{+d/2} \int_{\mathbb{R}_+} (x - s(t)) \mathbb{1}_{z \leq K_{1 \rightarrow 0}(x, Y_t, s(t))} N_{1 \rightarrow 0}(dt, dx, dz) \right. \\ \quad \quad \left. + \int_{-d/2}^{+d/2} \int_{\mathbb{R}_+} (x - X_{t^-}) \mathbb{1}_{z \leq K_{0 \rightarrow 1}^{\text{rev}}(x, Y_t, s(t))} N_{0 \rightarrow 1}^{\text{rev}}(dt, dx, dz) \right], \\ dY_t = -\eta_y^{-1} \partial_y w_{\alpha_t}(X_t, Y_t) dt + \sqrt{2\eta_y^{-1} k_B T} dB_t^y, \end{array} \right.$$

where $\eta_{x,y}$ are drag coefficients, and $(B_t^x)_{t \geq 0}$ and $(B_t^y)_{t \geq 0}$ are independent Brownian motions.⁴⁰ Notice that, in the second equation, the motion of X_t is deterministic when the head is attached, like in the two state model presented in Section 3.2.1.

The peculiarity of this model lays in the asymmetry between the attachment and the detachment jumps, which results from the different system's dimensionality in the attached and detached states. When the motor is detached, it evolves in a two dimensional space (X_t, Y_t) , while when it is attached, $X_t = s(t)$ so the dynamics becomes one dimensional. Hence, when an attachment jump occurs from a random configuration (X_t, Y_t) , the dynamics is projected on a one dimensional space,

⁴⁰ The meaning of the integrals of the form $\int_0^t \int_{\mathbb{R}_+} F(t, z) N(dt, dz)$ is explained in more details with extra references and numerical implementation in Section 2.2 and 4.1 of Chaintron et al., "A Jump-Diffusion Stochastic Formalism for Muscle Contraction Models at Multiple Timescales," 2023.

parametrized by $s(t)$. Hence, the value of X_t after the jump is fully determined by the position of the site.

The situation is different with the detachment, since there is no a priori value prescribed for X_t after the jump. This discrete-to-continuous detachment jump must then select a random location x for the detached myosin head. The probability law that chooses this new location has to be defined carefully to preserve the thermodynamic compatibility.

This problem was solved⁴¹ by considering the total jumps $(0, x, y, s) \rightarrow (1, s, y, s) \rightarrow (0, x, y, s)$ and writing the detailed balance conditions

$$\begin{cases} K_{0 \rightarrow 1}(x, y, s) = h_x \exp\left[-\frac{w_1(s, y) - w_0(x, y)}{k_B T}\right] K_{0 \rightarrow 1}^{\text{rev}}(x, y, s), \\ K_{1 \rightarrow 0}(x, y, s) = h_x^{-1} \exp\left[-\frac{(w_0(x, y) - \mu_T) - w_1(s, y)}{k_B T}\right] K_{1 \rightarrow 0}^{\text{rev}}(x, y, s), \end{cases} \quad (3.4)$$

where h_x is a characteristic length for x , taken equal to the characteristic length of the power stroke. Provided Eq. 3.4, only two rates have to be calibrated. From the rate $K_{1 \rightarrow 0}$ one can define the global detachment rate, describing the frequency of the detachment, considering all detached positions x that can be reached from an attached configuration $(1, s, y, s)$

$$k_{1 \rightarrow 0}(y, s) = \int_{-d/2}^{d/2} K_{1 \rightarrow 0}(x, y, s) dx,$$

A similar rate $k_{0 \rightarrow 1}^{\text{rev}}$ can be defined for the reverse attachment jump rate $K_{0 \rightarrow 1}^{\text{rev}}$. The rates $k_{1 \rightarrow 0}$ and $k_{0 \rightarrow 1}^{\text{rev}}$ are analog to the rates presented in Section 3.2.1. In the numerical implementation of the jump-diffusion process, the global rates $k_{1 \rightarrow 0}$ and $k_{0 \rightarrow 1}^{\text{rev}}$ are used to terminate the time between consecutive jumps. When a detachment jump occurs, the jump amplitude is drawn from the probability law $k_{1 \rightarrow 0}(y, s)^{-1} K_{1 \rightarrow 0}(x, y, s) dx$ (or $k_{0 \rightarrow 1}^{\text{rev}}(y, s)^{-1} K_{0 \rightarrow 1}^{\text{rev}}(x, y, s) dx$)⁴².

The model developed by Chaintron et al.⁴³ has been calibrated to reproduce data obtained on rat trabeculae in various experimental studies. In Figure 3.9, we show an extract of the results illustrating the Hill force-velocity curve. The model faithfully reproduces the fast transient response to rapid load changes⁴⁴, and can be used to predict the thermodynamic efficiency of the contraction.

3.4.4 Mean field approximation

We here recall that the active force produced by the motors, τ_c enters the macroscopic balance law through the active stress (see Figure 2.2)

$$\underline{\underline{\Sigma}}_a = \frac{T_c + \nu \dot{e}_c}{(1 + 2\underline{\underline{\tau}} \cdot \underline{\underline{e}} \cdot \underline{\underline{\tau}})^{\frac{1}{2}}} \underline{\underline{\tau}} \otimes \underline{\underline{\tau}}, \quad \text{with } T_c = \rho_m \tau_c, \text{ and } \dot{e}_c = \dot{x}_c / \ell_{\text{fib}}, \quad (3.5)$$

⁴¹ Chaintron et al. (“A Jump-Diffusion Stochastic Formalism for Muscle Contraction Models at Multiple Timescales,” 2023)

⁴² see Section 4.1 and 4.2 of *ibid.* for the details

⁴³ *ibid.*

⁴⁴ see figure 6 and 7 of *ibid.* For the details about the calibration procedure, we refer to Kimmig and Caruel, “Hierarchical Modeling of Force Generation in Cardiac Muscle,” 2020 and Chaintron et al., “A Jump-Diffusion Stochastic Formalism for Muscle Contraction Models at Multiple Timescales,” 2023

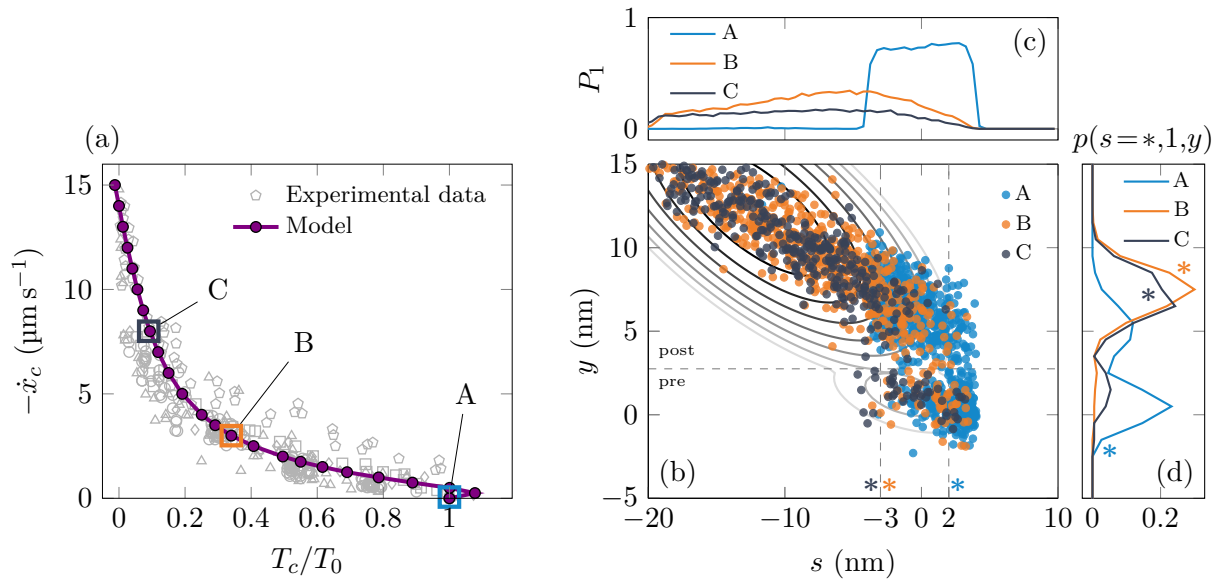


Figure 3.9: Hill force-velocity curve produced by the stochastic jump-diffusion model of Chaintron et al. The curve is obtained by computing the average force of 10^5 realizations in the steady state regime under imposed sliding velocity. (a) steady state force T_c (normalized to isometric force T_0) as a function of the shortening velocity $-\dot{x}_c$. (b) distribution of the system in the attached state. The level sets reproduce the energy landscape. The colored dots show three snapshots of the stochastic realizations corresponding to the points A, B and C shown in (a) for a subset of 5×10^3 randomly chosen realizations. (c) Distributions of attached heads at points A, B and C. (d) Distribution of the conformational variable Y_t in the double well potential for selected relative position s [marked * beside the vertical lines in (b)] of the binding site. Reprinted from Chaintron et al., “A Jump-Diffusion Stochastic Formalism for Muscle Contraction Models at Multiple Timescales,” 2023 with the permission of AIP Publishing, ©2023.

where \dot{x}_c is the relative sliding velocity between the filament. In the jump diffusion model presented in the previous section, if one considers a cluster of N motors, the force τ_c reads

$$\tau_c = \kappa \frac{1}{N} \sum_{i=1}^N \alpha_t^i (X_t^i + Y_t^i). \quad (3.6)$$

This force, produced by the attached motors, is linked to the sliding velocity \dot{x}_c by the macroscopic balance law (3.5), which effectively creates a mechanical coupling between the force generating units. Notice that this coupling has no effect on the detached motors.

Most of the existing models are based on the assumption that, in the regime of a large number N of motors, the total macroscopic force T_c defined in Eq. 3.6, which in principle is random and depends on the state of the (attached) motors, can in fact be considered deterministic and given by

$$T_c = \rho \kappa \mathbb{E}[\alpha_t (X_t + Y_t)],$$

where the expectation is taken by averaging over the statistical distribution of a single motor. This assumption reduces the study of a system of N interacting motors to that of a single one interacting with a surrounding mean-field, which is generally given by the solution of a nonlinear partial differential equation like Eq. 3.1 in the case of the Huxley-Hill model. In the case of the jump-diffusion model presented above, the computation of the active force necessitates the simulation of a large number of stochastic realizations of the processes α_t , X_t and Y_t . In a finite element simulation framework this operation has to be performed at each material point, which comes at a high computational cost. This limitation has been addressed by Kimmig and Caruel,⁴⁵ who derived several reduced version of the jump-diffusion model.

⁴⁵ “Hierarchical Modeling of Force Generation in Cardiac Muscle,” 2020

3.4.5 Reduced models

i Associated publications

The reduced models presented in this section are from *ibid.* with preliminary results from Bestel, Clément, and Sorine, “*A Biomechanical Model of Muscle Contraction*” 2001; Chapelle et al., “*An Energy-Preserving Muscle Tissue Model: Formulation and Compatible Discretizations*,” 2012 and Caruel, Chabiniok, et al., “*Dimensional Reductions of a Cardiac Model for Effective Validation and Calibration*,” 2014.

The first reduced model is obtained by eliminating the dynamics of the conformational variables X_t and Y_t , see Figure 3.10. This elimination is justified by the separation of timescales between the power stroke conformational change and the attachment-detachment process. The approximation consists in considering that X_t and Y_t quickly relax towards equilibrium, and are therefore distributed according to the classical

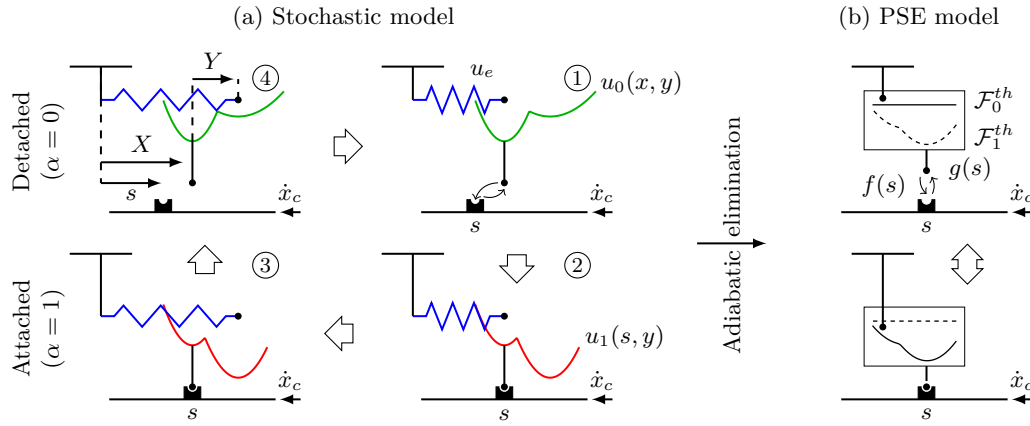


Figure 3.10: Model reduction using the adiabatic elimination of X_t and Y_t . The jump diffusion model can be reduced to a two state model analogous to the Huxley-Hill model with effective free energy potentials. Reproduced from Kimmig and Caruel, “*Hierarchical Modeling of Force Generation in Cardiac Muscle*,” 2020 with permission, ©2020 from Springer Nature.

Boltzmann density at fixed $s(t)$. The ensuing model has only two states see 3.10 and becomes analogous to the classical Huxley-Hill model (see Eq. 3.1), with the peculiarity that the free energies characterizing the two states and the transition rates are derived from a more refined model.

The system can be further simplified by considering the moments of the distribution $P_1(s, t)$ of heads in the attached states:⁴⁶

$$M_p = \frac{1}{d} \int_{s_-}^{s_+} s^p P_1(s, t) ds.$$

Using the conservation equation (3.1) we can write the following unclosed system of ordinary differential equations (ODE)

$$\dot{M}_p(t) = p \dot{x}_c M_{p-1}(t) + f_p - \frac{1}{d} \int_{s_-}^{s_+} (f(s) + g(s)) s^p P_1(s, t) ds,$$

with $f_p = \frac{1}{d} \int_{s_-}^{s_+} s^p f(s) ds$. This system of ODEs is equivalent to solving Eqs. 3.1, but specific closure relations can limit its size. For instance, if we assume that (i) the sum $f(s) + g(s)$ is independent of s ⁴⁷ and that the energy of the attached state is quadratic (as in the classical Huxley-Hill model), the moment equations reduce to

$$\begin{cases} \dot{K}_c(t) = -(f + g)K_c(t) + f_0 K_\infty, \\ \dot{T}_c(t) = -(f + g)T_c(t) + \dot{x}_c K_c(t) + (s_0 f_0 + f_1) K_\infty, \end{cases}$$

where $K_c = \rho \kappa M_0$, $K_\infty = \rho \kappa$, and $T_c = \rho \kappa (s_0 M_0 + M_1)$ depend on the 0th and 1st order moments. In the steady state regime, the predicted force-velocity relation is linear:

$$T_c^\infty = \frac{f_0 K_\infty}{(f + g)^2} \dot{x}_c + \frac{s_0 f_0 + f_1}{f + g} K_\infty,$$

⁴⁶ We here consider a single site model, see Kimmig and Caruel, “*Hierarchical Modeling of Force Generation in Cardiac Muscle*,” 2020 for the multi-site formulation.

⁴⁷ Bestel, Clément, and Sorine, “*A Biomechanical Model of Muscle Contraction*” 2001.

⁴⁸ “Hierarchical Modeling of Force Generation in Cardiac Muscle,” 2020

which is incompatible with observations, see Figure 3.9.

However, Kimmig and Caruel⁴⁸ showed that, despite its simplicity, a linear force velocity relation satisfactorily reproduces the mechanical output of a muscle fiber in a regime compatible with the deformation rates observed in a contracting heart.

3.5 Ongoing work

3.5.1 Molecular dynamics study of the Lymn–Taylor cycle

i Associated publications

This topic is the motivation of R. Manevy’s the PhD thesis at MSME. It is done in collaboration with A. Houdusse from Institut Curie. This work has been presented in several conferences and workshop: Caruel, Detrez, et al., “Umbrella Sampling for the estimation of the free energy barrier of Pi release in Myosin” 2022; Manevy, Caruel, et al., “Identification of Free Energy Barriers Associated With Transition In Myosin cycle Using Umbrella Sampling” 2021; Manevy, Detrez, et al., “Étude Mécanique d’une Protéine Du Muscle” 2021. A journal article is in preparation.

The objective of this work is to close the gap between structural mechanisms of the molecular motors functioning inferred from crystallographic data and more coarse theoretical models. The strategy is to project the high-dimension dynamics of the molecular system onto a low dimension manifold, enabling physiological timescale simulations based on Stochastic Differential Equations alike the ones presented in section Section 3.4.3.

For instance, the parameters characterizing energy landscape that is used to describe the power stroke are usually calibrated using data from fast load change experiments performed on muscle fiber.⁴⁹ One could also *compute* this energy landscape from molecular dynamics simulations.

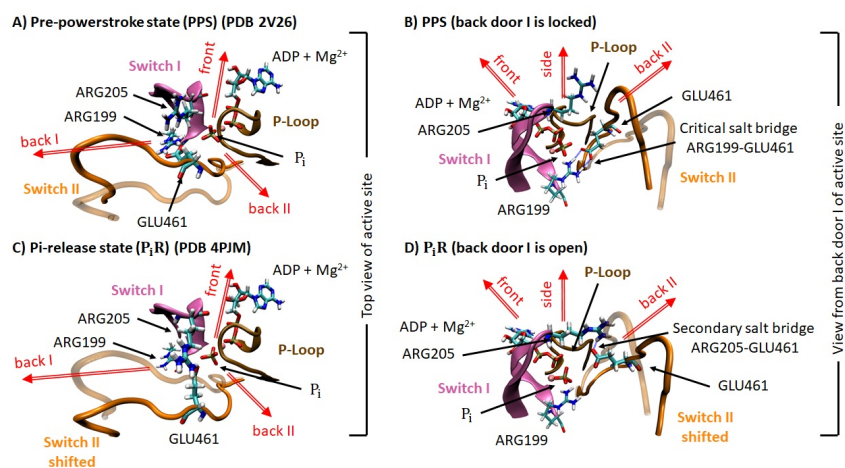
In the PhD work of R. Manevy, we studied the step of the actin-myosin interaction cycle where the inorganic phosphate (P_i), a product of the ATP hydrolysis, is released from the active site. The interplay between this escape from the active site and the power stroke conformational change is a subject of debate: is the release occurring before or after the working stroke, or can they occur simultaneously?⁵⁰

To test different escape pathways and their associated energetic costs, we performed Umbrella Sampling simulations starting with two crystallographic structures and several local configurations of the P_i within the active site, see Figure 3.11.

The constraint is the distance between the P_i and the magnesium ion associated with ADP in the active site. By increasing this distance in a

⁴⁹ Caruel, Moireau, and Chapelle, “Stochastic Modeling of Chemical–Mechanical Coupling in Striated Muscles,” 2019; Kimmig and Caruel, “Hierarchical Modeling of Force Generation in Cardiac Muscle,” 2020; Marcucci and Truskinovsky, “Mechanics of the Power Stroke in Myosin II,” 2010.

⁵⁰ see Llinas et al., “How Actin Initiates the Motor Activity of Myosin,” 2015, for a review on the topic



This video is available online: <https://youtu.be/2ZPqOfjERYU>

Figure 3.12: Umbrella sampling simulation of the escape of P_i from the active site. The video shows the interactions between the nucleotides binding loops during the umbrella sampling simulation for different protonation states of the P_i (named P_iR A to E). The simulations are displayed from the point of view of the back door I. The color code is similar to Figure 3.11. Courtesy of F. Detrez (MSME). Data produced by R. Manevy.

step-by-step manner, we force the inorganic phosphate out of the active site. The potential of mean force characterizing this process can be reconstructed, giving an estimate of the energy barrier associated with the escape pathway taken by the P_i . An example of the escape process is illustrated in Figure 3.12. Only the structures surrounding the active site are shown for clarity.

We found that the initial condition of the simulation, and in particular the orientation of the P_i within the active site, greatly affects the escape pathway and the associated potential of mean force. The statistical validation of these observations are work in progress.

3.5.2 Purely mechanical model of the actin-myosin interaction

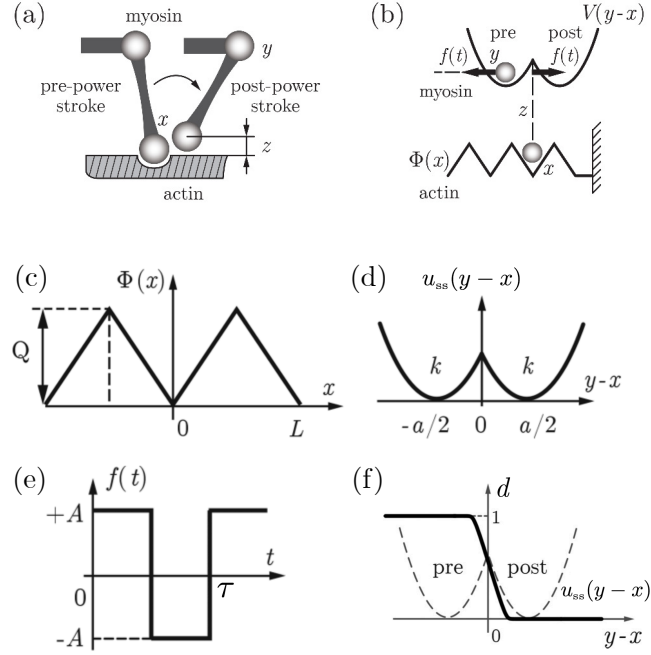
i Associated publication

This work is a follow-up of our collaboration with L. Truskinovsky and R. Sheshka. Preliminary work can be found in Sheshka and Truskinovsky, “*Power-Stroke-Driven Actomyosin Contractility*,” 2014 and section 4.2 of Caruel and Truskinovsky, “*Physics of Muscle Contraction*,” 2018.

In Section 3.4.3, we presented a hybrid chemical-mechanical framework of the actin-myosin interaction. As mentioned in Section 3.2, there exists a category of models where the dynamics of the molecular motor

Figure 3.11: Active site of the Myosin VI structures pre-powerstroke state (PPS) (PDB 2V26) (A and B) and P_i -release state (P_iR) (PDB 4PJM) (C and D). The P-Loop (residues 150 to 157) in brown, Switch I (residues 195 to 205) in pink and Switch II (residues 456 to 467) in orange are represented in cartoon. Other subdomains of the structure are not represented (see Figure 3.1). P_i , ADP, Mg^{2+} , ARG199 and ARG205 of Switch I, GLU461 of Switch II are represented in licorice with color code C cyan, H white, O red, N blue, P brown, and Mg^{2+} light pink. In each panel, Switch II is represented both in solid transparent to show its displacement between the PPS and the P_iR conformation. The P_i release pathways observed during our US simulations are represented by red double arrows following the terminology of Cecchini, Alexeev and Karplus (“*Pi Release from Myosin: A Simulation Analysis of Possible Pathways*,” 2010). The Switch II displacement is characteristic of the opening and closing of the back door I escape pathway for P_i .

Figure 3.13: Illustration of the stochastic mechanical model proposed by Sheshka and Truskinovsky [(a) and (b)]. (c) actin interaction potential ϕ ; (b) power stroke potential u_{ss} ; (d) bi-quadratic representation of the power stroke energy landscape; (e) colored component of the noise taking the form of a periodic force acting on the variable $y - x$; (f) representation of biochemical-mechanical coupling through the variable d representing the affinity of the myosin head to actin, depending on the power stroke state. Reprinted with permission from Sheshka and Truskinovsky, “Power-Stroke-Driven Actomyosin Contractility.” 2014, ©2014 by the American Physical Society.



is represented as a Langevin-type drift-diffusion process with a colored noise. The prototypical example of this class of models was proposed by Magnasco, see Eq. 3.3.

In Figure 3.13 we present an extension of Magnasco’s model that includes the power stroke mechanism. The molecular motor is parametrized by the position of the head X_t and the position of the tip of the lever arm Y_t . Both variables are endowed with Langevin stochastic dynamics. The associated potential includes.

- the energy landscape Φ which represents the interaction between the tip of the head and the actin track (a),
- the bistable potential u_{ss} representing the power stroke conformational change energetics (b).

As in Magnasco’s model, the colored component of the noise is a piecewise constant periodic force f that operates on the variable $Y_t - X_t$, i.e. on the power stroke, see Figure 3.13 (c). The action of this periodic force on the power stroke is the mechanical representation of the energy input provided by ATP hydrolysis. The directionality of the motion can be achieved either by making the actin interaction potential Φ non symmetric or by introducing a control mechanism $d(Y_t - X_t) \in [0, 1]$, that mimicks the coupling between mechanics and biochemistry in the Lymn–Taylor cycle. The potential of the system can then be written as

$$G(x, y, d, t) = d\Phi(x) + u_{ss}(y - x) + f(t)(y - x) - f_{\text{ext}}y, \quad (3.7)$$

where f_{ext} is the external force. The dynamics of the system is then written as

$$\begin{cases} dX_t = -\partial_x G(X_t, Y_t, d, t)dt + \sqrt{2D}dB_t^x, \\ dY_t = -\partial_y G(X_t, Y_t, d, t)dt + \sqrt{2D}dB_t^y. \end{cases}$$

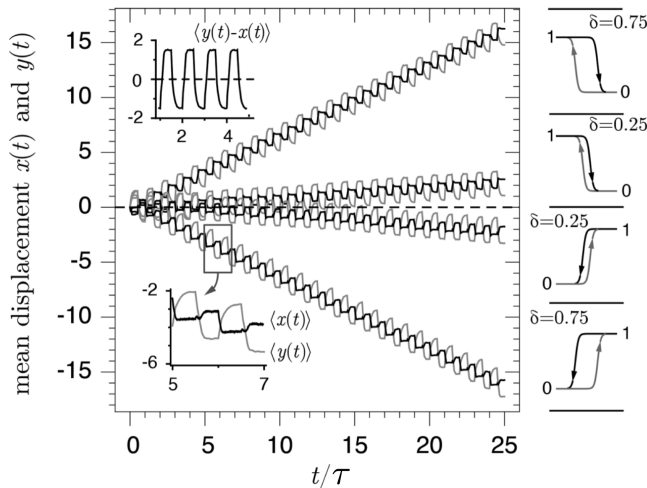


Figure 3.14: Particle trajectory produced in a load-free setting by a mechanical stochastic model with biochemical-mechanical coupling including memory effect. The coupling parameter d dependence on the power stroke state $y - x$ takes the form of a hysteresis (see right column). Changing the width of this hysteresis has a strong impact on the steady state velocity of the molecular motor. Reprinted with permission from Sheshka and Truskinovsky, “Power-Stroke-Driven Actomyosin Contractility.” 2014, ©2014 by the American Physical Society.

In Eq. 3.7, the coupling d characterizes the strength of the attachment. When $d = 1$, the actin potential affects on the evolution of X_t , effectively modeling the attachment. When $d = 0$, the interaction with actin is turned “off”, which represents the detached state.

Considering the dependence of d on the power stroke conformation $Y_t - X_t$ shown in Figure 3.13 (f), the multiplicative combination of d and Φ effectively mimicks the loss of affinity of the myosin head for actin as the power stroke conformational change happens. At the beginning of the power stroke $Y_t - X_t \approx -a/2$, so $d = 1$. Therefore, the gradient actin potential participates in driving the position X_t . After the completion of the power stroke $Y_t - X_t \approx a/2$, so $d = 0$. Therefore, the contribution of the actin potential to the motion of the head vanishes, mimicking a detached state.

An interesting characteristic of this family of model involving a control parameter is that directionality can be achieved even if all the potentials are symmetric, like shown in Figure 3.13. More refined version of the coupling d can incorporate memory effect which can, according to the preliminary results of Sheshka and Truskinovsky,⁵¹ augments the mechanical performance of the motor, see Figure 3.14.

⁵¹ “Power-Stroke-Driven Actomyosin Contractility.” 2014.

3.6 Other project: nano diffusion in the bone tissue

i Associated publications

The results of this work are published in Prakash, Lemaire, Di Tommaso, et al., “Transport Properties of Water Molecules Confined between Hydroxyapatite Surfaces,” 2017 and Prakash, Lemaire, Caruel, et al., “Anisotropic Diffusion of Water Molecules in Hydroxyapatite Nanopores,” 2017.

The biomechanics team of the MSME laboratory actively work on the mechanics of bone remodeling at various scales. Biochemical signaling for bone remodeling involves ionic diffusion within nanopores that connect bone cells to each other. We used molecular dynamics tools to simulate confined diffusion at the nanoscale and determine the physical parameters (diffusion tensor, viscosities, etc.) associated with the flow in the nanopores. This work enabled the determination of relevant parameters for a multiscale model of bone remodeling and also contributed to the understanding of the molecular mechanism of intercellular signaling within the bone tissue.⁵²

⁵² For more details we refer to Prakash, Lemaire, Di Tommaso, et al., “*Transport Properties of Water Molecules Confined between Hydroxyapatite Surfaces*,” 2017 and Prakash, Lemaire, Caruel, et al., “*Anisotropic Diffusion of Water Molecules in Hydroxyapatite Nanopores*,” 2017.

⁵³ Sznitman, “*Topics in propagation of chaos*,” 1991.

⁵⁴ Chaintron and Diez (“*Propagation of chaos: A review of models, methods and applications. I. Models and methods*,” 2022a); Chaintron and Diez (“*Propagation of chaos: A review of models, methods and applications. II. Applications*,” 2022b)

⁵⁵ Pertici, Bongini, et al., “*A Myosin II Nanomachine Mimicking the Striated Muscle*,” 2018.

3.7 Remaining challenges and future work

3.7.1 Beyond the mean-field hypothesis

- In the applied mathematics and statistical physics literature, the fact that the mean-field model summarized in Section 3.4.4 actually describes the large N limit of the original model is called the propagation of chaos phenomenon.⁵³ It finds its roots in the kinetic theory of gas dynamics but has found applications in a wide range of domains, including biology, game theory or deep learning. The quantitative study of this phenomenon, and in particular of the regime in which it occurs, is an active field of research at the interface between probability theory, partial differential equations and statistical physics.⁵⁴

A natural follow-up of the work on the jump-diffusion model presented in Section 3.4.3 is thus to reconsider the mean-field hypothesis and model a finite size cluster of interacting molecular motors. This line of research was started by Caruel, Allain and Truskinovsky (“*Muscle as a Metamaterial Operating Near a Critical Point*,” 2013) and will be presented in more detailed in the next chapter.

The question raised is the representation of the mode of interaction between the motors. One approach consists in considering short range elastic interactions between motors that are attached on the same actin filament. In this way, next-to-nearest neighbors cooperative mechanisms can emerge and propagate inside the contractile unit. This extension of a finite size system will also be useful to compare the model predictions with experimental measurements performed on synthetic nanomachines mimicking the muscle contractile units.⁵⁵

3.7.2 Molecular dynamics simulations

The potential next steps of R. Manevy’s thesis discussed in Section 3.5.1 are to extend the current study to the other steps of the Lymn–Taylor cycle and to strengthen of the methodology used for determining the adequate collective variables characterizing the conformational changes.

This work heavily relies on the availability of crystallographic structures serving as initial (or final) condition for these simulations. These structures are not always available in the protein databank, which limits the applicability of a model calibration approach based solely on molecular dynamics simulations. In particular, it still seems difficult to simulate detachment or attachments events using these techniques before establishing the structural basis of the affinity of myosin for actin.

Choosing appropriate collective variables to describe the motion of the protein during a conformational change is not easy. The energy landscape characterizing the protein is high-dimensional and very rugged so that (i) the collective variables found numerically may not be the most representative (i.e. the fastest) and (ii) the sampling of the effective free energy landscape ineffective. Our future work will involve exploration of various sampling methods and potential use of AI based techniques.⁵⁶

⁵⁶ Zhang et al., "[Artificial Intelligence Enhanced Molecular Simulations](#)," 2023.

Chapter 4

Microscale: the contractile unit

4.1 Background: muscle contractile units and models

4.1.1 The muscle contractile unit

The representative structure of the contractile apparatus above the single molecular motor is the *contractile unit*, a bundle of ~300 myosin motors protruding from the same myosin half-thick filament and interacting with six surrounding actin thin filaments. In the cross-section, each thick filament is at the center of a hexagon formed by the surrounding thin filaments, see Figure 1.2. Even though the structure of the contractile is three-dimensional, it is usually represented as a 1D chain of motors interacting with a single actin filament like in Figure 4.1. Within the sarcomeres, the contractile units are linked by cytoskeletal proteins whose role will be presented in Chapter 5.

Since the molecular motors are connected to a set of common backbones, they necessarily interact. Therefore, a change of state of one element can change the position of the backbone, which can affect the state other elements at short range or long range. Studying the mechanisms of these interactions and their effects on the mechanical output of the contractile unit is the topic of this Chapter. One important question raised is to what extent finite size effect impact the response of the contractile unit. This question is intimately linked to the potential limitation of the usual mean-field approach mentioned in Section 3.4.4 and Section 3.7.1. swift force decay giving The main problem with this intermediate scale is the lack of specific experimental data since classical experimental setups usually involve more macroscopic samples or single molecules. To study the specifics of the contractile unit behavior, one has to resolve to artificial reconstruction.

Recently the team lead by Dr. P. Bianco from the PhysioLab (University of Florence, Italy) has succeeded in reconstructing a minimal functional contractile unit (called the nanomachine) out of purified actin and myosin proteins, able to reproduce the performance of the functional unit of the muscle.¹ A dual laser optical trap holds a bead to which an actin filament is glued. This actin filament is brought to the vicinity of the side of a microneedle covered with myosin motors.

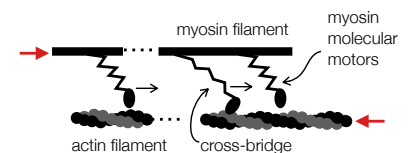


Figure 4.1: Schematic unidimensional representation of a contractile unit. Adapted from Chaintron, Caruel, and Kimmig, “*Modeling Actin-Myosin Interaction: Beyond the Huxley–Hill Framework*,” 2023, CC BY 4.0

¹ Pertici, Bianchi, et al., “*A Myosin II-Based Nanomachine Devised for the Study of Ca²⁺-Dependent Mechanisms of Muscle Regulation*,” 2020; Pertici, Bongini, et al., “*A Myosin II Nanomachine Mimicking the Striated Muscle*,” 2018.

² Kalganov et al., “Forces Measured with Micro-Fabricated Cantilevers during Actomyosin Interactions Produced by Filaments Containing Different Myosin Isoforms and Loop 1 Structures,” 2013; Kaya et al., “Coordinated Force Generation of Skeletal Myosins in Myofilaments through Motor Coupling,” 2017; Plaçais et al., “Spontaneous Oscillations of a Minimal Actomyosin System under Elastic Loading,” 2009; Walcott, D. M. Warshaw, and Debold, “Mechanical Coupling between Myosin Molecules Causes Differences between Ensemble and Single-Molecule Measurements,” 2012.

³ Guérin, Prost, and Joanny, “Dynamical Behavior of Molecular Motor Assemblies in the Rigid and Crossbridge Models,” 2011; Guérin, Prost, Martin, et al., “Coordination and Collective Properties of Molecular Motors,” 2010; Jülicher and Prost, “Spontaneous Oscillations of Collective Molecular Motors,” 1997; Jülicher and Prost, “Cooperative Molecular Motors,” 1995; Plaçais et al., “Spontaneous Oscillations of a Minimal Actomyosin System under Elastic Loading,” 2009.

⁴ Guérin, Prost, and Joanny, “Dynamical Behavior of Molecular Motor Assemblies in the Rigid and Crossbridge Models,” 2011.

⁵ In this respect, this formulation slightly differs from the classical Huxley-Hill model, because the latter considers four rates see Jülicher, Ajdari, and Prost, “Modeling Molecular Motors,” 1997 and Section 3.2.1.

Previous works on similar systems, reported interesting dynamical regimes with various spontaneous oscillations motifs.² It should be mentioned, however, that these observations result from a non-physiological loading setup since the alignment between the actin filament and the array of motors cannot be maintained upon the detachment of motors. In such condition, the detachment of the first motor, generates a cascade of detachments resulting in swift force decay giving and an overall sawtooth oscillatory pattern. This behavior is not observed in the nanomachine developed by the PhysioLab, since the motors are kept close to the actin filament. With this setup, the systems can generate an isometric tension, i.e. a steady force, with a minimum of 8 to 10 motors.

Such artificial contractile unit represents a unique tool for understanding the most basic principles of muscle physiology, with full control on the nature of the proteins involved, their number, and their chemical environment etc. It could be used for instance to test the effect of drugs or mutations on the basic mechanical output of this minimal system, which represents a major asset for the development of new drugs.

4.1.2 Contractile unit modeling

Collective dynamics of molecular motors within a contractile unit has been studied since the late 1990s notoriously by J. Prost and J.F. Joanny’s group at Institut Curie (Paris).³ They have shown in particular that the mechanical feedback induced by the presence of a shared mechanical load or a shared elastic backbone can lead to rich dynamical behaviours involving spontaneous oscillations.

A typical model of this type is a direct analog to the Huxley-Hill model (see Section 3.2.1), which can be formulated as follows.⁴ Considering the mean-field assumption mentioned in Section 3.4.4, let $\rho(x, t)$ be the density of attached molecular motors such that $\rho(x, t)dx$ is the number of motors in the attached state at time t whose positions are inside any interval of the type $[x + n\ell, x + n\ell + dx]$, where ℓ is the distance between consecutive binding sites and n is an integer. The myosin filament is considered rigid, and its position is denoted by X . The attachment and detachment rates are denoted by f and g , respectively, like in the two state Huxley Hill model, see Section 3.2.1. Notice that to maintain the system out of equilibrium these two rates should not satisfy the detailed balance.⁵

Writing the conservation of the myosin motors leads to the following partial differential equation

$$\partial_t \rho - \dot{X} \partial_x \rho = -g(x)\rho + f(x)(1/\ell - \rho).$$

The contractile unit is submitted to an external force F_e and experience a viscous drag $-\xi \dot{X}$. These external forces balance the force produced by the attached molecular motors F_m :

$$\xi \dot{X} = F_e + F_m,$$

with $F_m = N \int_0^\ell \rho(x, t) \partial_x u(x) dx$, where u denotes the interaction potential with actin and N is a scaling factor accounting for the volume density of motors. When the external force F_e is imposed, the force balance creates feedback on the population dynamics. The detailed analysis of the consequences of this feedback in various regimes can be found in the work of Guérin et al.⁶. A particularly interesting point being the broad variety of observable oscillatory responses depending on parameter values.⁷

4.2 Challenges

To put our work in perspective, we raise here a list of challenges relevant to the scale of the contractile unit.

1. As explained in Section 3.1.3, the use of synthetic contractile systems, like in the single molecule experimental setup, allows studying the most basic acto-myosin interaction mechanism. The nanomachine developed by Pertici et al.⁸, brings this experimental approach to a new level by allowing to reconstruct a minimal functioning contractile unit that was shown to behave as a scaled down muscle. The first challenge is to formulate a model of this class of experiments, where a finite number of interacting molecular motors are involved.
2. Simple mechanical feedback mediated by a connection to a common rigid backbone has already shown to trigger a broad range of dynamical regimes. However, the elastic interactions might be more complex, mixing short and long-range components. For instance, the actin and myosin filaments are in fact cross-linked not only by active molecular motors but also by the supposedly passive Myosin Binding Protein C (MyBP-C) and titin.⁹
3. The topic has not been mentioned yet but regulation mechanisms may be influenced by the mechanical interactions between the myosin motors within contractile units. These Regulation mechanisms are crucial in heart tissue undergoing rapid activation-deactivation cycles. During a heartbeat, full activation is never reached, keeping the percentage of attached motors below 15%. Although the cardiac tissue contains many motors (supporting mean-field approaches), individual contractile units may then involve at most 44 locally coupled attached motors, which questions the usual mean-field descriptions as associated models may fail to capture finite-size effects. For example, when mean-field models have multiple stable equilibria, finite-size systems often exhibit abrupt transitions between the equilibria over timescales that are exponential in (N) , which mean-field models do not reproduce.

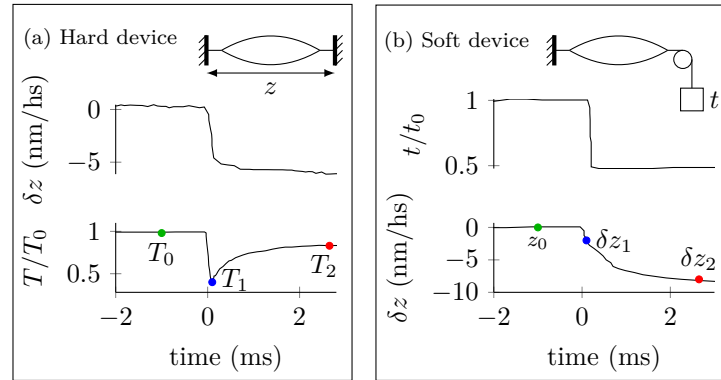
⁶ “*Dynamical Behavior of Molecular Motor Assemblies in the Rigid and Cross-bridge Models*,” 2011.

⁷ Variants of the above model were also studied in Guérin, Prost, and Joanny, “*Dynamic Instabilities in Assemblies of Molecular Motors with Finite Stiffness*,” 2010 and Plaçais et al., “*Spontaneous Oscillations of a Minimal Actomyosin System under Elastic Loading*,” 2009.

⁸ Pertici, Bongini, et al., “*A Myosin II Nanomachine Mimicking the Striated Muscle*,” 2018.

⁹ Tamborrini et al., “*Structure of the Native Myosin Filament in the Relaxed Cardiac Sarcomere*,” 2023 and Chapter 5

Figure 4.2: Fast timescale response of an activated muscle fiber, previously held in isometric conditions, consubmitted to swift load changes in hard (a, imposed shortening) and soft (b, imposed force drop) devices. The length changed are indicated in nanometer per half-sarcomere (nm/hs). Adapted from Caruel and Truskinovsky, “*Physics of Muscle Contraction*,” 2018, data from Piazzesi, Lucii, and Lombardi, “*The Size and the Speed of the Working Stroke of Muscle Myosin and Its Dependence on the Force*,” 2002; Piazzesi, Reconditi, Linari, Lucii, Sun, et al., “*Mechanism of Force Generation by Myosin Heads in Skeletal Muscle*,” 2002.



4.3 Contributions

i Associated publications

The majority of our work on contractile unit results from Caruel, Allain, and Truskinovsky, “*Muscle as a Metamaterial Operating Near a Critical Point*,” 2013, “*Mechanics of Collective Unfolding*,” 2015; Caruel and Truskinovsky, “*Statistical Mechanics of the Huxley-Simmons Model*,” 2016 and Caruel and Truskinovsky, “*Bi-Stability Resistant to Fluctuations*,” 2017. The results mentioned here have already been the object of a review in Sec. 2 of Caruel and Truskinovsky, “*Physics of Muscle Contraction*,” 2018. In Section 4.3.7 we will present an application of the results obtained in the context of muscle contraction to the understanding of the molecular processes driving neurotransmission.

4.3.1 Fast transient response of muscle fibers

Our contribution focuses on the fast timescale response of a muscle fiber submitted to swift load changes.¹⁰ The experiment consists in stimulating a muscle fiber up to isometric tetanus, where the tension reaches a steady state value denoted by T_0 , see Figure 4.2 (a). At $t = 0$, a load step is applied, either in length (soft device) or in tension (hard device). The first milliseconds of the response are illustrated in Figure 4.2. Simultaneously to a length step [see (a)], the tension drops to a level T_1 (phase 1) before rising up to a level T_2 within a few milliseconds (phase 2). In response to a force step, the fiber shortens simultaneously by an amount δz_1 (phase 1) and then more slowly by an amount δz_2 .

Importantly, in these fast timescale regimes the attachment-detachment events of individual myosin motors can be ignored, which means that the number of cross-bridges can be considered constant. This strong assumption is supported by several experimental studies showing that the first detachment events following the application of a quick change in load occur after a few milliseconds.¹¹ In the interval, the number of cross-

¹⁰ A. F. Huxley and Simmons, “*Proposed Mechanism of Force Generation in Striated Muscle*,” 1971; Podolsky, Nolan, and Zaveler, “*Cross-Bridge Properties Derived from Muscle Isotonic Velocity Transients*,” 1969.

¹¹ Reconditi, Linari, et al., “*The Myosin Motor in Muscle Generates a Smaller and Slower Working Stroke at Higher Load*,” 2004.

bridges is constant which allows detecting the conformational change in the attached motors.

In the following, we summarize our contribution to the understanding of the mechanics of this quick response, with a particular emphasis on the role played by the long-range elastic interactions on the synchronization of the power-strokes.

4.3.2 Mechanical model of a contractile unit

The mechanical model proposed for a contractile unit is represented in Figure 4.3. The main assumption of this model is to consider a parallel arrangement of cross-bridges. This simplified representation, where the contribution of the myosin and actin filaments to the elastic response is lumped into a linear series spring, is supported by the work of Ford, Huxley and Simmons, and Linari et al.¹²

In the contractile unit model, each cross-bridge is represented as a bistable snap-spring with the two configurations of the spring representing the pre- and post-power stroke conformation, respectively. As mentioned in Section 3.4.2, the dynamics of the conformational change can be described either using a jump process between two discrete states as formulated by Huxley and Simmons, or using a continuous Langevin dynamics in a double well potential as in the work of Marcucci and Truskinovsky.¹³ Both approaches were analysed. The advantage of the former is that it is fully analytic.

4.3.3 Purely mechanical response of a contractile unit

i Associated reference

The detailed analysis of the purely mechanical properties of the model is available in Caruel, Allain, and Truskinovsky, “*Mechanics of Collective Unfolding*,” 2015.

The mechanical behavior of the contractile model can be studied without considering the effect of temperature, shedding light on the mechanical origin of the interaction between the cross-bridges. In this context, under a given load, the system will equilibrate in local energy minima representing particular microstates. In the model represented in Figure 4.3, the cross-bridge can be interchanged without changing the energy of the microstate. Hence, the energy of a microstate is fully characterized by the fraction p of cross-bridges in the post-power stroke conformation.

To illustrate the behavior of the system in the absence of temperature, we first consider a system with a rigid backbone (consider $\lambda_b \rightarrow +\infty$ in the model of Figure 4.3). The energy and the tension of all metastable states (each characterized by a value of p) can be computed as function of the loading in hard and soft devices, see 4.4. In both cases, the configuration

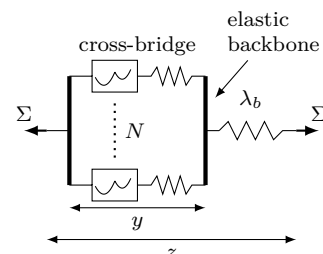


Figure 4.3: Mechanical model of a contractile unit with N cross-bridges assembled in parallel and connected in series to a common elastic backbone with stiffness λ_b . z : total elongation of the contractile unit; y : elongation of the cluster of cross-bridges; Σ : tension generated by the system. Figure adapted from Caruel and Truskinovsky, *ibid*.

¹² Ford, A. F. Huxley, and Simmons, “*The Relation between Stiffness and Filament Overlap in Stimulated Frog Muscle Fibres*.” 1981; Linari, Dobbie, et al., “*The Stiffness of Skeletal Muscle in Isometric Contraction and Rigor*,” 1998. This mechanical representation is valid at high load where the number of bound myosin motors is high. At low load this model has to be modified to incorporate the contribution of Titin, see Pertici, Caremani, and Reconditi, “*A Mechanical Model of the Half-Sarcomere Which Includes the Contribution of Titin*,” 2019; J. D. Powers et al., “*Contracting Striated Muscle Has a Dynamic I-band Spring with an Undamped Stiffness 100 Times Larger than the Passive Stiffness*,” 2020; Squarci et al., “*Titin Activates Myosin Filaments in Skeletal Muscle by Switching from an Extensible Spring to a Mechanical Rectifier*,” 2023.

¹³ A. F. Huxley and Simmons, “*Proposed Mechanism of Force Generation in Striated Muscle*,” 1971; Marcucci and Truskinovsky, “*Mechanics of the Power Stroke in Myosin II*,” 2010.

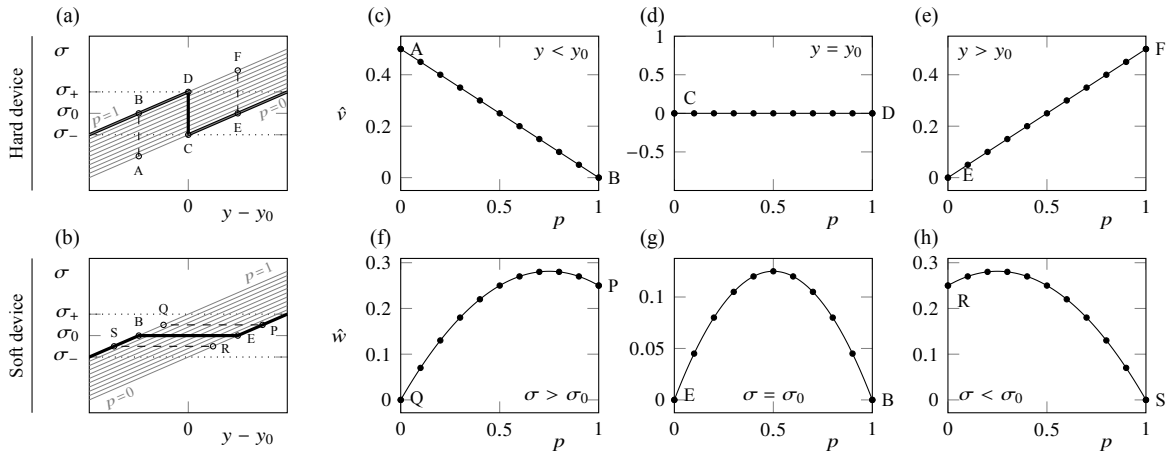


Figure 4.4: Equilibrium response of the contractile unit model with a discrete power-stroke representation at zero temperature and without an elastic backbone ($\lambda_b \rightarrow \infty$). [(a) and (b)] Tension-elongation relations corresponding to the metastable states (gray) and along the global minimum path (thick lines), in hard (a) and soft (b) devices. (c-e) [respectively (f-h)] Energy levels of the metastable states corresponding to $p = 0, 0.1, \dots, 1$, at different elongations y (respectively tensions σ). Corresponding transitions ($E \rightarrow B$, $P \rightarrow Q$, ...) are shown in (a) and (b). Reprinted from Caruel and Truskinovsky, “*Physics of Muscle Contraction*,” 2018.

that minimizes the energy is homogenous ($p = 0$ or $p = 1$), see [(a) and (b)]. The global equilibrium response is therefore characterized by a sharp transition at $y = y_0$ in hard device and $\sigma = \sigma_0$ in soft device.

The difference between the two responses can be investigated by representing the energy of the metastable states as function of p at these transition points, see [(d)-(g)]. In the hard device case at $y = y_0$ (d), all configurations have the same energy. However, in the soft device case at $\sigma = \sigma_0$ (g), mixed states ($0 < p < 1$) have energies higher than the homogenous states. The origin of this difference is the long range elastic interaction: In the soft device case, isolated pre- and post- power stroke cross-bridges would have different lengths [corresponding to points B and E in (b)], but within the cluster, they are constrained to an intermediate elongation which necessarily compresses (respectively elongates) pre-power stroke (respectively post-power stroke) cross-bridges. Hence, the increased energy of the mixed configurations. This simple mechanical feedback is of long-range nature: all cross-bridges are affected equally by the conformational change of a single one.¹⁴ This generic mechanical cross-talk may be present in many other biological systems, ranging from epigenetics to hair-cells.¹⁵ We now present how temperature interferes with these purely mechanical long-range interactions.

¹⁴ More results are available in Caruel, Allain, and Truskinovsky, “*Mechanics of Collective Unfolding*,” 2015 and a similar study is carried out when an elastic backbone is present (mixed device) in Caruel and Truskinovsky, “*Physics of Muscle Contraction*,” 2018.

¹⁵ *ibid.*

4.3.4 Equilibrium statistical mechanics in length clamp

The first model of the fast transient response of muscle fibers was proposed by Huxley and Simmons to interpret the experimental results obtained for imposed length steps.¹⁶ The model has been reformulated by Caruel and Truskinovsky¹⁷ and its statistical mechanical properties were derived by drawing on a formal analogy with a paramagnetic Ising model. The power stroke being modeled as a two state jump process, each cross-bridge is analog to an “elastic” spin pertaining to a parallel bundle confined between rigid backbones (consider the limit $\lambda_b \rightarrow \infty$ in Figure 4.3). In such system, the spins are uncoupled, which implies that the properties of the bundle of cross-bridge are obtained by simply rescaling the properties of a single unit.

One of the most important characteristics of the thermal equilibrium of this model is illustrated in Figure 4.5. The response depends on the non-dimensional ratio between elastic and thermal energies $\beta = \kappa a^2 / (k_B T)$, where κ is the stiffness of the myosin head, a is the power-stroke characteristic length, k_B is the Boltzmann constant and T is the absolute temperature. A salient feature of the system is the presence of a pseudo-critical temperature $\beta = \beta_c = 4$, beyond which the energy becomes a non-convex function of the applied elongation y and the tension-elongation curve shows a region of negative stiffness.

4.3.5 Equilibrium statistical mechanics in soft and mixed devices

The analysis of the Huxley and Simmons’ model in a length clamp setup (hard device) shows that the system does not experience any phase transition. However, the pseudo-critical temperature $\beta = 4$ signals the presence of a genuine second order phase transition if one considers the system in a force clamp setup (soft device). This can be anticipated by observing on Figure 4.5 that, for $\beta > 4$ there exist a load interval $[\sigma_-, \sigma_+]$ within which the same load σ can correspond to three different elongations. In the soft device condition, the Huxley and Simmons’ model is in fact a direct analog to the Curie-Wiess model.

The phase transition comes directly from the competition between the long range mechanical interactions which tend to increase the free energy of mixed states (see Section 4.3.3) and the entropy which tends to decrease the free energy of these states. Hence, the mechanical feedback dominates at low temperature but diminishes when the thermal energy allows the cross-bridges to easily flip conformation thanks to fluctuations.

A detailed analysis of this phase transition and its consequences on the thermal equilibrium properties and dynamical response to load steps has been published in Caruel and Truskinovsky, “*Bi-Stability Resistant to Fluctuations*,” 2017. The main results in the thermodynamic limit and when

¹⁶ A. F. Huxley and Simmons, “*Proposed Mechanism of Force Generation in Striated Muscle*,” 1971.

¹⁷ “*Statistical Mechanics of the Huxley-Simmons Model*,” 2016.

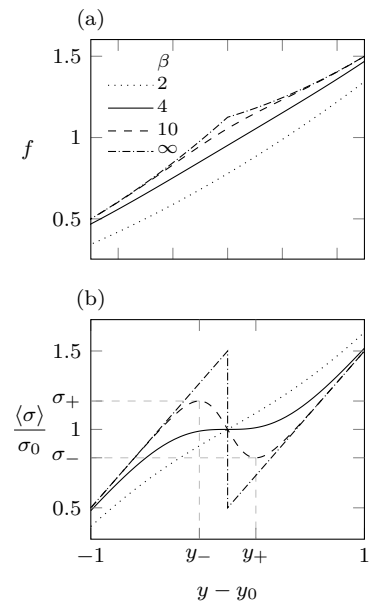
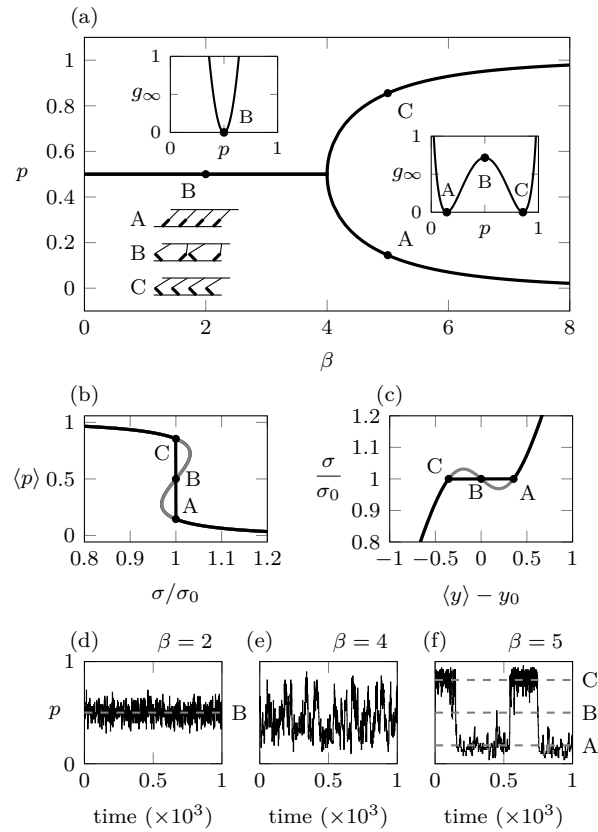


Figure 4.5: Thermal equilibrium response of the Huxley and Simmons model (“*Proposed Mechanism of Force Generation in Striated Muscle*,” 1971) in a length clamp setup, where the elongation $y - y_0$ is imposed. (a) free energy (b) normalized tension. The different curves correspond to different values of the non-dimensional parameter $\beta = \kappa a^2 / (k_B T)$ representing the ratio between the characteristic elastic energy and the characteristic thermal energy in the system. Above the “critical” temperature $\beta = 4$ (dashed and dot-dashed lines), the system shows a region of negative stiffness. Adapted with permission from Caruel and Truskinovsky, “*Statistical Mechanics of the Huxley-Simmons Model*,” 2016, ©2016 by the American Physical Society.

Figure 4.6: Phase transition of the Huxley and Simmons model (“*Proposed Mechanism of Force Generation in Striated Muscle*,” 1971) loaded in a soft device. The fraction of cross-bridge in the post-power-stroke conformation is denoted by p . (a) pitchfork bifurcation showing the location of the equilibrium free energy minima (A and C) and local maximum (B). The inserts show the free energy for $\beta = 2$ (left) and $\beta = 5$ (right). (b) and (c) show $\langle p \rangle$ and the normalized tension σ/σ_0 in the post-bifurcation regime where for a given load (here $\sigma = \sigma_0$) two stable configurations (A and C) exist. [(d)-(f)] shows a simulation of the system for $\sigma = \sigma_0$ before (d), at (e) and after (f) the bifurcation. Adapted from Caruel and Truskinovsky, “*Physics of Muscle Contraction*,” 2018.



the load $\sigma = \sigma_0$ are summarized in Figure 4.6. The free energy is represented as a function of the fraction p of cross-bridges in the post-power-stroke configuration. Before the bifurcation ($\beta < 4$), thermal agitation prevails, resulting into a single stable configuration around $p = 1/2$ (see B). After the bifurcation, the cross-bridge segregate into metastable relatively homogenous states (see A and C). In this regime, the conformational changes are synchronized, but as the barrier between the states A and B (see insert in (a)) increases with N synchronization is exponentially slower for large clusters.

The above analysis can be extended to the situation where the stiffness of the backbone is finite, see Figure 4.3. In this case, the bundle of cross-bridges is loaded in a *mixed device*.¹⁸ The new parameter $\lambda_b = \kappa_f/(N\kappa)$ represents the stiffness of the filament κ_f relative to the combined stiffness of the N cross-bridges forming the bundle. The hard and soft devices limits response can be viewed as the limit $\lambda_b \rightarrow +\infty$ and $\lambda_b \rightarrow 0$ ($z \rightarrow \infty$), respectively. For the Huxley and Simmons’ “spin” model, the critical temperature now reads $\beta_c = 4(1 + \lambda_b)$ and therefore depends on N . This result shows the importance of considering finite size contractile units.

The consequence of this phase transition is summarized in Figure 4.7. The phase diagram (a) shows three phases in the (β, λ_b) space, labelled I, II and III. We recall that the pure hard and soft device loadings correspond to the limits $\lambda_b \rightarrow \infty$ and $\lambda_b = 0$, respectively. Phase I is the

¹⁸ The details of this analysis can be found in Caruel and Truskinovsky, “*Physics of Muscle Contraction*,” 2018

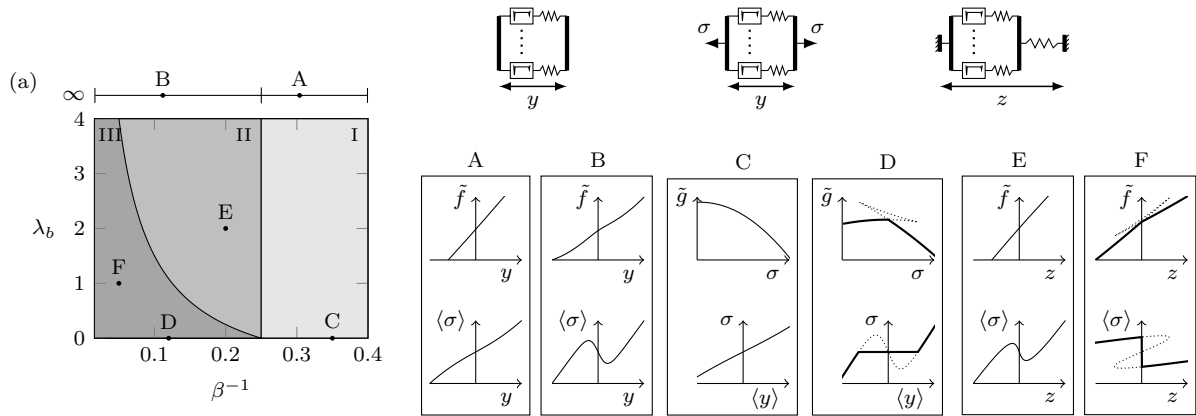


Figure 4.7: Summary of the thermal equilibrium response of the Huxley and Simmons (*“Proposed Mechanism of Force Generation in Striated Muscle,”* 1971) model in hard, soft and mixed device. The phase diagram (a) show the phases boundaries as function of the nondimensional parameters β (temperature), and λ_b (backbone elasticity). The pure hard and soft device behaviors corresponds to the lines at $\lambda_b \rightarrow \infty$ and $\lambda_b = 0$, respectively. The typical responses in each phase (labelled A-F) are shown on the right panels. The top row of these panels illustrates the free energies in thermal equilibrium (thick lines) and the metastable and unstable branches (dotted lines). The bottom row shows the corresponding tension-elongation relation. Adapted from Caruel and Truskinovsky, *“Physics of Muscle Contraction,”* 2018.

region where thermal effects dominates. In a hard device [(a) and (b)], the systems does not show negative stiffness and no metastability. The first phase transition is at $\beta = 4$ and concerns the soft device response. In the post-bifurcation regime (phase II), the hard device response is characterized by negative stiffness and the soft device response shows metastability (dotted lines in D) with an equilibrium response that includes a jump (thick lines in D), see Figure 4.6. In the third phase (III) that appears for $\beta > 4(1 + \lambda_b)$ in a mixed device, the system also shows metastability [dotted lines in (F)] and a jump in the equilibrium response [thick lines in (F)].

Overall this study reveals that the response of a system of parallel cross-bridges depends on the type of loading. This finding may affect the behavior also at larger scales. This point is discussed further in Chapter 5.

To match the experimental results obtained from the fast load changes, it is necessary to consider a regularized version of the Huxley and Simmons’ model as explained in Section 3.4.2. Qualitatively, the behavior of the regularized model is similar to the Huxley and Simmons’ model, though it partially loses its analytical transparency.¹⁹ The mixed device model of the system calibrated on the experimental data showed that the contractile unit might operate close to the critical line (between phase II and III using the notations of Figure 4.7).²⁰

A follow-up of this work was proposed by Borja da Rocha and Truskinovsky, where quenched disorder was added to the model adding third

¹⁹ We refer to Section 2.2 of *ibid.* for the details.

²⁰ This finding was published in Caruel, Allain, and Truskinovsky, *“Muscle as a Metamaterial Operating Near a Critical Point,”* 2013.

²¹ Borja da Rocha and Truskinovsky, “Functionality of Disorder in Muscle Mechanics,” 2019.

dimension to the phase diagram. Again, the author showed that the system was poised to criticality.²¹

4.3.6 Effective dynamical model of a contractile unit

The above analysis has shown that the presence of long-range interactions at the level of individual contractile units may create metastable states associated with power stroke synchronization. The timescale for the synchronization depends exponentially on the number of units in the cluster. These results show a limitation of the classical mean-field approach, which cannot capture finite size effect. A legitimate question at this stage is whether it is possible to derive another effective model of a contractile unit that would be faster to simulate than the fully detailed model but still capturing finite size effects. A preliminary attempt was made in Caruel, “*Mechanics of Fast Force Recovery in Striated Muscles*” 2011 (Chap. 6) by trying to project the high dimensional dynamics of the contractile unit model introduced in Section 4.3.2 on a low dimension manifold.

For the classical spin model a natural *collective* variable could be the fraction p of cross-bridges in the post-power-stroke conformation. An effective one-dimensional energy landscape was derived in Caruel, Allain, and Truskinovsky, “*Mechanics of Collective Unfolding*,” 2015, for the soft device (imposed load) case, and a “coarse grained” dynamical model was proposed and validated numerically in pre- and post-bifurcation regimes in Caruel and Truskinovsky, “*Bi-Stability Resistant to Fluctuations*,” 2017.

Results for the regularized model are still preliminary, since the choice of the collective variable is less obvious. Two strategies were tested in Caruel, “*Mechanics of Fast Force Recovery in Striated Muscles*” 2011 (Chap. 6). The first one uses the cluster elongation y (see Figure 4.3) as a collective variable and assumes that the conformations of the cross-bridges relaxes quickly to equilibrium (adiabatic elimination). The second strategy is based on a weak coupling approximation. In this approximation, it is assumed that the cross-bridges are independent conditionally on the position of the backbone.

The latter approximation seems more promising but a more rigorous mathematical treatment is required.

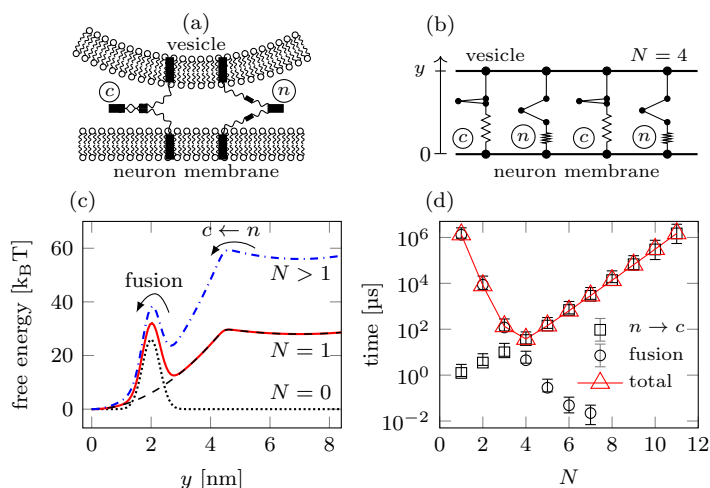


Figure 4.8: Mechanical modeling synaptic vesicle fusion mediated by SNAREpins. (a) Two SNAREpins bridging the vesicle and the neuron membranes before fusion. One SNAREpins is unzipped (n) and the other is zippered (c). (b) mechanical model of 4 SNAREpins between rigid membranes. (c) free energy landscape of the system. Black, dotted: fusion barrier without SNAREs; dashed line, energy landscape of a single SNAREpin; solid red and dot dashed blue: total free energy with one and four SNAREpins, respectively. (d) Influence of the number of SNAREpins on the simulated passage times over the zippering ($n \rightarrow c$, squares) and fusion (circle) barriers, and on the fusion time (red triangles). Adapted from Manca et al., “SNARE Machinery Is Optimized for Ultrafast Fusion,” 2019 ©2019 CC BY-NC-ND 4.0.

4.3.7 Application of the contractile unit model to neurotransmission

i Associated publications

This work was published in Manca et al., “SNARE Machinery Is Optimized for Ultrafast Fusion,” 2019 and a follow-up study was recently issued in Caruel and Pincet, “Dual-Ring SNAREpin Machinery Tuning for Fast Synaptic Vesicle Fusion,” 2024.

A collaboration was initiated with the groups of J.E. Rothman (Yale University) and F. Pincet in 2015 on the mechanical modeling of the molecular processes driving the synaptic neurotransmitters release.

Information is transmitted from one neuron to the next in chemical form through the synaptic cleft that separates the membranes of the neurons. The neurotransmitters are “stored” inside the emitting neuron within vesicles that are docked near the membrane. The incoming electrical signal triggers the massive release of Ca^{2+} ions in the cytoplasm of the emitting neuron, which results in the fusion of the vesicles membranes with the neuron membrane, and the release of their content in the cleft. The key step of the process is the fusion. This molecular topological transformation requires a large amount of energy (about $25 k_B T$): a spontaneous fusion would take more than 1 s, while it happens in less than 1ms in the brain.

The physiological speed is achieved thanks to a bundle of bistable proteins called SNAREpins,²² that bridge the vesicle and the neuron membrane prior to fusion, see Figure 4.8 (a). Their collective conformational change resembles a zippering that pulls the two membranes toward each other, see Figure 4.8 (a).

The system evolves under no external forces other than the viscous drag on the vesicle and the thermal noise. Using a slightly modified version of the Huxley and Simmons’ contractile unit model, Manca et al. predicted

²² soluble N-ethylmaleimide-sensitive factor attachment protein receptors. The role played by these proteins in membrane fusion in living systems has been discovered by J.E. Rothman, who won the Nobel-Prize in 2013.

that the time to reach fusion was a non-monotone function of the number of SNAREpins N showing an optimum around $N = 4$, see Figure 4.8 (d). The fusion model is the combination of two processes:

1. the collective zippering ($n \rightarrow c$), whose timescale augments with N , due to an increasing energy barrier [see Figure 4.8 (c) and (d)],
2. overcoming the fusion energy barrier, whose timescale decreases with N since more SNAREpins can exert more force.

The counterintuitive finding that more SNAREpins actually slow down the process is directly linked to the result of Section 4.3.5: Under a fixed load (here 0 force), the long-range interaction generates internal frustration that increases the energy of mixed microstate. The result of this feedback is an energy barrier between the two homogenous states (fully zippered or fully unzipped) that increases linearly with N , which makes the zippering process exponentially slower for larger clusters, see Figure 4.8 (c). The prediction of the model is in accordance with the actual molecular structure of the fusion machinery as explained in the recent review by Rothman et al. (*"Turbocharging Synaptic Transmission,"* 2023).

Recent work by Bera et al., suggests that the SNAREpins forms a double ring structure.²³ In a follow-up study²⁴ that considers a dual ring configuration, we show that the systems still shows an optimal configuration but that the relative positioning of the two rings on the vesicle may modify the fusion time by few orders of magnitude. Hence, this dual ring machinery has to be finely tuned as well.

²³ Bera et al., *"Synaptophysin Chaperones the Assembly of 12 SNAREpins under Each Ready-Release Vesicle,"* 2023.

²⁴ Caruel and Pincet, *"Dual-Ring SNAREpin Machinery Tuning for Fast Synaptic Vesicle Fusion,"* 2024.

4.4 Perspectives

A natural follow-up of our work on the fast transient response of muscle fiber is to use our contractile unit model in combination with a molecular motor model that includes the attachment-detachment process. The simplest approach is to consider a two state, attached-detached, model and implement for instance the reformulation of the Huxley's⁵⁷ model introduced by Chaintron, Caruel and Kimmig.²⁵ The framework would then be quite similar to the one used by Guérin et al,²⁶ but with a finite-size model that was calibrated and validated on physiological data. We will then be able to observe whether the different dynamical regimes predicted could be observed in realistic muscle contractile units. Another option are motor models proposed by Caruel, Moireau and Chapelle²⁷ by Chaintron et al.²⁸ or the fully mechanical model presented in Sheshka and Truskinovsky²⁹

A challenging research objective using these models will be to characterize finite-size effects, reconsider the mean-field hypothesis and suggest an enhanced reduced model of the contractile unit that is able to capture its metastable behavior. Precisely describing this behavior, even in simple models like the continuous Curie-Weiss model, remains an open question in probability and statistical physics.³⁰ Therefore, this perspective will necessitate advanced mathematical developments.

²⁵ *"Modeling Actin-Myosin Interaction: Beyond the Huxley-Hill Framework,"* 2023.

²⁶ *"Dynamical Behavior of Molecular Motor Assemblies in the Rigid and Cross-bridge Models,"* 2011.

²⁷ *"Stochastic Modeling of Chemical-Mechanical Coupling in Striated Muscles,"* 2019.

²⁸ *"A Jump-Diffusion Stochastic Formalism for Muscle Contraction Models at Multiple Timescales,"* 2023.

²⁹ *"Power-Stroke-Driven Actomyosin Contractility,"* 2014; see also Caruel and Truskinovsky, *"Physics of Muscle Contraction,"* 2018, Sec. 4.2

³⁰ Dawson and Gärtner, *"Large deviations and tunnelling for particle systems with mean field interaction,"* 1986.

Chapter 5

Mesoscale: myofibrils and fibers

This chapter presents the challenges and preliminary contributions to the modeling of muscle contraction at the mesoscale. Regulation mechanisms in muscle contraction, in particular in the heart, operate at this scale. They are currently the object of an intense research activity, so the content of the chapter should be considered more as a perspective for future work than a presentation of past contributions.

5.1 Background: anatomy of a myofibril

5.1.1 Definition of the Mesoscale

The definition of the “mesoscale” is ambiguous. We recall that the molecular scale is the nanometer, and the size of the power-stroke conformational change is ~ 10 nm, see Chapter 1. The scale of the tissue is the cm. In this section, we present in more details the anatomic structure of muscle fibers and suggest a definition of what to call the mesoscale.

A longitudinal cut of a sarcomere is shown on Figure 5.1. The sarcomere is delimited by two Z-lines, and it is symmetric with respect to the M-line. The distance between two consecutive Z-lines is typically $2\ \mu\text{m}$. The A-bands are the regions where the myosin motors interact with the actin filament. The center H-zone corresponds to the region of the thick filament where there are no motors. The I-band is the region containing only actin filaments.

The cross-section of a sarcomere is a crystalline hexagonal lattice of thick and thin filaments, see Figure 5.2. The unit cell of the lattice containing one thick filament for two thin filaments is a contractile unit. The side of the unit cell being $40\ \text{nm}$, there are about 600 contractile units per sarcomere.¹

Muscle fibrils (myofibrils) are successions of sarcomeres that span the whole length of a muscle cell, i.e. a few centimeters, and constitute the main component of its cytoplasm, see Figure 5.3. Their diameter is about $1\ \mu\text{m}$.² Each muscle cell (or fiber) contains about 10^4 myofibrils working in parallel. Muscle fibers are in turn bundled in fascicles which constitute the last step before the tissue scale. The typical diameter of a fascicle is $1\ \text{mm}$.

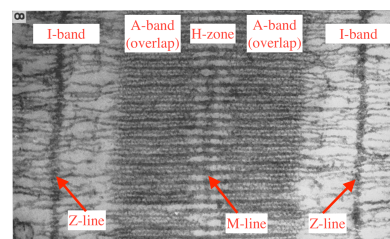


Figure 5.1: Longitudinal cut of a sarcomere. The sarcomere is delimited by two Z-lines. The two regions where the myosin and actin filaments overlap (A-band) are symmetric around the H-zone and the M-line. The I-band is the region where there is no myosin filament. Notice that the cross-bridge are visible in the A-bands. Adapted with permission from H. E. Huxley (*ibid.*), ©1957 from Rockefeller University Press Journals.

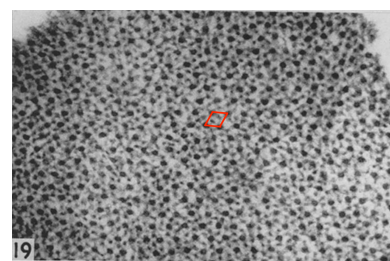


Figure 5.2: Transverse cut of a myofibril showing the hexagonal lattice of thick (myosin) and thin (actin) filaments. The red losange shows the unit cell of the lattice. Adapted with permission from *ibid.*, ©1957 from Rockefeller University Press Journals.

¹ Reconditi, “Recent Improvements in Small Angle X-Ray Diffraction for the Study of Muscle Physiology,” 2006.

² Mobley and B. R. Eisenberg, “Sizes of Components in Frog Skeletal Muscle Measured by Methods of Stereology,” 1975.

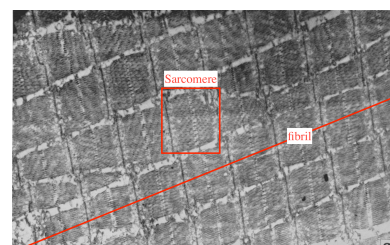
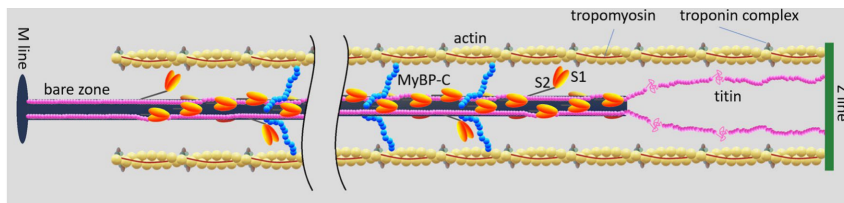


Figure 5.3: Longitudinal cut of a muscle fiber showing several myofibrils. Adapted with permission from *ibid.*, ©1957 from Rockefeller University Press Journals.

Figure 5.4: Schematic representation of a contractile unit proposed in Pertici, Caremani, and Reconditi (*“A Mechanical Model of the Half-Sarcomere Which Includes the Contribution of Titin,”* 2019), Reproduced with permission from Springer Nature.



According to the above description, one could argue that the muscle tissue has seven scales: molecular motors, contractile units, sarcomeres, fibrils, cells, fascicles and tissue, so it is not clear which one can be considered as the most representative “mesoscale”.

From the point of view of activation, the representative unit is the cell, since it is at their membrane that the electric signal from the motor neurons is converted in to a chemical signal in the cytoplasm. It thus seems reasonable to “merge” the fiber (cells) and the fibrils scales into one. Both myofibrils and fibers could be considered as slender continua, since their length is about 100 times to 1000 times larger than their diameter. The meso-scale structure could thus be defined as the elementary representative portion of this 1D continuum that would comprise a “sufficient” number of sarcomeres in the longitudinal direction.

The main assumption behind this representation is that the sarcomeres deform uniformly within a representative volume element or that non-uniformities average out. This would exclude strong localized phenomena. The homogeneity of the sarcomere deformation within the representative volume element depends primarily on the properties of the structures that connect these sarcomeres both in the longitudinal and transverse directions. Another question is whether the friction between the fascicles has some effect on the macroscopic properties of the tissue. A more thorough literature review is necessary to answer this second question.

Here, we choose to define the *mesoscale* as a representative set of contractile units that can serve as the basis of a 1D-homogenized model. One of the objective of the work on this scale will be to refine this definition and come up with an elementary representative volume.

³ R. W. Craig and Padrón, *“Molecular Structure of the Sarcomere”* 2004; Z. Wang et al., *“The Molecular Basis for Sarcomere Organization in Vertebrate Skeletal Muscle,”* 2021.

⁴ The Myosin Binding Protein C (MyBP-C) is a protein that connects the thick and thin filament within the sarcomere. Its function is still not fully understood, but it may play a fundamental role in the regulation of muscle contraction, see Heling, M. A. Geeves, and Kad, *“MyBP-C,”* 2020; Henderson et al., *“Overview of the Muscle Cytoskeleton”* 2017.

5.1.2 Cytoskeletal structural elements

In this section, we provide a quick overview of experimental findings supporting the need for detailed modeling of the mesoscale muscle structures. The following does not constitute a complete review; it rather points at good entry points to establish a more thorough state of the art. For an overview of the sarcomeric molecular structure we refer in particular to the work of Craig and Padrón. and Wang et al.³

The elastic network connecting the contractile units together has essentially three elements: the M-lines, the Z-disks and the titin proteins,⁴ see Figure 5.4.

- **Z-disks** (also called Z-lines) connect the sarcomeres together along the myofibril. It is a complex structure of proteins in which actin filaments and titin are anchored. In a relatively recent review, Frank and Frey⁵ underline the strategic position of the Z-disk “to sense, integrate, and transduce biomechanical stress signals”, and present an overview of their putative role in the development of severe cardiomyopathies.⁶
- **M-lines** connect the thick filaments in the hexagonal lattice transverse to the direction of the fibrils. Their role in the contraction mechanics has been reviewed by Lange et al.⁷ The authors argue that the M-lines “stabilize” the active fibrils by limiting the misalignment of the thick filaments while they exert force.⁸
- **Titin** is the largest protein in the human genome. It connects the two Z-lines of a sarcomere and runs along the thick filament. When the muscle is relaxed, there are no cross-bridges linking the actin and myosin filament and therefore, in the absence of titin, there would be no structure, apart from the fibers’ membrane themselves, preventing the sarcomeres from over stretching, as the filament would slide freely. This “safeguard” function was supported by numerous passive mechanical tests showing a non-linear hyperelastic behavior, with a strong “enthalpic” stiffening at large elongations, see Figure 5.5. In the next section, we will explain its central role in the regulation of the contraction.

⁵ “Cardiac Z-disc Signaling Network,” 2011

⁶ see also Wadmore, Azad, and Gehmlich, “The Role of Z-disc Proteins in Myopathy and Cardiomyopathy,” 2021

⁷ “The M-band: The Underestimated Part of the Sarcomere,” 2019

⁸ Agarkova et al., “M-Band: A Safeguard for Sarcomere Stability?,” 2003; Schoenauer et al., “Myomesin Is a Molecular Spring with Adaptable Elasticity,” 2005.

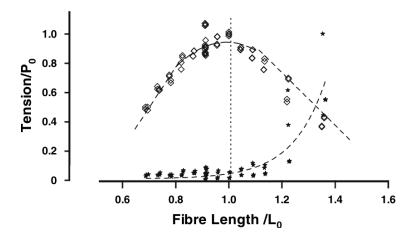


Figure 5.5: Variation of the isometric force with the sarcomere length in active (open diamonds, passive force subtracted) and passive (no activation, stars) conditions. The sarcomere length corresponding to the maximum force is $L_0 = 2.2 \mu\text{m}$. Actin and myosin filament do not overlap for $L/L_0 > 1.3$. Reproduced from *ibid.* reproduced with permission from SNCSC.

5.1.3 Three-filament theory of contraction and regulation

In view of the classical fiber mechanical measurements (Figure 5.5), it seemed that near physiological regimes, titin would work mostly in an “entropic” regime with negligible contribution to the total force. The physiological role of titin has been completely reconsidered in the past decade, in particular thanks to the work of W. Herzog and colleagues to which the terminology “three-filament theory” (actin-myosin-titin) can be attributed.⁹ In short, titin is sensitive to calcium ions and, as such, its properties in the passive and active regimes are in fact completely different.

The active contraction model involving titin is summarized in Figure 5.6. In the passive regime (A), the classical behavior is observed, with a very low stiffness at physiological sarcomere elongation. This low entropic stiffness is due to the PEVK domains of the molecule that unfold under tension. Upon activation and before the onset of actin-myosin interaction this stiffness slightly increases.¹⁰ When actin and myosin start to interact, titin proximal N2A calcium sensitive domain binds to actin, which result in drastic reduction of the titin’s length and thereby a 100-fold increase of its stiffness.¹¹ We refer to the review by Herzog and Schappacher-Tilp for further references on the experimental measurements.¹²

Based on the experimental observations, the mechanical model suggested by Ford, A.F. Huxley and Simmons¹³ has been revisited by Pertici, Care-

⁹ Schappacher-Tilp et al., “A Novel Three-Filament Model of Force Generation in Eccentric Contraction of Skeletal Muscles,” 2015.

¹⁰ K. Powers et al. (“Titin Force Is Enhanced in Actively Stretched Skeletal Muscle,” 2014)

¹¹ J. D. Powers et al., “Contracting Striated Muscle Has a Dynamic I-band Spring with an Undamped Stiffness 100 Times Larger than the Passive Stiffness,” 2020.

¹² Herzog and Schappacher-Tilp, “Molecular Mechanisms of Muscle Contraction,” 2023.

¹³ “The Relation between Stiffness and Filament Overlap in Stimulated Frog Muscle Fibres.” 1981; see Figure 4.3

Figure 5.6: Three-filaments theory of muscle contraction. Reprinted from Herzog and Schappacher-Tilp (*“Molecular Mechanisms of Muscle Contraction,”* 2023), ©2023, with permission from Elsevier

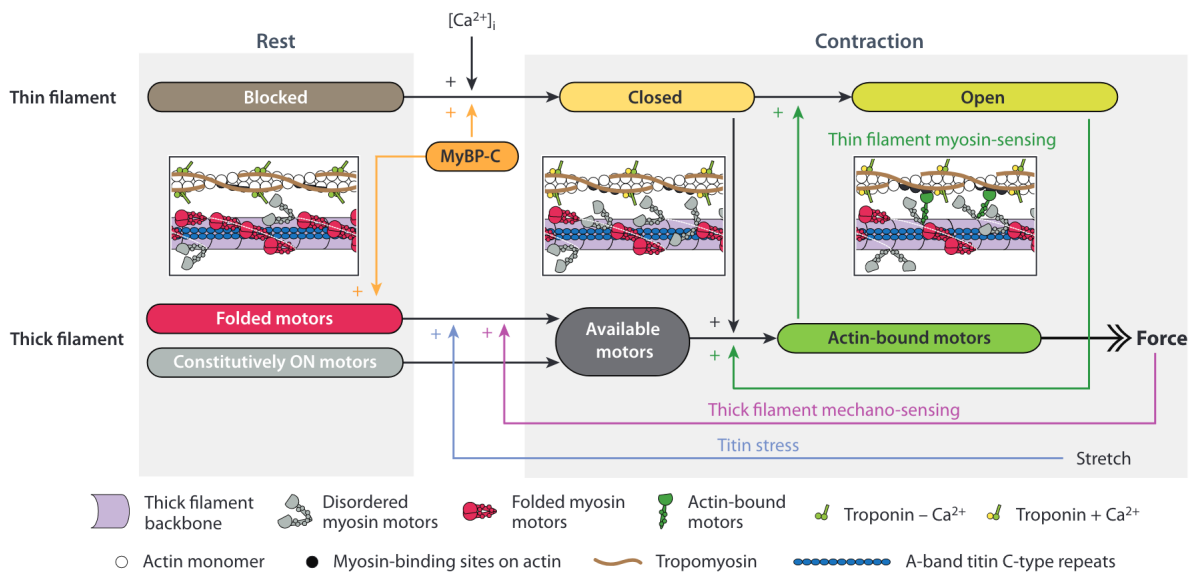
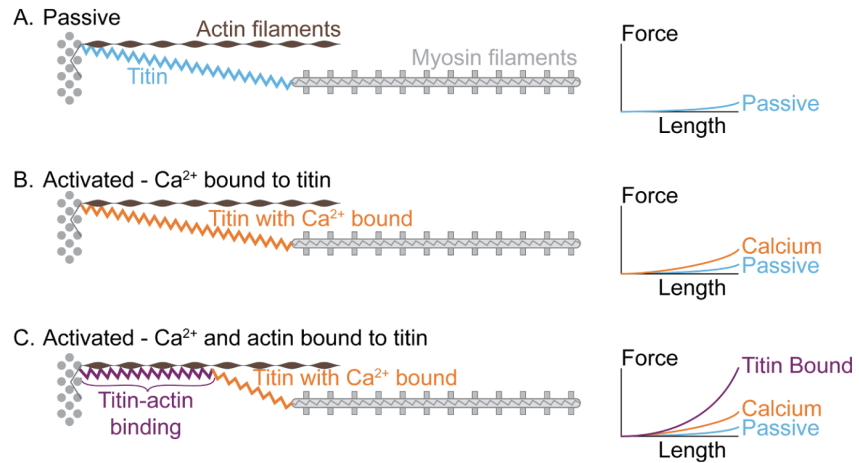


Figure 5.7: Dual regulation of muscle contraction. From Brunello and Fusi, *“Regulating Striated Muscle Contraction,”* 2024, CC BY 4.0.

¹⁴ “A Mechanical Model of the Half-Sarcomere Which Includes the Contribution of Titin,” 2019

¹⁵ Brunello, Bianco, et al., *“Structural Changes in the Myosin Filament and Cross-Bridges during Active Force Development in Single Intact Frog Muscle Fibres: Stiffness and X-ray Diffraction Measurements,”* 2006.

mani and Reconditi¹⁴ to incorporate the contribution of titin. The results confirm numerous previous studies showing that the original model of Ford A.F. Huxley and Simmons was inaccurate only at low force, which corresponds to the beginning of the contraction or to contraction at near maximal velocities.¹⁵

5.1.4 Contraction regulation mechanisms

We here provide a short presentation of the physiological mechanisms controlling the level of activation of the contractile machinery.¹⁶

The contraction is activated by the release of calcium ions in the cytoplasm of the muscle cells, see the top row of 5.7. The consensual mechanism is that the calcium ions (Ca^{2+}) bind to the regulatory units formed by the Troponin-Tropomyosin complexes that are coiled around the actin filament.¹⁷ In the relaxed state these complexes “cover” the actin binding

sites, which prevents myosin attachment (blocked state). The binding of Ca^{2+} to a regulatory unit induces a conformational change that partially reveals the binding site (closed state) and allows weak myosin binding. The binding of a myosin “locks” the regulatory unit and the attachment becomes strong (open state).

In the last decade, it became clear that there is also an activation mechanism associated with the thick filament, which is particularly important for heart contraction, see the bottom row of 5.7. In the relaxed state, the myosin motors are in a so-called OFF-state: the majority of the myosin heads are in an autoinhibitory conformation called the Interacting Head Motif (IHM), folded back on the thick filament.¹⁸ The thick filament activation is not directly due to calcium. It results from a positive force feedback transmitted by the thick filament itself and by the titin protein,¹⁹ which triggers the transition of the myosin motor from the OFF-state to the ON-state.²⁰

Numerous experimental results also support the idea that there is a cooperative mechanism at work in the actin filament as well (green vertical arrow in 5.7). The principle of this mechanism is that force generating myosin motors may propagate the regulatory unit conformational change without the need for extra calcium ions.²¹ Hence, the strong binding of a myosin motor can facilitate the binding of neighboring motors.

These recent observations clearly show that the single motor description is not sufficient to take into account these cooperative activation mechanisms. They also put the long-range mechanical feedback loop mediated by the cytoskeletal structural protein like titin at the center of the picture.

5.1.5 Non-affine deformation along muscle fibrils

Over the past two decades, experimental studies at the scale of single fibrils comprising a few sarcomeres have revealed the existence of non-uniformities (non-affine behavior) of the sarcomere lengths during contraction.²² A recent review of these studies reports on the important role played by the elastic network that connects the contractile units together in tailoring these non-uniformities and in determining the force production.²³ As mentioned in Section 1.4.3, these non-uniformities may play a significant role in the development of severe cardiomyopathies. One problem is that there is no experimental setup available to monitor individual contractile units. Individual sarcomere lengths can however be monitored.²⁴ Another issue is that little is known about the elastic properties of the Z and M-lines, so the calibration of these elements might be difficult.

We recall that one of the hypotheses usually made to formulate models of muscle contraction is that fibers can be modelled as a uniform continuum, see Section 2.1.3. This hypothesis implies an affine deformation of the fiber, which is not in accordance with the potential onset of sarcomere length non-uniformities. Hence, reconsidering the modeling of

¹⁶ The interested reader can find a more thorough up-to-date presentation with an extended list of reference in the recent Brunello and Fusi (*“Regulating Striated Muscle Contraction,”* 2024). We also refer to the introduction of Kimmig, *“Modélisation Multi-Échelles de La Contraction Musculaire: De La Dynamique Stochastique Des Moteurs Moléculaires à La Mécanique Des Milieux Continus”* 2019 and Kimmig, Caruel, and Chapelle, *“Varying Thin Filament Activation in the Framework of the Huxley’57 Model,”* 2022.

¹⁷ McKillop and M. Geeves, *“Regulation of the Interaction between Actin and Myosin Subfragment 1,”* 1993.

¹⁸ Woodhead and R. Craig, *“The Mesa Trail and the Interacting Heads Motif of Myosin II,”* 2020.

¹⁹ We recall that titin runs along the thick filament, and gets stiffer upon activation.

²⁰ Linari, Brunello, et al., *“Force Generation by Skeletal Muscle Is Controlled by Mechanosensing in Myosin Filaments,”* 2015; Reconditi, Caremani, et al., *“Myosin Filament Activation in the Heart Is Tuned to the Mechanical Task,”* 2017; Squarci et al., *“Titin Activates Myosin Filaments in Skeletal Muscle by Switching from an Extensible Spring to a Mechanical Rectifier,”* 2023.

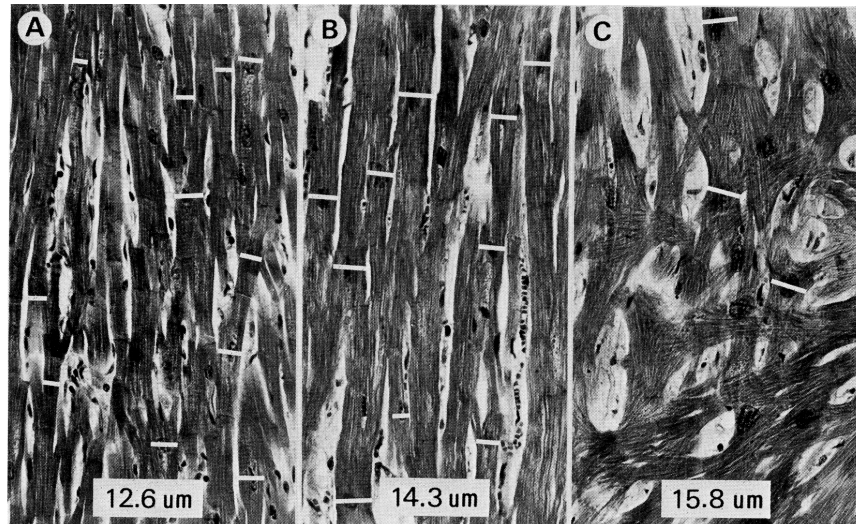
²¹ Caremani, Marcello, et al., *“The Force of the Myosin Motor Sets Cooperativity in Thin Filament Activation of Skeletal Muscles,”* 2022.

²² Li et al., *“Stretch Harmonizes Sarcomere Strain Across the Cardiomyocyte,”* 2023; Moo and Herzog, *“Single Sarcomere Contraction Dynamics in a Whole Muscle,”* 2018.

²³ Leite and Rassier, *“Sarcomere Length Non-Uniformity and Force Regulation in Myofibrils and Sarcomeres,”* 2020.

²⁴ Li et al., *“Stretch Harmonizes Sarcomere Strain Across the Cardiomyocyte,”* 2023; Lookin, Khokhlova, and Cazorla, *“Contractile State Dependent Sarcomere Length Variability in Isolated Guinea-Pig Cardiomyocytes,”* 2022; Moo and Herzog, *“Single Sarcomere Contraction Dynamics in a Whole Muscle,”* 2018.

Figure 5.8: Mesoscale structure of the cardiac tissue illustrating variability in fiber orientation. A: Normal adult heart; B hypertensive heart; C: Hypertrophic cardiomyopathy. Micrographs reproduced from Hoshino et al., “*Myocardial Fiber Diameter and Regional Distribution in the Ventricular Wall of Normal Adult Hearts, Hypertensive Hearts and Hearts with Hypertrophic Cardiomyopathy*,” 1983, ©1983 with permission from Wolters Kluwer Health, Inc..



muscle fibers in a multiscale framework would be necessary to capture potential effect of cardiomyopathies affecting the mechanical properties of cytoskeletal proteins.

5.1.6 Fiber orientations in the muscle tissue

A second hypothesis shared by macroscopic models of muscle contraction is that a single fiber orientation can be defined at each material point, see Figure 2.2. Figure 5.8 shows micrographs of cardiac tissue illustrating the orientation of fibers in a normal adult heart (A), a hypertensive heart (B) and in a heart with hypertrophic cardiomyopathy (C). It is clear that in the latter case the definition of a unique fiber orientation is not possible, at least in this sample.

Tueni, Allain and Genet proposed a multiscale model of the passive myocardium using different representations of the microscopic organisation of cardiomyocytes within the extracellular matrix.²⁵ The objective of this study is to determine which type of microstructure best reproduces the observed anisotropic passive response of tissue samples.²⁶ Such study could be extended considering the active mechanisms, in particular activation.

5.2 Challenges

The above developments of mesostructures based models are so far addressing only the passive behavior of the tissue, so they remain to be coupled to active rheological laws. Furthermore, our previous work on the collective behavior of molecular motors within a single contractile unit (see Chapter 4) has revealed the consequences of long-range elastic interactions existing between them. In particular, it has been shown that these interactions could lead to finite size collective effects like synchronized working strokes,²⁷ that usual mean-field model cannot

²⁵ Tueni, Allain, and Genet, “*On the Structural Origin of the Anisotropy in the Myocardium*,” 2023, see also Avazmohammadi et al., “*A Novel Constitutive Model for Passive Right Ventricular Myocardium*,” 2017

²⁶ Dokos et al., “*Shear Properties of Passive Ventricular Myocardium*,” 2002; Sommer et al., “*Biomechanical Properties and Microstructure of Human Ventricular Myocardium*,” 2015.

²⁷ Caruel, Allain, and Truskinovsky, “*Muscle as a Metamaterial Operating Near a Critical Point*,” 2013; Caruel and Truskinovsky, “*Physics of Muscle Contraction*,” 2018.

capture. These findings are compatible with the presence of non-affine deformation at the mesoscale, with for instance some contractile units being in one conformation while others being in another conformation, see Section 5.3.1. Such non-affine deformation are observed at the fibril scale, so understanding the mechanisms underpinning the onset of these inhomogeneities may be of importance for medical applications.

Another question is to find an adequate model of the regulations mechanisms. The role played by the cytoskeleton on these mechanisms might reveal to be the major determinant of the inter-sarcomere dynamics.²⁸ Finding a path towards a meaningful mesoscale model of muscle contraction activation and regulation is difficult because there is still no consensus on the underlying physiological mechanisms.

All these issues may lead to reconsidering the classical rheological representation presented in Section 2.1.3.

²⁸ Leite and Rassier, “Sarcomere Length Non-Uniformity and Force Regulation in Myofibrils and Sarcomeres,” 2020.

5.3 Contributions

5.3.1 Passive behavior of a simplified sarcomere chain

i Associated publications

The following results are presented in more details in Caruel and Truskinovsky, “*Physics of Muscle Contraction*,” 2018, Sec. 2.3.

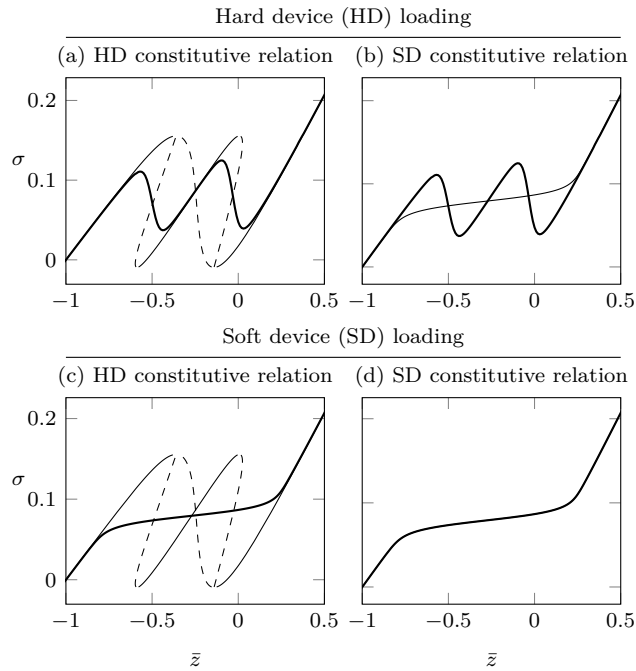
A first set of results rely on a statistical mechanical model of two antagonists contractile units and then of a chain of contractiles units. This work concerns only the coordination of power-stroke conformational changes with the same fixed number of myosin motors in each contractile unit. Hence, the study does not include the attachment-detachment side of the actin-myosin interaction and should thus be considered only in the context of the short timescale response to fast load changes.

We recall that the equilibrium tension-elongation relation of a single contractile unit depends on the loading device, see Section 4.3.5. In a hard device, the response can show a region of negative stiffness, while, at similar temperature, the soft device response is characterized by a plateau, see Figure 4.7 and associated discussion. In the post bifurcation regime (low temperature or low backbone stiffness, see phase III in Figure 4.7), the assembly of cross-bridges tends to behave synchronously: the vast majority of the proteins adopting the same conformation at any given time. The consequence of this property is that the deformation can differ from one contractile unit to the next. With such a behavior, one can expect the deformation associated with muscle contraction to be globally non-affine.

This intuition was confirmed by computing the equilibrium response, at zero and finite temperature, of two or more contractile units in series.²⁹ Interestingly, the equilibrium deformation in a hard device (im-

²⁹ Caruel and Truskinovsky (*ibid.*)

Figure 5.9: Thermal equilibrium response of a sarcomere in hard (a,b) and soft (c,d) devices loading conditions. Tick lines: thermal equilibrium response; thin lines: stable branches (local minima of the free energy); dashed line: unstable branches (local maxima of the free energy). Figure adapted from Caruel and Truskinovsky, “*Physics of Muscle Contraction*,” 2018.



³⁰ Leite and Rassier, “*Sarcomere Length Non-Uniformity and Force Regulation in Myofibrils and Sarcomeres*,” 2020; Shimamoto et al., “*Inter-Sarcomere Coordination in Muscle Revealed through Individual Sarcomere Response to Quick Stretch*,” 2009; Vilfan and T. Duke, “*Instabilities in the Transient Response of Muscle*,” 2003.

posed length) is non-affine which confirms previous numerical and experimental studies.³⁰ In contrary, in a soft device (imposed force), the systems never explores non-affine states.

Comparing the derived non-affine tension-elongation relations with those calculated under the premise that each contractile unit acts as a basic constitutive element with a predetermined tension-elongation relation is enlightening. To do so, we assume that the “constitutive” tension-elongation relation corresponds either to the soft or the hard device equilibrium response of a single contractile unit.

The single sarcomere responses obtained by combining such “phenomenological” units in series in hard and soft device loadings are shown in Figure 5.9. The thick lines show the thermal equilibrium tension-elongation relation computed exactly (using full ensemble averaging). The thin lines are obtained by assuming the constitutive relations.

If the chosen constitutive relation corresponds to that obtained following a hard device protocol [see (a) and (c)], we obtain several equilibrium states for a given total elongation, which is directly imposed by the non-convexity of the constitutive constraints. The global minimum path predicted by the “constitutive model” (thin lines) shows discontinuous transitions between stable branches which resemble continuous transitions along the actual hard device thermal equilibrium path, see the thick line in (a). If instead we use the soft device constitutive law for the description of individual half-sarcomeres [see (b) and (d), thin lines], the tension-elongation response becomes monotone and is therefore completely unrealistic regarding the hard-device thermal equilibrium path

(thick lines), see (b). It is however fit to the equilibrium response in a soft device, see (d).

These preliminary results show that the challenge in developing a macroscopic continuum theory for skeletal muscles arises from the model producing different constitutive relations for soft and hard devices, and the possibility that mixed loading conditions could lead to other relations. This complexity suggests that a local constitutive approach might not be sufficient for a medium governed by long-range interactions. Instead, it may be necessary to explore a nonlocal constitutive closure for the balance law system.

5.3.2 Coupling actin-myosin interaction mechanics and contraction regulation processes

i Associated reference

The work summarized in this section has been published in Kimmig, Caruel, and Chapelle, *“Varying Thin Filament Activation in the Framework of the Huxley’57 Model,”* 2022.

Numerous phenomenological models have been developed to investigate the interplay between force production and the thick and thin filament activation processes.³¹ These models have the common characteristic of not taking into account the relative sliding of actin and myosin filaments and its effect on the population densities occupying the different states. This effect may in fact play a major role in the regulation process, specially in the case of cardiac contraction.

Kimmig, Caruel and Chapelle recently worked on setting the framework for combining the two modeling aspects regarding the thin filament activation process.³² This work is the follow-up of a paper by Kimmig, Moireau and Chapelle³³ on the length dependent force generation, which was focusing on the thick filament regulation mechanisms.

The modeling framework is summarized in Figure 5.10. Within a sarcomere (a), models can be formulated to describe the interaction between myosin proteins and their neighboring actin filaments (b). For this interaction to take place, both myosin motors and actin binding sites needs to be active.³⁴ In the inactive state (OFF-state, 0), myosin motors are folded back on the thick filament and cannot interact with actin, see Figure 5.10 (e). Active motors (ON-state, 1) can attach only to an actin site that has been activated by the binding of a calcium ion to troponin, see state P in Figure 5.10 (f).

In the proposed model, the actin site is a unit that can exist in four different states depending on whether it is activated or not (N or P) and whether it is occupied by a myosin head or not (0 or 1). Kimmig, Caruel and Chapelle³⁵ show how the conservation law for the populations of these four states can be coupled to the attachment-detachment process

³¹ see Trayanova and Rice, *“Cardiac Electromechanical Models,”* 2011 for a review and Regazzoni, Dedè, and Quarteroni, *“Biophysically detailed mathematical models of multiscale cardiac active mechanics,”* 2020 for a more recent contribution. The approach proposed by Regazzoni, Dedè, and Quarteroni (*ibid.*) shows similarities with the one presented here, see the introduction of Kimmig, Caruel, and Chapelle, *“Varying Thin Filament Activation in the Framework of the Huxley’57 Model,”* 2022 for more explanations of the differences.

³² *ibid.*

³³ *“Hierarchical Modeling of Length-Dependent Force Generation in Cardiac Muscles and Associated Thermodynamically-Consistent Numerical Schemes,”* 2021

³⁴ Brunello and Fusi, *“Regulating Striated Muscle Contraction,”* 2024.

³⁵ *“Varying Thin Filament Activation in the Framework of the Huxley’57 Model,”* 2022

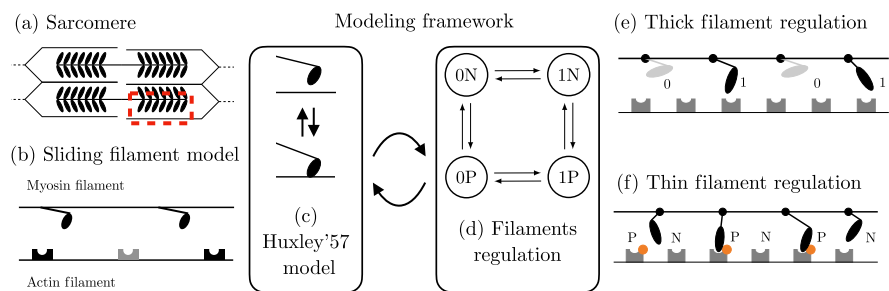


Figure 5.10: Modeling framework for coupling actin and myosin filament activation to the actin-myosin mechanical interaction. (a) Structure of a sarcomere ($\sim \mu\text{m}$). Using the symmetries in the sarcomere structure, its description can be made considering a half-myosin filament (dashed rectangle). (b) Actin sites and myosin heads interact with each other to form cross-bridges (cycling rate ~ 10 ms). The model aims to couple the actin-myosin interaction (c) and the thin and thick filament activations (d) in a mathematically consistent manner. (e) Thick filament regulation. As a result of sarcomere extension, a myosin head transitions between a state where it is not available for attachment (indexed by 0) to a state in which it is available for attachment (indexed by 1). (f) Thin filament regulation. As a result of sarcomere extension and calcium supply, an actin site transitions between a permissive state (denoted by P) in which it is available for myosin attachment and a non-permissive state (denoted by N) in which it is not available for myosin attachment. Reprinted from Kimmig, Caruel, and Chapelle, “*Varying Thin Filament Activation in the Framework of the Huxley’57 Model*,” 2022 © 2022, with permission from John Wiley & Sons Ltd.

of myosin heads, within the framework of the classical Huxley-Hill two-state model (see Section 3.2.1).

In this model, the internal variable $\gamma \in \{0, 1\}$ represent two pools of myosin heads, the value 0 (respectively 1) being associated to heads that are not available (respectively available) for attachment. The fraction of heads that are available is denoted by n_0 . We denote by $P_1(s, t, \gamma)$, the probability for a head pertaining to the pool γ , that is located at a distance s from its nearest binding site to be attached at time t .

We recall that in the classical Huxley-Hill model, the conservation for $P_1(s, t)$ reads (see Eq. 3.1)

$$\partial_t P_1(t, s) + \dot{x}_c(t) \partial_s P_1(t, s) = -g(s) P_1(t, s) + f(s) [1 - P_1(t, s)]$$

For a subset of heads located at a distance s from their nearest binding site, the state of the thin filament can be described by

- n_a the ratio of activated actin sites, which is considered as a prescribed parameter,
- $\bar{n}_a(s, t, \gamma)$ the ratio of activated actin sites occupied by a bound myosin head.

In the proposed model, the attachment and detachment rates depend on the state of the actin site (na , a : non activated or activated, respectively), and the availability of the myosin head γ . The rates corresponding to the different transitions of the four-state model shown in Figure 5.10 are then denoted by $f_{\gamma,a}$ and $f_{\gamma,na}$ for attachments, and $g_{\gamma,a}$ and $g_{\gamma,na}$ for detachments. Notice that, attachments to a non activated site, or of an unavailable head is by design possible, to preserve mathematical consistency, but the calibration will ensure that the corresponding rates will be low.

Using these quantities, the dynamics of P_1 and \bar{n}_a can be written as³⁶

$$\begin{cases} \frac{d}{dt} P_1(s, t, \gamma) = f_{\gamma,a} \bar{n}_a + f_{\gamma,na} (1 - P_1 - \bar{n}_a) \\ \quad - g_{\gamma,a} (n_a - \bar{n}_a) - g_{\gamma,na} (\bar{n}_a - n_a + P_1), \\ \frac{d}{dt} \bar{n}_a(s, t, \gamma) = \frac{|\dot{n}_a|_+}{1 - n_a} (1 - P_1 - \bar{n}_a) + g_{\gamma,a} (n_a - \bar{n}_a) \\ \quad - \frac{|\dot{n}_a|_-}{n_a} \bar{n}_a - f_{\gamma,a} \bar{n}_a, \end{cases} \quad (5.1)$$

where, the total time derivatives are defined by

$$\begin{aligned} \frac{d}{dt} P_1(s, t, 1) &= \partial_t P_1(s, t, 1) + \dot{x}_c \partial_s P_1(s, t, 1) + \frac{|\dot{n}_0|_+}{n_0} [P_1(s, t, 1) - P_1(s, t, 0)], \\ \frac{d}{dt} \bar{n}_a(s, t, 1) &= \partial_t \bar{n}_a(s, t, 1) - \dot{x}_c \partial_s \bar{n}_a(s, t, 1) + \frac{|\dot{n}_0|_+}{n_0} [\bar{n}_a(s, t, 1) - \bar{n}_a(s, t, 0)]. \end{aligned}$$

³⁶ The details of the computations leading to this system can be found in Kimmig, Caruel, and Chapelle, "Varying Thin Filament Activation in the Framework of the Huxley'57 Model," 2022, Section 2.2.2 and 2.2.3. We use the notations

$$\begin{aligned} |x|_+ &= \begin{cases} x, & \text{if } x \geq 0, \\ 0, & \text{otherwise,} \end{cases} \\ |x|_- &= \begin{cases} -x, & \text{if } x \leq 0, \\ 0, & \text{otherwise.} \end{cases} \end{aligned}$$

³⁷ *ibid.*

³⁸ Caremani, Pinzauti, et al., “*Size and Speed of the Working Stroke of Cardiac Myosin in Situ*,” 2016; Dobesh, Konhilas, and Tombe, “*Cooperative Activation in Cardiac Muscle: Impact of Sarcomere Length*,” 2002; Janssen and Hunter, “*Force, Not Sarcomere Length, Correlates with Prolongation of Isometric Contraction*,” 1995; Kentish et al., “*Comparison between the Sarcomere Length-Force Relations of Intact and Skinned Trabeculae from Rat Right Ventricle. Influence of Calcium Concentrations on These Relations*,” 1986; ter Keurs et al., “*Sarcomere Mechanics in Uniform and Non-Uniform Cardiac Muscle*,” 2008.

The model dynamics given by Eq. 5.1 was calibrated³⁷ based on experimental data obtained from isometric twitch contractions of cardiac trabeculae.³⁸

We postulate that $n_a(e_c, t, C) = n_{a,\infty}(e_c, C)n_{a,t}(e_c, t)$. The function $n_{a,\infty}$ accounts the variations of steady-state level of activation with the sarcomere extension e_c , and a level of calcium supply parameter C that accounts for the contractility. The function $n_{a,t}$ describes the time transients.

At this stage, both functions $n_{a,\infty}$ and C are fitted manually on data from various publications, which makes the model purely phenomenological, and thus not based on a physical description of the activation process per se. The objective was to set the framework where a physical model of activation can be coupled to a Huxley-Hill-like actin-myosin interaction model.

5.4 Perspectives

5.4.1 Anatomic structures

As we mentioned in Section 1.1.1, the muscle tissue has a hierarchical structure decomposed from the macroscale to the nanoscale as tissue, fascicles, fibers, fibrils, sarcomeres, contractile units, molecular motors. We termed “mesoscale”, structure ranging from the sarcomeres to fibers which is already containing three hierarchical levels. This chapter showed our contributions to the lowest levels of this hierarchy. To improve our current understanding of the multiscale mechanics of the muscle tissue in health and disease, emphasis has to be put on - the connective structure between sarcomeres in a more realistic model of a non-homogenous fiber, - the organisation of fibers within the extracellular matrix, which implies to reconsider the macroscopic model where, so far, only a single direction per material point is considered.

5.4.2 Modeling activation

Our understanding of the muscle contraction regulation mechanisms has made a considerable leap forwards over the past five years, see Section 5.1.4. The discovery of long-range cooperative mechanisms will necessarily result in the development of models of interacting contractile units where cytoskeletal proteins (titin, Z-lines, M-lines) will play a central role.

In conclusion, from this brief overview of the contraction mechanism at the mesoscale level, it seems clear that the classical approach which consists in considering a mean field approach for the modeling of actin-myosin interaction and a direct rescaling in a macroscale model, is largely insufficient.

Chapter 6

Conclusions, applications, and perspectives

6.1 Summary of the main contributions

This manuscript has highlighted our main contributions to the research on the modeling of muscle contraction at different scales. At the nanoscale (Chapter 3), we have formulated a stochastic jump-diffusion model of actin-myosin interaction, combining a continuous description of the power-stroke conformational change with a more classical discrete representation of the attachment-detachment process. In particular, we have shown that this extension of the classical Huxley-Hill framework can be made compatible with the thermodynamics principle provided an adequate detailed balance condition. This model can be robustly calibrated to reproduce state of the art mechanical experiments performed on muscle fibers.

At the microscale (Chapter 4), we investigated the role played by elastic interactions in the synchronisation of the cross-bridges conformational changes. The strength of these elastic interactions competes with the thermal agitation, which generate a phase transition analog to the ferromagnetic to paramagnetic transition of the Curie-Weiss model. We discuss the implication of such synchronisation on the behavior of sarcomeres submitted to fast load changes, which we show to be ensemble-dependent. We presented a direct application of this work where we show the effect of long-range mechanical interaction on the fine-tuning of the SNARE machinery in the process of neurotransmitter release.

Linking the nanoscale to the macroscale within a genuinely multiscale framework is where major efforts remain to be made (Chapter 5). Recent experimental studies have shed light on the essential role played by the cytoskeletal proteins in regulation processes involving long-range mechanical feedback loops within and in between contractile units. The nature of the internal elastic coupling can make difficult to define adequate “small parameters” necessary for applying standard upscaling techniques. A fully detailed 3D representation of the sarcomeric internal structure is possible but at a very high numerical cost, so new reduced models will have to be developed.

6.2 Applications

In this section, we present potential applications of our work.

6.2.1 Collective switching of systems with long-range interactions

i Associated publication

An extended version of this discussion can be found in Sec. 6 of Caruel and Truskinovsky, *“Physics of Muscle Contraction,”* 2018.

The prototypical nature of the main model formulated for the study of the collective conformational change among an ensemble of interconnected cross-bridges (see Chapter 4), makes it relevant to beyond the context of muscle contraction. It describes a molecular device capable of converting a continuous input (in the form of an external load change in the case of muscles) into an all-or-none output. Such conversion mechanism is ubiquitous in cellular physiology.

A first example is the cooperative zippering of SNAREpins presented in Section 4.3.7. Another example is provided by the transduction channels in the hair cells bundle of the auditory system. In these bundles, the motion induced by the sound waves trigger the opening and closing of elastic ion gates in response to the deformation of the cilia of the cells.¹ A last example is the analogy that can be drawn between the cross-bridge model and the models of collective unzipping for adhesive clusters containing bundles of bistable proteins, such as integrins or cadherins, connected to elastic substrates.²

Furthermore, collective conformational changes in distributed biological systems containing coupled bistable units can be driven not only mechanically, by applying forces or displacements, but also biochemically by, varying concentrations or chemical potentials of ligand molecules in the environment.³ The response of these so-called *allosteric* systems is ultrasensitive to changes in the ligand concentration, leading to all-or-none type of responses. The long range coupling is often provided by mechanical stresses inside membranes and macromolecular complexes. Notice that the actin filament activation mentioned in Section 5.1.4 belongs to this class of system.

Finally, our work on the cooperative power-stroke within contractile units has been used for the design of mechanical devices taking advantage of engineered long-range internal interactions.⁴ In these work, prototypes of modular metastructures are designed, showing exploitable metastable states and adjustable hysteresis. This type of structure can be used for instance for energy harvesting based on asymmetric design of the bistable elements, or for the control of wave propagation if the system, in the case of series connexion.⁵

¹ Bormuth et al., *“Transduction Channels’ Gating Can Control Friction on Vibrating Hair-Cell Bundles in the Ear,”* 2014.

² Erdmann and Schwarz, *“Impact of Receptor-Ligand Distance on Adhesion Cluster Stability,”* 2007; Gao, Qian, and Chen, *“Probing Mechanical Principles of Focal Contacts in Cell-Matrix Adhesion with a Coupled Stochastic-Elastic Modelling Framework,”* 2011; Yao and Gao, *“Mechanics of Robust and Releasable Adhesion in Biology,”* 2006.

³ J.-P. Changeux et al., *“On the Cooperativity of Biological Membranes,”* 1967; Monod, Wyman, and J. P. Changeux, *“On The Nature Of Allosteric Transitions: A Plausible Model.”* 1965.

⁴ R. L. Harne, Wu, and K. W. Wang, *“Mechanical Properties Adaptivity by the Design and Exploitation of Metastable States in a Modular Metastructure,”* 2015, *“Designing and Harnessing the Metastable States of a Modular Metastructure for Programmable Mechanical Properties Adaptation,”* 2016; Kidambi, R. L. Harne, and K. W. Wang, *“Energy Capture and Storage in Asymmetrically Multistable Modular Structures Inspired by Skeletal Muscle,”* 2017; Wu, R. Harne, and K. Wang, *“Exploring a Modular Adaptive Metastructure Concept Inspired by Muscle’s Cross-Bridge,”* 2016.

⁵ Nadkarni et al., *“Unidirectional Transition Waves in Bistable Lattices,”* 2016.

6.2.2 Simulation of muscle contraction

The benefits of using of multiscale models of biological tissue in clinical context are well identified. They are directly connected to the development of “numerical twins” to test surgical and monitoring procedures or drugs. One aim of modeling efforts is thus to provide tools that would be used routinely in the clinic, or tools that would be used for treatment design or clinical research purposes.

As an example of the first use case, we can highlight the start-up led by François Kimmig. This company, named [AnaestAssist](#), is the result of a collaboration between the Inria MÈDISIM team and the Anesthesia and Intensive Care unit at Lariboisière Hospital (APHP). AnaestAssist aims at providing an enhanced monitoring solution integrated with an alert and decision support tool. By utilizing real-time simulations that interact with data, AnaestAssist predicts the cardiovascular response to anesthetic pharmacology during surgery, thereby reducing the risk of hypotension.

To illustrate the second use case, we can mention the work of Pr Linari’s group (PhysioLab, University of Florence), who is involved in a synergistic european [research project](#) with clinicians on investigating the role of titin in skeletal muscle disorders and trying to correlate the phenotype to the genotype. One aspect of the methodology consists in testing samples from patients to measure the functional consequences of the genetic variations and finally improve the clinical diagnostic pipeline for skeletal muscle disorder. Modeling could be used to supplement this kind of procedure with simulations to bring additional mechanistic insight into clinical diagnostic and decision in the context of genetic cardiomyopathies.

A practical example for pharmaceutical development is to predict the effect of isolated using intense in silico screening on the tissue behavior using multiscale modeling. This modeling approach can be supplemented by experiments using reconstructed biomimetic systems using, for instance the nanomachine developed at the PhysioLab by the group of P. Bianco, see Section 4.1.1.

6.3 Perspective and future work

To pursue our research we identified the following projects.

6.3.1 Mesoscale modeling

As we have shown in Chapter 5, one of the biggest challenge currently addressed by physiologist and biophysicists working on muscle contraction is the understanding of the regulation mechanisms of contraction that involves the proteins connecting contractile units together.

To contribute to this effort, we aim at formulating a model of the myofibril lattice using effective contractile unit models. The reduced models should be obtained using adequate asymptotic representation of a fully explicit contractile unit stochastic model with a finite number of motors. To achieve this step we started a collaboration with the [CERMICS laboratory](#) (Center for Training and Research in Mathematics and Scientific Computing) at Ecole des Ponts, in particular with Pr. [Julien Reynnier](#) and Pr. [Tony Lelièvre](#). The questions addressed are the compatibility of this effective model with in-situ observations of the average molecular motors conformations in muscle fibers (in situ X-ray experiments), and the validity of the common mean-field approach.

A possible next step for that project is to formulate a homogenized model law of the mesoscale contractile unit network by considering appropriate continuum limits in the direction of the fiber. The ensuing equations characterizing the level of deformation and the corresponding force will be coupled to the continuum mechanics balance laws within the framework presented in Chapter 2. We will develop the numerical methods to implement the new multiscale contraction model in the existing heart simulation framework developed over the past years with the M Ξ DISIM Inria team.

6.3.2 Tissue engineering

A project we intend to pursue consists in determining the effects of the mesoscale structure on the mechanical output of bioprinted tissue. Bioprinting technologies have made tremendous progress in the past decade, to the point where it becomes feasible to test treatments on bioprinted samples and repair injured tissue.⁶ When addressing the issue of modeling muscle contraction at the mesoscale, using bioprinted tissue presents several advantages against classical approaches based on dissected animal tissues:

- Cells can be grown within a few days from standardized cell lines, which is simpler than using actual animal models.
- Many cells can be observed at once which means that some experiments can be parallelized.
- The bioprinter allows a good control of the microstructure: we could produce tissues with various distributions of fiber orientations for instance.
- The experiments may be more reproducible.

Such a project could be decomposed into four work packages:

1. **Develop the bioprinting protocol.** The objective is here to obtain a contracting tissue with desired microstructure
2. **Define the readouts.** We intend to measure the deformation field of the tissue and link this deformation to the microstructure. The deformation can be measured for instance using microbeads printed with the biomaterial. Microstructure can be characterized using standard microscopy techniques, like Two Photon Electro

⁶ Ma et al., “*Integrated Design and Fabrication Strategies Based on Bioprinting for Skeletal Muscle Regeneration*,” 2023.

Fluorescence. Intracellular component are typically observed using live stain imaging. Finally, the morphology of the tissue can be characterized using Atomic Force Microscopy, potentially in real time.

3. **Design adequate loading devices.** Mechanical tests on muscle fibers are performed only in 1D, in the direction of the fiber. However, in vivo, the tissue is subjected to more complex loadings, which we aim to reproduce in vitro. To reach this objective, the simplest way is to design first a biaxial traction machine. We can also use 3D fabricated surfaces covered with micropillar and measure local force by recording the micropillar deflexion. Traction Force microscopy is another solution.
4. **Formulate new models.** Here a first step is to improve the existing model to take into account fiber anisotropy in an already homogenized framework. The homogenization of a single fiber can then be addressed to determine if developed heterogeneities in the sarcomere deformation has a macroscopic signature. At a smaller scale, we can also propose more descriptive models of how mechanical forces can influence muscle activation and regulation physiological mechanisms, as mentioned previously.

References

- Agarkova, I. “M-Band: A Safeguard for Sarcomere Stability?” In: *J Muscle Res Cell M* 24.2/3 (2003), pp. 191–203. ISSN: 0142-4319. DOI: [10.1023/a:1026094924677](https://doi.org/10.1023/a:1026094924677).
- Ait Mou, Y. “Altered Myofilament Structure and Function in Dogs with Duchenne Muscular Dystrophy Cardiomyopathy”. In: *Journal of Molecular and Cellular Cardiology* 114 (2018), pp. 345–353. ISSN: 00222828. DOI: [10/gc4psp](https://doi.org/10/gc4psp).
- Ait-Mou, Y. “Titin Strain Contributes to the Frank–Starling Law of the Heart by Structural Rearrangements of Both Thin- and Thick-Filament Proteins”. In: *Proceedings of the National Academy of Sciences* 113.8 (2016), pp. 2306–2311. ISSN: 0027-8424, 1091-6490. DOI: [10.1073/pnas.1516732113](https://doi.org/10.1073/pnas.1516732113).
- Arbore, C. “Probing Force in Living Cells with Optical Tweezers: From Single-Molecule Mechanics to Cell Mechanotransduction”. In: *Biophysical Reviews* 11.5 (2019), pp. 765–782. ISSN: 1867-2450, 1867-2469. DOI: [10.1007/s12551-019-00599-y](https://doi.org/10.1007/s12551-019-00599-y).
- Avazmohammadi, R. “A Novel Constitutive Model for Passive Right Ventricular Myocardium: Evidence for Myofiber–Collagen Fiber Mechanical Coupling”. In: *Biomechanics and Modeling in Mechanobiology* 16.2 (2017), pp. 561–581. ISSN: 1617-7959, 1617-7940. DOI: [10.1007/s10237-016-0837-7](https://doi.org/10.1007/s10237-016-0837-7).
- Baker, J. L., Voth, G. A., “Effects of ATP and Actin-Filament Binding on the Dynamics of the Myosin II S1 Domain”. In: *Biophysical Journal* 105.7 (2013), pp. 1624–1634. ISSN: 00063495. DOI: [10/f5ckxr](https://doi.org/10/f5ckxr).
- Bastos, M. B. “Invasive Left Ventricle Pressure–Volume Analysis: Overview and Practical Clinical Implications”. In: *European Heart Journal* 41.12 (2020), pp. 1286–1297. ISSN: 0195-668X. DOI: [10.1093/eurheartj/ehz552](https://doi.org/10.1093/eurheartj/ehz552).
- Bera, M. “Synaptophysin Chaperones the Assembly of 12 SNAREpins under Each Ready-Release Vesicle”. In: *Proceedings of the National Academy of Sciences of the United States of America* 120.45 (2023), e2311484120. ISSN: 0027-8424. DOI: [10.1073/pnas.2311484120](https://doi.org/10.1073/pnas.2311484120).
- Bestel, J., Clément, F., Sorine, M., “A Biomechanical Model of Muscle Contraction”. In: *Medical Image Computing and Computer-Assisted Intervention – MICCAI 2001*. Ed. by G. Goos et al. Vol. 2208. Berlin, Heidelberg: Springer Berlin Heidelberg, 2001, pp. 1159–1161. DOI: [10.1007/3-540-45468-3_143](https://doi.org/10.1007/3-540-45468-3_143).
- Block, S. M., Goldstein, L. S. B., Schnapp, B. J., “Bead Movement by Single Kinesin Molecules Studied with Optical Tweezers”. In: *Nature* 348.6299 (1990), pp. 348–352. ISSN: 1476-4687. DOI: [10.1038/348348a0](https://doi.org/10.1038/348348a0).
- Borja da Rocha, H., Truskinovsky, L., “Functionality of Disorder in Muscle Mechanics”. In: *Physical Review Letters* 122.8 (2019), p. 088103. ISSN: 0031-9007, 1079-7114. DOI: [10/ggj7sz](https://doi.org/10/ggj7sz).

- Bormuth, V. “Transduction Channels’ Gating Can Control Friction on Vibrating Hair-Cell Bundles in the Ear”. In: *Proceedings of the National Academy of Sciences* 111.20 (2014), pp. 7185–7190. ISSN: 0027-8424, 1091-6490. DOI: [10/f53stg](https://doi.org/10/f53stg).
- Brunello, E., Bianco, P., “Structural Changes in the Myosin Filament and Cross-Bridges during Active Force Development in Single Intact Frog Muscle Fibres: Stiffness and X-ray Diffraction Measurements”. In: *Journal of Physiology* 577.3 (2006), pp. 971–984. DOI: [10.1113/jphysiol.2006.115394](https://doi.org/10.1113/jphysiol.2006.115394).
- Brunello, E., Fusi, L., “Regulating Striated Muscle Contraction: Through Thick and Thin”. In: *Annual Review of Physiology* 86.1 (2024), annurev-physiol-042222-022728. ISSN: 0066-4278, 1545-1585. DOI: [10.1146/annurev-physiol-042222-022728](https://doi.org/10.1146/annurev-physiol-042222-022728).
- Buonfiglio, V. “Force and Kinetics of Fast and Slow Muscle Myosin Determined with a Synthetic Sarcomere-like Nanomachine”. In: *Communications Biology* 7.1 (2024), pp. 1–12. ISSN: 2399-3642. DOI: [10.1038/s42003-024-06033-8](https://doi.org/10.1038/s42003-024-06033-8).
- Capitanio, M. “Ultrafast Force-Clamp Spectroscopy of Single Molecules Reveals Load Dependence of Myosin Working Stroke”. In: *Nature Methods* 9.10 (2012), pp. 1013–1019. ISSN: 1548-7091, 1548-7105. DOI: [10/f4bt6v](https://doi.org/10/f4bt6v).
- Caremani, M., Marcello, M., “The Force of the Myosin Motor Sets Cooperativity in Thin Filament Activation of Skeletal Muscles”. In: *Communications Biology* 5.1 (2022), pp. 1–12. ISSN: 2399-3642. DOI: [10.1038/s42003-022-04184-0](https://doi.org/10.1038/s42003-022-04184-0).
- Caremani, M., Melli, L., “Force and Number of Myosin Motors during Muscle Shortening and the Coupling with the Release of the ATP Hydrolysis Products: Chemo-mechanical Coupling during Muscle Shortening”. In: *J Physiol* 593.15 (2015), pp. 3313–3332. ISSN: 00223751. DOI: [10/f7kxch](https://doi.org/10/f7kxch).
- Caremani, M., Pinzauti, F., “Size and Speed of the Working Stroke of Cardiac Myosin in Situ”. In: *Proceedings of the National Academy of Sciences* 113.13 (2016), pp. 3675–3680. ISSN: 0027-8424, 1091-6490. DOI: [10/f8f2sh](https://doi.org/10/f8f2sh).
- Caruel, M. “Mechanics of Fast Force Recovery in Striated Muscles”. Ecole Polytechnique, 2011.
- Caruel, M., Allain, J.-M., Truskinovsky, L., “Muscle as a Metamaterial Operating Near a Critical Point”. In: *Physical Review Letters* 110.24 (2013), p. 248103. ISSN: 0031-9007, 1079-7114. DOI: [10/gmtzn5](https://doi.org/10/gmtzn5).
- “Mechanics of Collective Unfolding”. In: *Journal of the Mechanics and Physics of Solids* 76 (2015), pp. 237–259. ISSN: 00225096. DOI: [10/f639qf](https://doi.org/10/f639qf).
- Caruel, M., Chabiniok, R., “Dimensional Reductions of a Cardiac Model for Effective Validation and Calibration”. In: *Biomechanics and Modeling in Mechanobiology* 13.4 (2014), pp. 897–914. ISSN: 1617-7959, 1617-7940. DOI: [10/gmtzn6](https://doi.org/10/gmtzn6).
- Caruel, M., Detrez, F., “Umbrella Sampling for the estimation of the free energy barrier of Pi release in Myosin”. In: *27th Congress of the European Society of Biomechanics*. Porto, Portugal, 2022. URL: <https://hal-upec-upem.archives-ouvertes.fr/hal-03727763>.
- Caruel, M., Moireau, P., Chapelle, D., “Stochastic Modeling of Chemical–Mechanical Coupling in Striated Muscles”. In: *Biomechanics and Modeling in Mechanobiology* 18.3 (2019), pp. 563–587. ISSN: 1617-7959, 1617-7940. DOI: [10.1007/s10237-018-1102-z](https://doi.org/10.1007/s10237-018-1102-z).
- Caruel, M., Pincet, F., “Dual-Ring SNAREpin Machinery Tuning for Fast Synaptic Vesicle Fusion”. In: *Biomolecules* 14.5 (2024), p. 600. ISSN: 2218-273X. DOI: [10.3390/biom14050600](https://doi.org/10.3390/biom14050600).

- Caruel, M., Truskinovsky, L., “Statistical Mechanics of the Huxley-Simmons Model”. In: *Physical Review E* 93.6 (2016), p. 062407. ISSN: 2470-0045, 2470-0053. DOI: [10/gkpp6d](https://doi.org/10/gkpp6d).
- “Bi-Stability Resistant to Fluctuations”. In: *Journal of the Mechanics and Physics of Solids* 109 (2017), pp. 117–141. ISSN: 00225096. DOI: [10/gcgxxs](https://doi.org/10/gcgxxs).
- “Physics of Muscle Contraction”. In: *Reports on Progress in Physics* 81.3 (2018), p. 036602. ISSN: 0034-4885, 1361-6633. DOI: [10/gf8wq6](https://doi.org/10/gf8wq6).
- Cecchini, M., Alexeev, Y., Karplus, M., “Pi Release from Myosin: A Simulation Analysis of Possible Pathways”. In: *Structure* 18.4 (2010), pp. 458–470. ISSN: 09692126. DOI: [10.1016/j.str.2010.01.014](https://doi.org/10.1016/j.str.2010.01.014).
- Chabiniok, R. “Multiphysics and Multiscale Modelling, Data–Model Fusion and Integration of Organ Physiology in the Clinic”. In: *Interface Focus* 6.2 (2016), p. 20150083. DOI: [10.1098/rsfs.2015.0083](https://doi.org/10.1098/rsfs.2015.0083).
- Chaintron, L.-P., Caruel, M., Kimmig, F., “Modeling Actin-Myosin Interaction: Beyond the Huxley–Hill Framework”. In: *MathematicS In Action* 12.1 (2023), pp. 191–226. DOI: [10.5802/msia.38](https://doi.org/10.5802/msia.38).
- Chaintron, L.-P., Diez, A., “Propagation of chaos: A review of models, methods and applications. I. Models and methods”. In: *Kinetic and Related Models* 15.6 (2022), pp. 895–1015. DOI: [10.3934/krm.2022017](https://doi.org/10.3934/krm.2022017).
- “Propagation of chaos: A review of models, methods and applications. II. Applications”. In: *Kinetic and Related Models* 15.6 (2022), pp. 1017–1173. DOI: [10.3934/krm.2022018](https://doi.org/10.3934/krm.2022018).
- Chaintron, L.-P. “A Jump-Diffusion Stochastic Formalism for Muscle Contraction Models at Multiple Timescales”. In: *Journal of Applied Physics* 134.19 (2023), p. 194901. ISSN: 0021-8979. DOI: [10.1063/5.0158191](https://doi.org/10.1063/5.0158191). eprint: https://pubs.aip.org/aip/jap/article-pdf/doi/10.1063/5.0158191/18212771/194901_1_5.0158191.pdf.
- Changeux, J.-P. “On the Cooperativity of Biological Membranes”. In: *Proceedings of the National Academy of Sciences* 57.2 (1967), pp. 335–341. ISSN: 0027-8424, 1091-6490. DOI: [10/brqnsf](https://doi.org/10/brqnsf).
- Chapelle, D. “An Energy-Preserving Muscle Tissue Model: Formulation and Compatible Discretizations”. In: *International Journal For Multiscale Computational Engineering* 10.2 (2012), pp. 189–211.
- Cheng, Y.-S., Leite, F. d. S., Rassier, D. E., “The Load Dependence and the Force-Velocity Relation in Intact Myosin Filaments from Skeletal and Smooth Muscles”. In: *Am J Physiol-cell Ph* 318.1 (2020), pp. C103–C110. ISSN: 0363-6143. DOI: [10.1152/ajpcell.00339.2019](https://doi.org/10.1152/ajpcell.00339.2019).
- Colorado-Cervantes, J. I. “Patient-Specific Modeling of Left Ventricle Mechanics”. In: *Acta Mechanica Sinica* 38.1 (2022), p. 621211. ISSN: 0567-7718, 1614-3116. DOI: [10.1007/s10409-021-09041-0](https://doi.org/10.1007/s10409-021-09041-0).
- Craig, R. W., Padrón, R., “Molecular Structure of the Sarcomere”. In: *Myology*. 3rd ed. The McGraw-Hill Companies, Inc, 2004, pp. 129–144. ISBN: 0-07-137180-X.
- Damon, B. M. “Skeletal Muscle Diffusion Tensor-MRI Fiber Tracking: Rationale, Data Acquisition and Analysis Methods, Applications and Future Directions”. In: *NMR in Biomedicine* 30.3 (2017), e3563. ISSN: 1099-1492. DOI: [10.1002/nbm.3563](https://doi.org/10.1002/nbm.3563).
- Dawson, D. A., Gärtner, J., “Large deviations and tunnelling for particle systems with mean field interaction”. In: *CR Math. Rep. Acad. Sci. Canada* 8.6 (1986), pp. 387–392. URL: <https://m>

athreports.ca/article/large-deviations-and-tunnelling-for-particle-systems-with-mean-field-interaction/.

- Day, S. M., Tardiff, J. C., Ostap, E. M., “Myosin Modulators: Emerging Approaches for the Treatment of Cardiomyopathies and Heart Failure”. In: *The Journal of Clinical Investigation* 132.5 (2022). ISSN: 0021-9738. DOI: [10.1172/JCI148557](https://doi.org/10.1172/JCI148557).
- de Tombe, P. P., ter Keurs, H. E., “Force and Velocity of Sarcomere Shortening in Trabeculae from Rat Heart. Effects of Temperature.” In: *Circulation Research* 66.5 (1990), pp. 1239–1254. ISSN: 0009-7330, 1524-4571. DOI: [10/gmtztb](https://doi.org/10/gmtztb).
- Debold, E. P. “Recent Insights into the Relative Timing of Myosin’s Powerstroke and Release of Phosphate”. In: *Cytoskeleton* 78.9 (2021), pp. 448–458. ISSN: 1949-3592. DOI: [10.1002/cm.21695](https://doi.org/10.1002/cm.21695).
- Dobesh, D. P., Konhilas, J. P., Tombe, P. P., “Cooperative Activation in Cardiac Muscle: Impact of Sarcomere Length”. In: *American Journal of Physiology-Heart and Circulatory Physiology* 282.3 (2002), H1055–H1062. ISSN: 0363-6135. DOI: [10.1152/ajpheart.00667.2001](https://doi.org/10.1152/ajpheart.00667.2001).
- Dokos, S. “Shear Properties of Passive Ventricular Myocardium”. In: *American Journal of Physiology-Heart and Circulatory Physiology* 283.6 (2002), H2650–H2659. ISSN: 0363-6135. DOI: [10.1152/ajpheart.00111.2002](https://doi.org/10.1152/ajpheart.00111.2002).
- Dominguez, R. “Crystal Structure of a Vertebrate Smooth Muscle Myosin Motor Domain and Its Complex with the Essential Light Chain: Visualization of the Pre-Power Stroke State”. In: *Cell* 94.5 (1998), pp. 559–571. ISSN: 0092-8674, 1097-4172. DOI: [10.1016/S0092-8674\(00\)81598-6](https://doi.org/10.1016/S0092-8674(00)81598-6). pmid: [9741621](https://pubmed.ncbi.nlm.nih.gov/9741621/). URL: [https://www.cell.com/cell/abstract/S0092-8674\(00\)81598-6](https://www.cell.com/cell/abstract/S0092-8674(00)81598-6).
- Duke, T. A. J. “Molecular Model of Muscle Contraction”. In: *Proceedings of the National Academy of Sciences* 96.6 (1999), pp. 2770–2775. ISSN: 0027-8424, 1091-6490. DOI: [10/d4xwdb](https://doi.org/10/d4xwdb).
- Eisenberg, E., Hill, T. L., “A Cross-Bridge Model of Muscle Contraction”. In: *Progress in Biophysics and Molecular Biology* 33 (1979), pp. 55–82. ISSN: 00796107. DOI: [10/bdpfkn](https://doi.org/10/bdpfkn).
- Erdmann, T., Schwarz, U. S., “Impact of Receptor-Ligand Distance on Adhesion Cluster Stability”. In: *Eur. Phys. J. E* 22.2 (2007), pp. 123–137. ISSN: 1292-8941, 1292-895X. DOI: [10/cvn2q5](https://doi.org/10/cvn2q5).
- Filipovic, N. “SILICOFM Platform, Multiscale Modeling of Left Ventricle from Echocardiographic Images and Drug Influence for Cardiomyopathy Disease”. In: *Computer Methods and Programs in Biomedicine* 227 (2022), p. 107194. ISSN: 0169-2607. DOI: [10.1016/j.cmpb.2022.107194](https://doi.org/10.1016/j.cmpb.2022.107194).
- Finer, J. T., Simmons, R. M., Spudich, J. A., “Single Myosin Molecule Mechanics: Piconewton Forces and Nanometre Steps”. In: *Nature* 368.6467 (1994), pp. 113–119. ISSN: 1476-4687. DOI: [10.1038/368113a0](https://doi.org/10.1038/368113a0).
- Fischer, S. “Structural Mechanism of the Recovery Stroke in the Myosin Molecular Motor”. In: *Proceedings of the National Academy of Sciences* 102.19 (2005), pp. 6873–6878. ISSN: 0027-8424, 1091-6490. DOI: [10/d3s2fb](https://doi.org/10/d3s2fb).
- Foëx, P., Leone, B. J., “Pressure-Volume Loops: A Dynamic Approach to the Assessment of Ventricular Function”. In: *Journal of Cardiothoracic and Vascular Anesthesia. Emerging Technologies: Advances and Complications in Cardiac Anesthesia and Surgery* 8.1 (1994), pp. 84–96. ISSN: 1053-0770. DOI: [10.1016/1053-0770\(94\)90020-5](https://doi.org/10.1016/1053-0770(94)90020-5).
- Ford, L. E., Huxley, A. F., Simmons, R. M., “The Relation between Stiffness and Filament Overlap in Stimulated Frog Muscle Fibres.” In: *The Journal of Physiology* 311.1 (1981), pp. 219–249.

- ISSN: 00223751. DOI: [10/gmjmmmd](https://doi.org/10/gmjmmmd). URL: <https://onlinelibrary.wiley.com/doi/10.1113/jphysiol.1981.sp013582>.
- Frank, D., Frey, N., “Cardiac Z-disc Signaling Network”. In: *Journal of Biological Chemistry* 286.12 (2011), pp. 9897–9904. ISSN: 00219258. DOI: [10.1074/jbc.R110.174268](https://doi.org/10.1074/jbc.R110.174268). URL: <https://linkinghub.elsevier.com/retrieve/pii/S0021925820538118>.
- Gao, H., Qian, J., Chen, B., “Probing Mechanical Principles of Focal Contacts in Cell-Matrix Adhesion with a Coupled Stochastic-Elastic Modelling Framework”. In: *Journal of the Royal Society Interface* 8.62 (2011), pp. 1217–1232. DOI: [10.1098/rsif.2011.0157](https://doi.org/10.1098/rsif.2011.0157).
- George, M. “Novel Drug Targets in Clinical Development for Heart Failure.” In: *Eur J Clin Pharmacol* 70.7 (2014), pp. 765–74. ISSN: 0031-6970. DOI: [10.1007/s00228-014-1671-4](https://doi.org/10.1007/s00228-014-1671-4).
- Gerull, B. “Mutations of TTN, Encoding the Giant Muscle Filament Titin, Cause Familial Dilated Cardiomyopathy”. In: *Nat Genet* 30.2 (2002), pp. 201–204. ISSN: 1061-4036. DOI: [10.1038/ng815](https://doi.org/10.1038/ng815).
- Göktepe, S., Menzel, A., Kuhl, E., “The Generalized Hill Model: A Kinematic Approach towards Active Muscle Contraction”. In: *Journal of the Mechanics and Physics of Solids* 72 (2014), pp. 20–39. ISSN: 00225096. DOI: [10/f24qpv](https://doi.org/10/f24qpv).
- Granzier, H. “Titin: Physiological Function and Role in Cardiomyopathy and Failure”. In: *Heart Fail Rev* 10.3 (2005), pp. 211–223. ISSN: 1382-4147, 1573-7322. DOI: [10/bqqzhh](https://doi.org/10/bqqzhh).
- Guérin, T., Prost, J., Joanny, J.-F., “Dynamic Instabilities in Assemblies of Molecular Motors with Finite Stiffness”. In: *Physical Review Letters* 104.24 (2010), p. 248102. ISSN: 0031-9007, 1079-7114. DOI: [10/cmftsw](https://doi.org/10/cmftsw). URL: <https://link.aps.org/doi/10.1103/PhysRevLett.104.248102>.
- Guérin, T., Prost, J., Joanny, J.-F., “Dynamical Behavior of Molecular Motor Assemblies in the Rigid and Crossbridge Models”. In: *Eur. Phys. J. E* 34.6 (2011), p. 60. ISSN: 1292-8941, 1292-895X. DOI: [10/dwphkc](https://doi.org/10/dwphkc).
- Guérin, T., Prost, J., Martin, P., “Coordination and Collective Properties of Molecular Motors: Theory”. In: *Current Opinion in Cell Biology* 22.1 (2010), pp. 14–20. ISSN: 09550674. DOI: [10/c4hrnm](https://doi.org/10/c4hrnm).
- Harne, R. L., Wu, Z., Wang, K. W., “Mechanical Properties Adaptivity by the Design and Exploitation of Metastable States in a Modular Metastructure”. In: *ASME 2015 Conference on Smart Materials, Adaptive Structures and Intelligent Systems* (2015), V001T01A014–V001T01A014. DOI: [10.1115/smasis2015-9018](https://doi.org/10.1115/smasis2015-9018).
- “Designing and Harnessing the Metastable States of a Modular Metastructure for Programmable Mechanical Properties Adaptation”. In: *Journal of Mechanical Design* 138.2 (2016), p. 021402. ISSN: 1050-0472, 1528-9001. DOI: [10/gfw466](https://doi.org/10/gfw466).
- Heling, L. W. H. J., Geeves, M. A., Kad, N. M., “MyBP-C: One Protein to Govern Them All”. In: *Journal of Muscle Research and Cell Motility* 41.1 (2020), pp. 91–101. ISSN: 0142-4319, 1573-2657. DOI: [10.1007/s10974-019-09567-1](https://doi.org/10.1007/s10974-019-09567-1). URL: <http://link.springer.com/10.1007/s10974-019-09567-1>.
- Henderson, C. A. “Overview of the Muscle Cytoskeleton”. In: *Comprehensive Physiology*. John Wiley & Sons, Ltd, 2017, pp. 891–944. ISBN: 978-0-470-65071-4. DOI: [10.1002/cphy.c160033](https://doi.org/10.1002/cphy.c160033). URL: <https://onlinelibrary.wiley.com/doi/abs/10.1002/cphy.c160033>.
- Herwig, M. “Modulation of Titin-Based Stiffness in Hypertrophic Cardiomyopathy via Protein Kinase D”. In: *Front Physiol* 11 (2020), p. 240. ISSN: 1664-042X. DOI: [10.3389/fphys.2020.00240](https://doi.org/10.3389/fphys.2020.00240).

- Herzog, W., Schappacher-Tilp, G., “Molecular Mechanisms of Muscle Contraction: A Historical Perspective”. In: *Journal of Biomechanics* 155 (2023), p. 111659. ISSN: 00219290. DOI: [10.1016/j.biomech.2023.111659](https://doi.org/10.1016/j.biomech.2023.111659). URL: <https://linkinghub.elsevier.com/retrieve/pii/S0021929023002282>.
- Hill, T. L. “Theoretical Formalism for the Sliding Filament Model of Contraction of Striated Muscle Part I”. In: *Prog Biophys Mol Bio* 28 (1974), pp. 267–340. ISSN: 00796107. DOI: [10/cwsfsx](https://doi.org/10/cwsfsx).
- “Theoretical Formalism for the Sliding Filament Model of Contraction of Striated Muscle Part II”. In: *Progress in Biophysics and Molecular Biology* 29 (1976), pp. 105–159. ISSN: 00796107. DOI: [10/b4z7px](https://doi.org/10/b4z7px).
- Hinson, J. T. “Titin Mutations in iPSCs Define Sarcomere Insufficiency as a Cause of Dilated Cardiomyopathy”. In: *Science* 349.6251 (2015), pp. 982–986. DOI: [10/f7qjd4](https://doi.org/10/f7qjd4).
- Holzbaur, E. L., Goldman, Y. E., “Coordination of Molecular Motors: From in Vitro Assays to Intracellular Dynamics”. In: *Current Opinion in Cell Biology* 22.1 (2010), pp. 4–13. ISSN: 09550674. DOI: [10/djb3hh](https://doi.org/10/djb3hh).
- Hoshino, T. “Myocardial Fiber Diameter and Regional Distribution in the Ventricular Wall of Normal Adult Hearts, Hypertensive Hearts and Hearts with Hypertrophic Cardiomyopathy”. In: *Circulation* 67.5 (1983), pp. 1109–1116. DOI: [10.1161/01.CIR.67.5.1109](https://doi.org/10.1161/01.CIR.67.5.1109).
- Houdusse, A., Auguin, D., “Small Molecules Modulating Force Production: A Promising Strategy to Treat Myosin-Associated Diseases”. In: *Biophysical Journal* 123.3 (2024), 466a. ISSN: 0006-3495. DOI: [10.1016/j.bpj.2023.11.2821](https://doi.org/10.1016/j.bpj.2023.11.2821).
- Houdusse, A., Sweeney, H., “How Myosin Generates Force on Actin Filaments”. In: *Trends in Biochemical Sciences* 41.12 (2016), pp. 989–997. ISSN: 09680004. DOI: [10/f9c8jf](https://doi.org/10/f9c8jf).
- Huxley, A. F. “Muscle Structure and Theories of Contraction”. In: *Progress in biophysics and biophysical chemistry* 7 (1957), pp. 255–318. DOI: [10.1016/S0096-4174\(18\)30128-8](https://doi.org/10.1016/S0096-4174(18)30128-8).
- Huxley, A. F., Simmons, R. M., “Proposed Mechanism of Force Generation in Striated Muscle”. In: *Nature* 233.5321 (1971), pp. 533–538. DOI: [10.1038/233533a0](https://doi.org/10.1038/233533a0).
- Huxley, H. E. “The Double Array of Filaments in Cross-Striated Muscle”. In: *The Journal of Biophysical and Biochemical Cytology* 3.5 (1957), pp. 631–648. ISSN: 0095-9901. PMID: [13475381](https://pubmed.ncbi.nlm.nih.gov/13475381/). URL: <https://www.ncbi.nlm.nih.gov/pmc/articles/PMC2224118/>.
- Hwang, Y. “A Reverse Stroke Characterizes the Force Generation of Cardiac Myofilaments, Leading to an Understanding of Heart Function”. In: *Proceedings of the National Academy of Sciences* 118.23 (2021), e2011659118. ISSN: 0027-8424, 1091-6490. DOI: [10.1073/pnas.2011659118](https://doi.org/10.1073/pnas.2011659118).
- Janssen, P. M., Hunter, W. C., “Force, Not Sarcomere Length, Correlates with Prolongation of Isosarcometric Contraction”. In: *American Journal of Physiology-Heart and Circulatory Physiology* 269.2 (1995), H676–H685. ISSN: 0363-6135, 1522-1539. DOI: [10/gmtz3f](https://doi.org/10/gmtz3f).
- Jülicher, F., Prost, J., “Spontaneous Oscillations of Collective Molecular Motors”. In: *Physical Review Letters* 78.23 (1997), pp. 4510–4513. DOI: [10.1103/physrevlett.78.4510](https://doi.org/10.1103/physrevlett.78.4510).
- Jülicher, F., Prost, J., “Cooperative Molecular Motors”. In: *Physical Review Letters* 75.13 (1995), pp. 2618–2621.
- Jülicher, F., Ajdari, A., Prost, J., “Modeling Molecular Motors”. In: *Reviews of Modern Physics* 69.4 (1997), pp. 1269–1282. ISSN: 0034-6861, 1539-0756. DOI: [10/dvk9kt](https://doi.org/10/dvk9kt).

- Kalaganov, A. “Forces Measured with Micro-Fabricated Cantilevers during Actomyosin Interactions Produced by Filaments Containing Different Myosin Isoforms and Loop 1 Structures”. In: *Biochimica et Biophysica Acta (BBA) - General Subjects* 1830.3 (2013), pp. 2710–2719. ISSN: 0304-4165. DOI: [10.1016/j.bbagen.2012.11.022](https://doi.org/10.1016/j.bbagen.2012.11.022).
- Kaya, M. “Coordinated Force Generation of Skeletal Myosins in Myofilaments through Motor Coupling”. In: *Nat Commun* 8.1 (2017), p. 16036. ISSN: 2041-1723. DOI: [10/gbkxhq](https://doi.org/10/gbkxhq).
- Kentish, J. C. “Comparison between the Sarcomere Length-Force Relations of Intact and Skinned Trabeculae from Rat Right Ventricle. Influence of Calcium Concentrations on These Relations.” In: *Circulation Research* 58.6 (1986), pp. 755–768. ISSN: 0009-7330, 1524-4571. DOI: [10.1161/01.res.58.6.755](https://doi.org/10.1161/01.res.58.6.755).
- Kidambi, N., Harne, R. L., Wang, K. W., “Energy Capture and Storage in Asymmetrically Multistable Modular Structures Inspired by Skeletal Muscle”. In: *Smart Mater. Struct.* 26.8 (2017), p. 085011. ISSN: 0964-1726, 1361-665X. DOI: [10/gmc7xc](https://doi.org/10/gmc7xc).
- Kimmig, F. “Modélisation Multi-Échelles de La Contraction Musculaire: De La Dynamique Stochastique Des Moteurs Moléculaires à La Mécanique Des Milieux Continus”. 2019.
- Kimmig, F., Caruel, M., “Hierarchical Modeling of Force Generation in Cardiac Muscle”. In: *Biomechanics and Modeling in Mechanobiology* 19.6 (2020), pp. 2567–2601. ISSN: 1617-7959. DOI: [10.1007/s10237-020-01357-w](https://doi.org/10.1007/s10237-020-01357-w).
- Kimmig, F., Caruel, M., Chapelle, D., “Varying Thin Filament Activation in the Framework of the Huxley’57 Model”. In: *International Journal for Numerical Methods in Biomedical Engineering* 38.12 (2022), e3655. ISSN: 2040-7947. DOI: [10.1002/cnm.3655](https://doi.org/10.1002/cnm.3655).
- Kimmig, F., Chapelle, D., Moireau, P., “Thermodynamic Properties of Muscle Contraction Models and Associated Discrete-Time Principles”. In: *Advanced Modeling and Simulation in Engineering Sciences* 6.1 (2019), p. 6. ISSN: 2213-7467. DOI: [10/gmtzrb](https://doi.org/10/gmtzrb).
- Kimmig, F., Moireau, P., Chapelle, D., “Hierarchical Modeling of Length-Dependent Force Generation in Cardiac Muscles and Associated Thermodynamically-Consistent Numerical Schemes”. In: *Comput Mech* (2021), pp. 1–36. ISSN: 0178-7675. DOI: [10.1007/s00466-021-02051-z](https://doi.org/10.1007/s00466-021-02051-z).
- Lange, S. “The M-band: The Underestimated Part of the Sarcomere”. In: *Biochimica Et Biophysica Acta Bba - Mol Cell Res* 1867 (J. Biol. Chem. 286 2011 2019), p. 118440. ISSN: 0167-4889. DOI: [10.1016/j.bbamcr.2019.02.003](https://doi.org/10.1016/j.bbamcr.2019.02.003).
- LeGrice, I. J. “Laminar Structure of the Heart: Ventricular Myocyte Arrangement and Connective Tissue Architecture in the Dog”. In: *American Journal of Physiology-Heart and Circulatory Physiology* 269.2 (1995), H571–H582. ISSN: 0363-6135. DOI: [10.1152/ajpheart.1995.269.2.H571](https://doi.org/10.1152/ajpheart.1995.269.2.H571).
- Leite, F. d. S., Rassier, D. E., “Sarcomere Length Non-Uniformity and Force Regulation in Myofibrils and Sarcomeres”. In: *Biophys J* 119.12 (2020), pp. 2372–2377. ISSN: 0006-3495. DOI: [10.1016/j.bpj.2020.11.005](https://doi.org/10.1016/j.bpj.2020.11.005).
- Li, J. “Stretch Harmonizes Sarcomere Strain Across the Cardiomyocyte”. In: *Circulation Research* 133.3 (2023), pp. 255–270. DOI: [10.1161/CIRCRESAHA.123.322588](https://doi.org/10.1161/CIRCRESAHA.123.322588).
- Linari, M., Brunello, E., “Force Generation by Skeletal Muscle Is Controlled by Mechanosensing in Myosin Filaments”. In: *Nature* 528.7581 (2015), pp. 276–279. DOI: [10.1038/nature15727](https://doi.org/10.1038/nature15727).

- Linari, M., Dobbie, I., “The Stiffness of Skeletal Muscle in Isometric Contraction and Rigor: The Fraction of Myosin Heads Bound to Actin”. In: *Biophysical Journal* 74.5 (1998), pp. 2459–2473. ISSN: 00063495. DOI: [10/bkzqv6](https://doi.org/10/bkzqv6). URL: <https://linkinghub.elsevier.com/retrieve/pii/S0006349598779548>.
- Linke, W. A. “Stretching the Story of Titin and Muscle Function”. In: *Journal of Biomechanics* 152 (2023), p. 111553. ISSN: 0021-9290. DOI: [10.1016/j.jbiomech.2023.111553](https://doi.org/10.1016/j.jbiomech.2023.111553).
- Linke, W. A., Krüger, M., “The Giant Protein Titin as an Integrator of Myocyte Signaling Pathways”. In: *Physiology* 25.3 (2010), pp. 186–198. ISSN: 1548-9213, 1548-9221. DOI: [10/d6nqv](https://doi.org/10/d6nqv).
- Llinas, P. “How Actin Initiates the Motor Activity of Myosin”. In: *Developmental Cell* 33.4 (2015), pp. 401–412. ISSN: 15345807. DOI: [10/f7cvg8](https://doi.org/10/f7cvg8).
- Lookin, O., Khokhlova, A., Cazorla, O., “Contractile State Dependent Sarcomere Length Variability in Isolated Guinea-Pig Cardiomyocytes”. In: *Frontiers in Physiology* 13 (2022). ISSN: 1664-042X. DOI: [10.3389/fphys.2022.857471](https://doi.org/10.3389/fphys.2022.857471).
- Lynn, R. W., Taylor, E. W., “Mechanism of Adenosine Triphosphate Hydrolysis by Actomyosin”. In: *Biochemistry* 10.25 (1971), pp. 4617–4624. DOI: [10/dvbcct](https://doi.org/10/dvbcct).
- Ma, H. “Integrated Design and Fabrication Strategies Based on Bioprinting for Skeletal Muscle Regeneration: Current Status and Future Perspectives”. In: *Materials & Design* 225 (2023), p. 111591. ISSN: 0264-1275. DOI: [10.1016/j.matdes.2023.111591](https://doi.org/10.1016/j.matdes.2023.111591).
- Magnasco, M. O. “Forced Thermal Ratchets”. In: *Physical Review Letters* 71.10 (1993), pp. 1477–1481. ISSN: 0031-9007. DOI: [10/dtk497](https://doi.org/10/dtk497).
- Malik, F. I. “Cardiac Myosin Activation: A Potential Therapeutic Approach for Systolic Heart Failure”. In: *Science* 331.6023 (2011), pp. 1439–1443. ISSN: 0036-8075, 1095-9203. DOI: [10/d5qnp](https://doi.org/10/d5qnp).
- Manca, F. “SNARE Machinery Is Optimized for Ultrafast Fusion”. In: *Proceedings of the National Academy of Sciences* 116.7 (2019), pp. 2435–2442. ISSN: 0027-8424, 1091-6490. DOI: [10/gmn5g3](https://doi.org/10/gmn5g3).
- Manevy, R., Caruel, M., “Identification of Free Energy Barriers Associated With Transition In Myosin cycle Using Umbrella Sampling”. In: *Workshop Les Houches Protein Dynamics*. Congrès virtuel, 2021.
- Manevy, R., Detrez, F., “Étude Mécanique d’une Protéine Du Muscle”. In: *Journée Thématique Biomécanique et Biomatériaux F2M*. online, 2021.
- Manganotti, J. “Coupling Reduced-Order Blood Flow and Cardiac Models through Energy-Consistent Strategies: Modeling and Discretization”. In: *Advanced Modeling and Simulation in Engineering Sciences* 8.1 (2021), p. 21. ISSN: 2213-7467. DOI: [10.1186/s40323-021-00206-4](https://doi.org/10.1186/s40323-021-00206-4). URL: <https://doi.org/10.1186/s40323-021-00206-4>.
- Månsson, A. “Actomyosin-ADP States, Interhead Cooperativity, and the Force-Velocity Relation of Skeletal Muscle”. In: *Biophysical Journal* 98.7 (2010), pp. 1237–1246. ISSN: 00063495. DOI: [10/crwdh6](https://doi.org/10/crwdh6).
- “Actomyosin Based Contraction: One Mechanokinetic Model from Single Molecules to Muscle?” In: *J Muscle Res Cell Motil* 37.6 (2016), pp. 181–194. ISSN: 0142-4319, 1573-2657. DOI: [10/f9sbhb](https://doi.org/10/f9sbhb).
 - “Comparing Models with One versus Multiple Myosin-Binding Sites per Actin Target Zone: The Power of Simplicity”. In: *Journal of General Physiology* 151.4 (2019), pp. 578–592. ISSN: 0022-1295. DOI: [10.1085/jgp.201812301](https://doi.org/10.1085/jgp.201812301).

- “Hypothesis: Single Actomyosin Properties Account for Ensemble Behavior in Active Muscle Shortening and Isometric Contraction”. In: *Int J Mol Sci* 21.21 (2020), p. 8399. DOI: [10.3390/ijms21218399](https://doi.org/10.3390/ijms21218399).
- Marcucci, L., Truskinovsky, L., “Mechanics of the Power Stroke in Myosin II”. In: *Physical Review E* 81.5 (2010), p. 051915. ISSN: 1539-3755, 1550-2376. DOI: [10/c9xrzx](https://doi.org/10/c9xrzx).
- Maron, B. J., Maron, M. S., “Hypertrophic Cardiomyopathy”. In: *The Lancet* 381.9862 (2013), pp. 242–255. DOI: [10.1016/s0140-6736\(12\)60397-3](https://doi.org/10.1016/s0140-6736(12)60397-3).
- Marston, S. “Force Measurements From Myofibril to Filament”. In: *Frontiers in Physiology* 12 (2022), p. 817036. ISSN: 1664-042X. DOI: [10.3389/fphys.2021.817036](https://doi.org/10.3389/fphys.2021.817036).
- McKillop, D., Geeves, M., “Regulation of the Interaction between Actin and Myosin Subfragment 1: Evidence for Three States of the Thin Filament”. In: *Biophysical Journal* 65.2 (1993), pp. 693–701. ISSN: 00063495. DOI: [10.1016/S0006-3495\(93\)81110-X](https://doi.org/10.1016/S0006-3495(93)81110-X).
- McNeill Alexander, R., Newsom-Davis, J. M., “Striated Muscle; Human Biceps Muscle”. In: *Encyclopaedia Britannica*. 2015.
- Ménétreay, J. “The Structure of the Myosin VI Motor Reveals the Mechanism of Directionality Reversal”. In: *Nature* 435.7043 (2005), pp. 779–785. ISSN: 1476-4687. DOI: [10.1038/nature03592](https://doi.org/10.1038/nature03592).
- Milićević, B. “Huxley Muscle Model Surrogates for High-Speed Multi-Scale Simulations of Cardiac Contraction”. In: *Computers in Biology and Medicine* 149 (2022), p. 105963. ISSN: 0010-4825. DOI: [10.1016/j.compbiomed.2022.105963](https://doi.org/10.1016/j.compbiomed.2022.105963). URL: <https://www.sciencedirect.com/science/article/pii/S0010482522006965>.
- Mobley, B. A., Eisenberg, B. R., “Sizes of Components in Frog Skeletal Muscle Measured by Methods of Stereology”. In: *Journal of General Physiology* 66.1 (1975), pp. 31–45. ISSN: 0022-1295, 1540-7748. DOI: [10/cm8s33](https://doi.org/10/cm8s33).
- Molloy, J. E. “Single-Molecule Mechanics of Heavy Meromyosin and Si Interacting with Rabbit or Drosophila Actins Using Optical Tweezers”. In: *Biophysical Journal* 68 (1995), p. 6.
- Monod, J., Wyman, J., Changeux, J. P., “On The Nature Of Allosteric Transitions: A Plausible Model.” In: *J. Mol. Biol.* 12 (1965), pp. 88–118.
- Moo, E. K., Herzog, W., “Single Sarcomere Contraction Dynamics in a Whole Muscle”. In: *Scientific Reports* 8.1 (1 2018), p. 15235. ISSN: 2045-2322. DOI: [10.1038/s41598-018-33658-7](https://doi.org/10.1038/s41598-018-33658-7). URL: <https://www.nature.com/articles/s41598-018-33658-7>.
- Morita, H. “Shared Genetic Causes of Cardiac Hypertrophy in Children and Adults”. In: *New England Journal of Medicine* 358.18 (2008), pp. 1899–1908. DOI: [10.1056/nejmoa075463](https://doi.org/10.1056/nejmoa075463).
- Nadkarni, N. “Unidirectional Transition Waves in Bistable Lattices”. In: *Physical Review Letters* 116.24 (2016), p. 244501. ISSN: 0031-9007, 1079-7114. DOI: [10/gf2mms](https://doi.org/10/gf2mms).
- Nag, S. “Mavacamten, a Precision Medicine for Hypertrophic Cardiomyopathy: From a Motor Protein to Patients”. In: *Science Advances* 9.30 (2023), eabo7622. DOI: [10.1126/sciadv.abo7622](https://doi.org/10.1126/sciadv.abo7622).
- Nardinocchi, P., Teresi, L., “On the Active Response of Soft Living Tissues”. In: *Journal of Elasticity* 88.1 (2007), pp. 27–39. ISSN: 0374-3535, 1573-2681. DOI: [10.1007/s10659-007-9111-7](https://doi.org/10.1007/s10659-007-9111-7).
- Niellas-Vallespin, S. “Assessment of Myocardial Microstructural Dynamics by In Vivo Diffusion Tensor Cardiac Magnetic Resonance”. In: *Journal of the American College of Cardiology* 69.6 (2017), pp. 661–676. ISSN: 0735-1097. DOI: [10.1016/j.jacc.2016.11.051](https://doi.org/10.1016/j.jacc.2016.11.051).

- Nobile, F., Quarteroni, A., Ruiz-Baier, R., “An Active Strain Electromechanical Model for Cardiac Tissue: Active strain in cardiac electromechanics”. In: *International Journal for Numerical Methods in Biomedical Engineering* 28.1 (2012), pp. 52–71. ISSN: 20407939. DOI: [10/bn6kcq](https://doi.org/10/bn6kcq).
- Pertici, I., Bianchi, G., “A Myosin II-Based Nanomachine Devised for the Study of Ca²⁺-Dependent Mechanisms of Muscle Regulation”. In: *Int J Mol Sci* 21.19 (2020), p. 7372. DOI: [10.3390/ijms21197372](https://doi.org/10.3390/ijms21197372).
- Pertici, I., Bongini, L., “A Myosin II Nanomachine Mimicking the Striated Muscle”. In: *Nat Commun* 9.1 (2018), p. 3532. ISSN: 2041-1723. DOI: [10/gd69s3](https://doi.org/10/gd69s3).
- Pertici, I., Caremani, M., Reconditi, M., “A Mechanical Model of the Half-Sarcomere Which Includes the Contribution of Titin”. In: *Journal of Muscle Research and Cell Motility* 40.1 (2019), pp. 29–41. ISSN: 0142-4319, 1573-2657. DOI: [10/gmtzrp](https://doi.org/10/gmtzrp). URL: <http://link.springer.com/10.1007/s10974-019-09508-y>.
- Piazzesi, G., Lombardi, V., “A Cross-Bridge Model That Is Able to Explain Mechanical and Energetic Properties of Shortening Muscle”. In: *Biophysical Journal* 68.5 (1995), pp. 1966–1979. ISSN: 00063495. DOI: [10/c3nkhz](https://doi.org/10/c3nkhz).
- Piazzesi, G., Lucii, L., Lombardi, V., “The Size and the Speed of the Working Stroke of Muscle Myosin and Its Dependence on the Force”. In: *The Journal of Physiology* 545.1 (2002), pp. 145–151. ISSN: 0022-3751, 1469-7793. DOI: [10/dtj3gc](https://doi.org/10/dtj3gc).
- Piazzesi, G., Reconditi, M., Linari, M., Lucii, L., Bianco, P., “Skeletal Muscle Performance Determined by Modulation of Number of Myosin Motors Rather Than Motor Force or Stroke Size”. In: *Cell* 131.4 (2007), pp. 784–795. ISSN: 00928674. DOI: [10/bmsfz4](https://doi.org/10/bmsfz4).
- Piazzesi, G., Reconditi, M., Linari, M., Lucii, L., Sun, Y.-B., “Mechanism of Force Generation by Myosin Heads in Skeletal Muscle”. In: *Nature* 415.6872 (2002), pp. 659–662. ISSN: 0028-0836, 1476-4687. DOI: [10/frsg7p](https://doi.org/10/frsg7p).
- Pinzauti, F. “The Force and Stiffness of Myosin Motors in the Isometric Twitch of a Cardiac Trabecula and the Effect of the Extracellular Calcium Concentration”. In: *The Journal of Physiology* 596.13 (2018), pp. 2581–2596. ISSN: 00223751. DOI: [10/gmtzp9](https://doi.org/10/gmtzp9).
- Plaçaïs, P.-Y. “Spontaneous Oscillations of a Minimal Actomyosin System under Elastic Loading”. In: *Physical Review Letters* 103.15 (2009), p. 158102. ISSN: 0031-9007, 1079-7114. DOI: [10/cdjrvz](https://doi.org/10/cdjrvz).
- Podolsky, R., Nolan, A. C., Zaveler, S. A., “Cross-Bridge Properties Derived from Muscle Isotonic Velocity Transients.” In: *Proceedings of the National Academy of Sciences of the United States of America* 64.2 (1969), pp. 504–511.
- Pollard, T. D. “Evolution of Research on Cellular Motility over Five Decades”. In: *Biophysical Reviews* 10.6 (2018), pp. 1503–1508. ISSN: 1867-2450, 1867-2469. DOI: [10/gqjswp](https://doi.org/10/gqjswp).
- Powers, J. D. “Contracting Striated Muscle Has a Dynamic I-band Spring with an Undamped Stiffness 100 Times Larger than the Passive Stiffness”. In: *The Journal of Physiology* 598.2 (2020), pp. 331–345. ISSN: 0022-3751, 1469-7793. DOI: [10/gm3sgx](https://doi.org/10/gm3sgx).
- Powers, K. “Titin Force Is Enhanced in Actively Stretched Skeletal Muscle”. In: *Journal of Experimental Biology* (2014), jeb.105361. ISSN: 1477-9145, 0022-0949. DOI: [10.1242/jeb.105361](https://doi.org/10.1242/jeb.105361).
- Prakash, M., Lemaire, T., Caruel, M., “Anisotropic Diffusion of Water Molecules in Hydrox-yapatite Nanopores”. In: *Physics and Chemistry of Minerals* 44.7 (2017), pp. 509–519. ISSN: 0342-1791, 1432-2021. DOI: [10/gbphjp](https://doi.org/10/gbphjp).

- Prakash, M., Lemaire, T., Di Tommaso, D., “Transport Properties of Water Molecules Confined between Hydroxyapatite Surfaces: A Molecular Dynamics Simulation Approach”. In: *Applied Surface Science* 418 (2017), pp. 296–301. ISSN: 01694332. DOI: [10/gmtzzr](https://doi.org/10/gmtzzr).
- Protti, I. “Looking Back, Going Forward: Understanding Cardiac Pathophysiology from Pressure–Volume Loops”. In: *Biology* 13.1 (2024), p. 55. ISSN: 2079-7737. DOI: [10.3390/biology13010055](https://doi.org/10.3390/biology13010055).
- RabieeRad, M. “Novel Treatments of Hypertrophic Cardiomyopathy in GDMT for Heart Failure: A State-of-art Review”. In: *Current Problems in Cardiology* 48.9 (2023), p. 101740. ISSN: 01462806. DOI: [10.1016/j.cpcardiol.2023.101740](https://doi.org/10.1016/j.cpcardiol.2023.101740).
- Rayment, I., Holden, H. M., “Structure of the Actin-Myosin Complex and Its Implications for Muscle Contraction”. In: *Science* 261.5117 (1993), pp. 58–65. ISSN: 0036-8075, 1095-9203. DOI: [10/cjj44w](https://doi.org/10/cjj44w).
- Rayment, I., Rypniewski, W. R., “Three-Dimensional Structure of Myosin Subfragment-1: A Molecular Motor”. In: *Science* 261.5117 (1993), pp. 50–58.
- Reconditi, M. “Recent Improvements in Small Angle X-Ray Diffraction for the Study of Muscle Physiology”. In: *Reports on Progress in Physics* 69.10 (2006), pp. 2709–2759. ISSN: 0034-4885, 1361-6633. DOI: [10.1088/0034-4885/69/10/R01](https://doi.org/10.1088/0034-4885/69/10/R01). URL: <https://iopscience.iop.org/article/10.1088/0034-4885/69/10/R01>.
- Reconditi, M., Caremani, M., “Myosin Filament Activation in the Heart Is Tuned to the Mechanical Task”. In: *Proc Natl Acad Sci USA* 114.12 (2017), pp. 3240–3245. ISSN: 0027-8424, 1091-6490. DOI: [10/f9vq5m](https://doi.org/10/f9vq5m).
- Reconditi, M., Linari, M., “The Myosin Motor in Muscle Generates a Smaller and Slower Working Stroke at Higher Load”. In: *Nature* 428.6982 (2004), pp. 578–581. ISSN: 0028-0836, 1476-4687. DOI: [10/dfh49n](https://doi.org/10/dfh49n). URL: <http://www.nature.com/articles/nature02380>.
- Regazzoni, F., Dedè, L., Quarteroni, A., “Biophysically detailed mathematical models of multi-scale cardiac active mechanics”. In: *PLOS Computational Biology* 16.10 (2020), e1008294. ISSN: 1553-734X. DOI: [10.1371/journal.pcbi.1008294](https://doi.org/10.1371/journal.pcbi.1008294).
- Regazzoni, F., Salvador, M., “A Machine Learning Method for Real-Time Numerical Simulations of Cardiac Electromechanics”. In: *Computer Methods in Applied Mechanics and Engineering* 393 (2022), p. 114825. ISSN: 0045-7825. DOI: [10.1016/j.cma.2022.114825](https://doi.org/10.1016/j.cma.2022.114825). URL: <https://www.sciencedirect.com/science/article/pii/S004578252200144X>.
- Robert-Paganin, J. “Force Generation by Myosin Motors: A Structural Perspective”. In: *Chem. Rev.* 120.1 (2020), pp. 5–35. ISSN: 0009-2665, 1520-6890. DOI: [10/gmtzrv](https://doi.org/10/gmtzrv).
- Rock, R. S. “Myosin VI Is a Processive Motor with a Large Step Size”. In: *Proceedings of the National Academy of Sciences* 98.24 (2001), pp. 13655–13659. DOI: [10.1073/pnas.191512398](https://doi.org/10.1073/pnas.191512398).
- Roots, H., Offer, G. W., Ranatunga, K. W., “Comparison of the Tension Responses to Ramp Shortening and Lengthening in Intact Mammalian Muscle Fibres: Crossbridge and Non-Crossbridge Contributions”. In: *Journal of Muscle Research and Cell Motility* 28.2-3 (2007), pp. 123–139. ISSN: 0142-4319, 1573-2657. DOI: [10/d9dff9](https://doi.org/10/d9dff9). URL: <http://link.springer.com/10.1007/s10974-007-9110-0>.
- Rosignol, P. “Heart Failure Drug Treatment”. In: *Lancet* 393.10175 (2019), pp. 1034–1044. ISSN: 0140-6736. DOI: [10.1016/s0140-6736\(18\)31808-7](https://doi.org/10.1016/s0140-6736(18)31808-7).

- Rothman, J. E. “Turbocharging Synaptic Transmission”. In: *FEBS Letters* 597.18 (2023), pp. 2233–2249. ISSN: 1873-3468. DOI: [10.1002/1873-3468.14718](https://doi.org/10.1002/1873-3468.14718). URL: <https://onlinelibrary.wiley.com/doi/abs/10.1002/1873-3468.14718>.
- Saper, G., Hess, H., “Synthetic Systems Powered by Biological Molecular Motors”. In: *Chemical Reviews* 120.1 (2020), pp. 288–309. ISSN: 0009-2665, 1520-6890. DOI: [10.1021/acs.chemrev.9b00249](https://doi.org/10.1021/acs.chemrev.9b00249).
- Schappacher-Tilp, G. “A Novel Three-Filament Model of Force Generation in Eccentric Contraction of Skeletal Muscles”. In: *PLOS ONE* 10.3 (2015), e0117634. DOI: [10.1371/journal.pone.0117634](https://doi.org/10.1371/journal.pone.0117634).
- Schoenauer, R. “Myomesin Is a Molecular Spring with Adaptable Elasticity”. In: *J Mol Biol* 349.2 (2005), pp. 367–379. ISSN: 0022-2836. DOI: [10.1016/j.jmb.2005.03.055](https://doi.org/10.1016/j.jmb.2005.03.055).
- Sheshka, R., Truskinovsky, L., “Power-Stroke-Driven Actomyosin Contractility.” In: *Phys Rev E* 89.1 (2014), pp. 012708–12. DOI: [10.1103/physreve.89.012708](https://doi.org/10.1103/physreve.89.012708).
- Shimamoto, Y. “Inter-Sarcomere Coordination in Muscle Revealed through Individual Sarcomere Response to Quick Stretch”. In: *Proceedings of the National Academy of Sciences* 106.29 (2009), pp. 11954–11959. ISSN: 0027-8424, 1091-6490. DOI: [10/crcjzf](https://doi.org/10.1073/pnas.2009.09.11954).
- Smith, D. A., Mijailovich, S. M., “Toward a Unified Theory of Muscle Contraction. II: Predictions with the Mean-Field Approximation”. In: *Ann Biomed Eng* 36.8 (2008), pp. 1353–1371. ISSN: 0090-6964, 1573-9686. DOI: [10/ctxn66](https://doi.org/10.1002/abme.10666).
- Smith, D., Geeves, M., “Strain-Dependent Cross-Bridge Cycle for Muscle”. In: *Biophys J* 69.2 (1995), pp. 524–537. ISSN: 0006-3495. DOI: [10.1016/s0006-3495\(95\)79926-x](https://doi.org/10.1016/s0006-3495(95)79926-x).
- “Strain-Dependent Cross-Bridge Cycle for Muscle. II. Steady-state Behavior”. In: *Biophysical Journal* 69.2 (1995), pp. 538–552. ISSN: 00063495. DOI: [10.1016/S0006-3495\(95\)79927-1](https://doi.org/10.1016/S0006-3495(95)79927-1).
- Smith, D., Geeves, M., “Towards a Unified Theory of Muscle Contraction. I: Foundations”. In: *Ann Biomed Eng* 36.10 (2008), pp. 1624–1640. ISSN: 0090-6964, 1573-9686. DOI: [10/b3tnkk](https://doi.org/10.1002/abme.10666).
- Sommer, G. “Biomechanical Properties and Microstructure of Human Ventricular Myocardium”. In: *Acta Biomaterialia* 24 (2015), pp. 172–192. ISSN: 1742-7061. DOI: [10.1016/j.actbio.2015.06.031](https://doi.org/10.1016/j.actbio.2015.06.031).
- Spudich, J. A. “Optical Traps to Study Properties of Molecular Motors”. In: *Cold Spring Harbor Protocols* 2011.11 (2011), pdb.top066662. ISSN: 1940-3402, 1559-6095. DOI: [10.1101/pdb.top066662](https://doi.org/10.1101/pdb.top066662).
- Squarci, C. “Titin Activates Myosin Filaments in Skeletal Muscle by Switching from an Extensible Spring to a Mechanical Rectifier”. In: *Proceedings of the National Academy of Sciences* 120.9 (2023), e2219346120. DOI: [10.1073/pnas.2219346120](https://doi.org/10.1073/pnas.2219346120). URL: <https://www.pnas.org/doi/10.1073/pnas.2219346120>.
- Stojanovic, B. “Multi-scale Striated Muscle Contraction Model Linking Sarcomere Length-dependent Cross-bridge Kinetics to Macroscopic Deformation”. In: *J. Comput. Sci.* (2019), p. 101062. DOI: [10.1016/j.jocs.2019.101062](https://doi.org/10.1016/j.jocs.2019.101062).
- Streeter Jr. D. D., Bassett, D. L., “An Engineering Analysis of Myocardial Fiber Orientation in Pig’s Left Ventricle in Systole”. In: *The Anatomical Record* 155.4 (1966), pp. 503–511. ISSN: 1097-0185. DOI: [10.1002/ar.1091550403](https://doi.org/10.1002/ar.1091550403).
- Sugiura, S., Okada, J.-I., “UT-Heart: A Finite Element Model Designed for the Multiscale and Multiphysics Integration of Our Knowledge on the Human Heart”. In: *Computational Systems*

- Biology in Medicine and Biotechnology: Methods and Protocols*. Ed. by S. Cortassa and M. A. Aon. New York, NY: Springer US, 2022, pp. 221–245. ISBN: 978-1-07-161831-8. DOI: [10.1007/978-1-0716-1831-8_10](https://doi.org/10.1007/978-1-0716-1831-8_10).
- Sugiura, S., Washio, T., “Multi-Scale Simulations of Cardiac Electrophysiology and Mechanics Using the University of Tokyo Heart Simulator”. In: *Progress in Biophysics and Molecular Biology* 110.2 (2012), pp. 380–389. ISSN: 0079-6107. DOI: [10.1016/j.pbiomolbio.2012.07.001](https://doi.org/10.1016/j.pbiomolbio.2012.07.001).
- Svoboda, K. “Direct Observation of Kinesin Stepping by Optical Trapping Interferometry”. In: *Nature* 365.6448 (1993), pp. 721–727. ISSN: 1476-4687. DOI: [10.1038/365721a0](https://doi.org/10.1038/365721a0).
- Sznitman, A.-S. “Topics in propagation of chaos”. In: *Ecole d’été de probabilités de Saint-Flour XIX–1989* 1464 (1991), pp. 165–251. DOI: [10.1007/BFb0085169](https://doi.org/10.1007/BFb0085169).
- Tamborrini, D. “Structure of the Native Myosin Filament in the Relaxed Cardiac Sarcomere”. In: *Nature* (2023), pp. 1–9. ISSN: 1476-4687. DOI: [10.1038/s41586-023-06690-5](https://doi.org/10.1038/s41586-023-06690-5). URL: <https://www.nature.com/articles/s41586-023-06690-5>.
- ter Keurs, H. E. “Sarcomere Mechanics in Uniform and Non-Uniform Cardiac Muscle: A Link between Pump Function and Arrhythmias”. In: *Progress in Biophysics and Molecular Biology* 97.2-3 (2008), pp. 312–331. ISSN: 00796107. DOI: [10/b3qk99](https://doi.org/10/b3qk99).
- Tozzini, V. “Coarse-Grained Models for Proteins”. In: *Current Opinion in Structural Biology* 15.2 (2005), pp. 144–150. ISSN: 0959440X. DOI: [10/bj7js5](https://doi.org/10/bj7js5).
- Trayanova, N. A., Rice, J. J., “Cardiac Electromechanical Models: From Cell to Organ”. In: *Front. Physio.* 2 (2011). ISSN: 1664-042X. DOI: [10/cdpd7s](https://doi.org/10/cdpd7s).
- Tueni, N., Allain, J.-M., Genet, M., “On the Structural Origin of the Anisotropy in the Myocardium: Multiscale Modeling and Analysis”. In: *Journal of the Mechanical Behavior of Biomedical Materials* 138 (2023), p. 105600. ISSN: 1751-6161. DOI: [10.1016/j.jmbbm.2022.105600](https://doi.org/10.1016/j.jmbbm.2022.105600).
- Veigel, C. “Load-Dependent Kinetics of Force Production by Smooth Muscle Myosin Measured with Optical Tweezers”. In: *Nature Cell Biology* 5.11 (2003), pp. 980–986. ISSN: 1465-7392, 1476-4679. DOI: [10/d7nctr](https://doi.org/10/d7nctr). URL: <http://www.nature.com/articles/ncb1060>.
- Velden, J. “Research Priorities in Sarcomeric Cardiomyopathies”. In: *CARDIOVASCULAR RESEARCH* 105.4 (2015), pp. 449–456. DOI: [10.1093/cvr/cvv019](https://doi.org/10.1093/cvr/cvv019).
- Vilfan, A., Duke, T., “Instabilities in the Transient Response of Muscle”. In: *Biophysical Journal* 85.2 (2003), pp. 818–827.
- Wadmore, K., Azad, A. J., Gehmlich, K., “The Role of Z-disc Proteins in Myopathy and Cardiomyopathy”. In: *Int J Mol Sci* 22.6 (2021), p. 3058. DOI: [10.3390/ijms22063058](https://doi.org/10.3390/ijms22063058).
- Walcott, S., Warshaw, D. M., Debold, E. P., “Mechanical Coupling between Myosin Molecules Causes Differences between Ensemble and Single-Molecule Measurements”. In: *Biophysical Journal* 103.3 (2012), pp. 501–510. ISSN: 00063495. DOI: [10/f37d3b](https://doi.org/10/f37d3b).
- Wang, H., Oster, G., “Ratchets, Power Strokes, and Molecular Motors”. In: *Applied Physics A* 75.2 (2002), pp. 315–323. ISSN: 0947-8396, 1432-0630. DOI: [10/d99s9z](https://doi.org/10/d99s9z).
- Wang, Z. “The Molecular Basis for Sarcomere Organization in Vertebrate Skeletal Muscle”. In: *Cell* 184.8 (2021), 2135–2150.e13. ISSN: 00928674. DOI: [10.1016/j.cell.2021.02.047](https://doi.org/10.1016/j.cell.2021.02.047). URL: <https://linkinghub.elsevier.com/retrieve/pii/S0092867421002361>.
- Warshaw, D. “The In Vitro Motility Assay: A Window Into the Myosin Molecular Motor”. In: *Physiology* 11.1 (1996), pp. 1–7. ISSN: 1548-9213, 1548-9221. DOI: [10/gqjsw9](https://doi.org/10/gqjsw9).

- Woodhead, J. L., Craig, R., “The Mesa Trail and the Interacting Heads Motif of Myosin II”. In: *Archives of Biochemistry and Biophysics* 680 (2020), p. 108228. ISSN: 0003-9861. DOI: [10.1016/j.abb.2019.108228](https://doi.org/10.1016/j.abb.2019.108228).
- Woody, M. S., Winkelmann, D. A., “Single Molecule Mechanics Resolves the Earliest Events in Force Generation by Cardiac Myosin”. In: *eLife* 8 (2019), e49266. ISSN: 2050-084X. DOI: [10/gf9vhg](https://doi.org/10/gf9vhg).
- Woody, M. S., Greenberg, M. J., “Positive Cardiac Inotrope Omecamtiv Mecarbil Activates Muscle despite Suppressing the Myosin Working Stroke”. In: *Nat Commun* 9.1 (2018), p. 3838. ISSN: 2041-1723. DOI: [10/gfemsk](https://doi.org/10/gfemsk).
- Wu, Z., Harne, R., Wang, K., “Exploring a Modular Adaptive Metastructure Concept Inspired by Muscle’s Cross-Bridge”. In: *Journal of Intelligent Material Systems and Structures* 27.9 (2016), pp. 1189–1202. ISSN: 1045-389X, 1530-8138. DOI: [10/f8jtf3](https://doi.org/10/f8jtf3).
- Yanagida, T. “Single Molecule Analysis of the Actomyosin Motor”. In: *Current Opinion in Cell Biology* 12.1 (2000), pp. 20–25. ISSN: 09550674. DOI: [10/cwnq9w](https://doi.org/10/cwnq9w).
- Yao, H., Gao, H., “Mechanics of Robust and Releasable Adhesion in Biology: Bottom-up Designed Hierarchical Structures of Gecko”. In: *Journal of the Mechanics and Physics of Solids* 54.6 (2006), pp. 1120–1146. ISSN: 00225096. DOI: [10/cp4dsc](https://doi.org/10/cp4dsc).
- Zhang, J. “Artificial Intelligence Enhanced Molecular Simulations”. In: *Journal of Chemical Theory and Computation* 19.14 (2023), pp. 4338–4350. ISSN: 1549-9618. DOI: [10.1021/acs.jctc.3c00214](https://doi.org/10.1021/acs.jctc.3c00214).

LA CONTRACTION MUSCULAIRE EN QUATRE ÉCHELLES

Matthieu Caruel

Résumé

Cet ouvrage présente une synthèse des travaux scientifiques menés par Matthieu Caruel entre 2008 et 2025. Ces recherches portent sur la modélisation multi-échelle de la contraction musculaire, motivées par le développement d'outils de simulation numérique pour des applications dans le domaine de la santé. En partant de la description macroscopique du tissu dans le cadre de la mécanique des milieux continus, l'auteur introduit la notion de contrainte active générée par les moteurs moléculaires. Cette interaction peut être représentée par divers modèles mathématiques, formulés soit dans un cadre déterministe de dynamique des populations, soit dans un cadre stochastique de processus de Markov.

M. Caruel met ensuite en lumière le rôle des interactions mécaniques induites par les structures anatomiques à l'échelle micrométrique, dans l'émergence d'effets collectifs au sein des populations de protéines interagissantes. Ces résultats suggèrent une reformulation du cadre classique de modélisation, fondé jusqu'à présent sur un couplage direct entre l'échelle moléculaire et l'échelle tissulaire.

L'auteur souligne la nécessité de ces développements théoriques en s'appuyant sur divers résultats expérimentaux ayant démontré le rôle fondamental des interactions mécaniques supramoléculaires, à l'échelle dite mésoscopique, dans les processus physiologiques régulant la contraction.

Abstract

This work presents a synthesis of the scientific research conducted by Matthieu Caruel between 2008 and 2025. The research focuses on multiscale modeling of muscle contraction, driven by the development of numerical simulation tools for health applications. Starting with the macroscopic description of the tissue within the framework of continuum mechanics, the author introduces the concept of active stress generated by molecular motors. This interaction can be represented by various mathematical models, formulated either in a deterministic framework of population dynamics or in a stochastic framework of Markov processes.

M. Caruel then highlights the role played by mechanical interactions induced by anatomical structures at the micrometric scale in the emergence of collective effects within populations of interacting proteins. These findings suggest a reformulation of the classical modeling framework based so far on a direct coupling between the molecular scale and the tissue scale.

The author emphasizes the necessity of such theoretical developments by presenting various experimental results that have demonstrated the fundamental role of supramolecular mechanical interactions, at the so-called mesoscopic scale, in the physiological processes regulating contraction.